最近の高エネルギー ガンマ線天文学の発展

Recent developments in high-energy gamma-ray astrophysics

森　正樹

東京大学宇宙線研究所

首都大学東京 理工学研究科物理学専攻素粒子理論セミナー

2006年11月9日

Detection of gamma-rays (1)

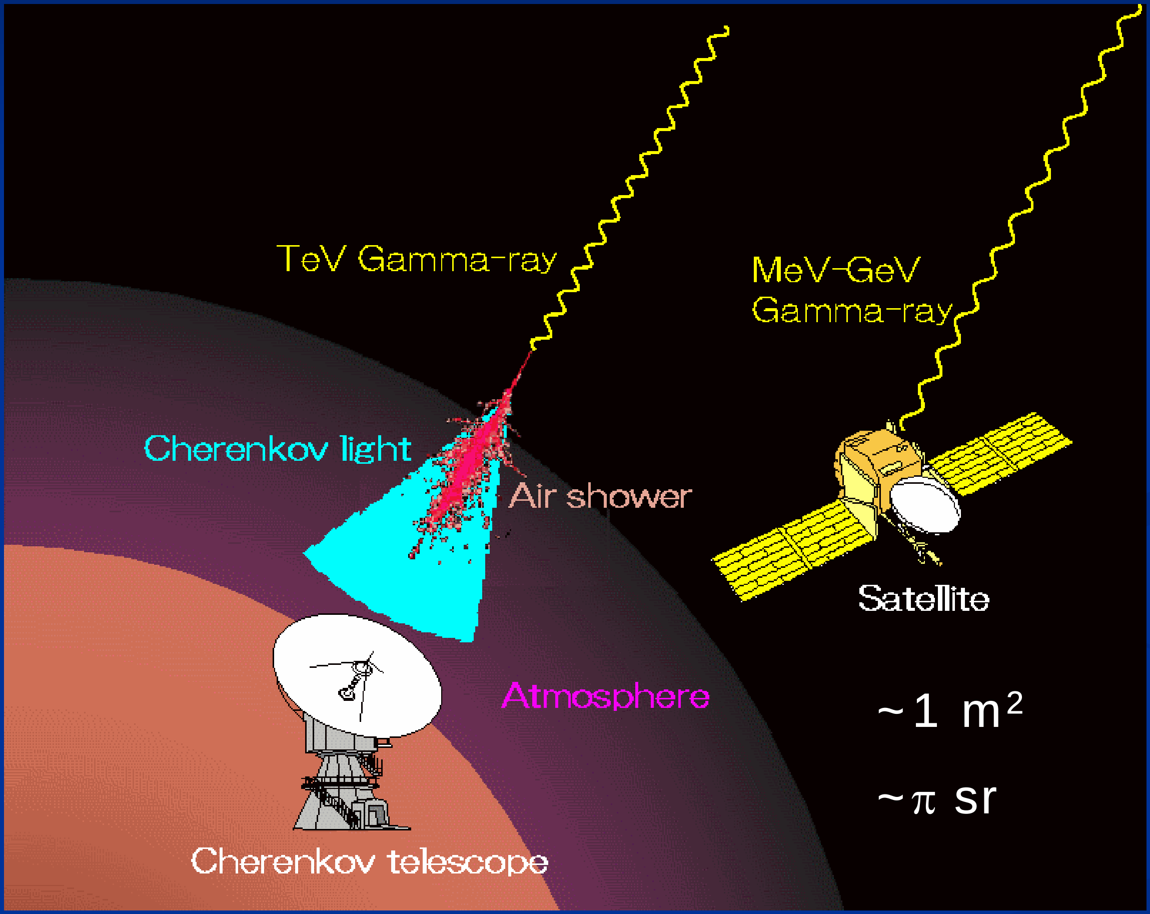

$\sim 1\ m^2$

$\sim \pi$ sr

$A \sim 10^4 m^2$

$\Omega \sim 10^{-2}$sr

> TeV gamma-rays

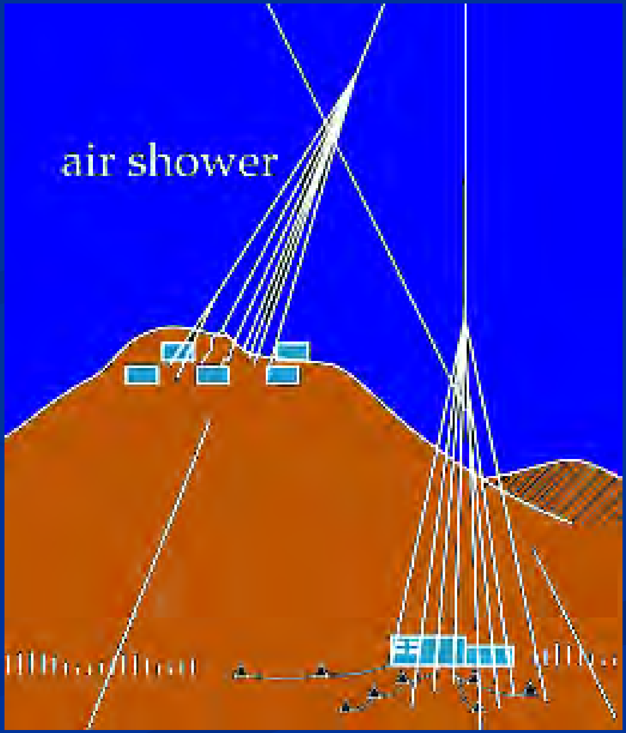

Atmospheric Cherenkov telescopes

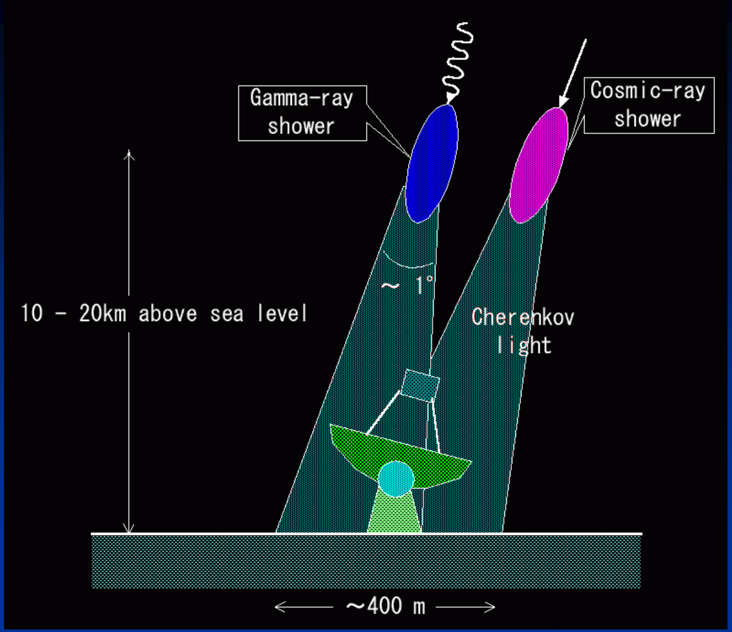

Cherenkov light from gamma-ray showers

Lateral distribution & Timing distribution

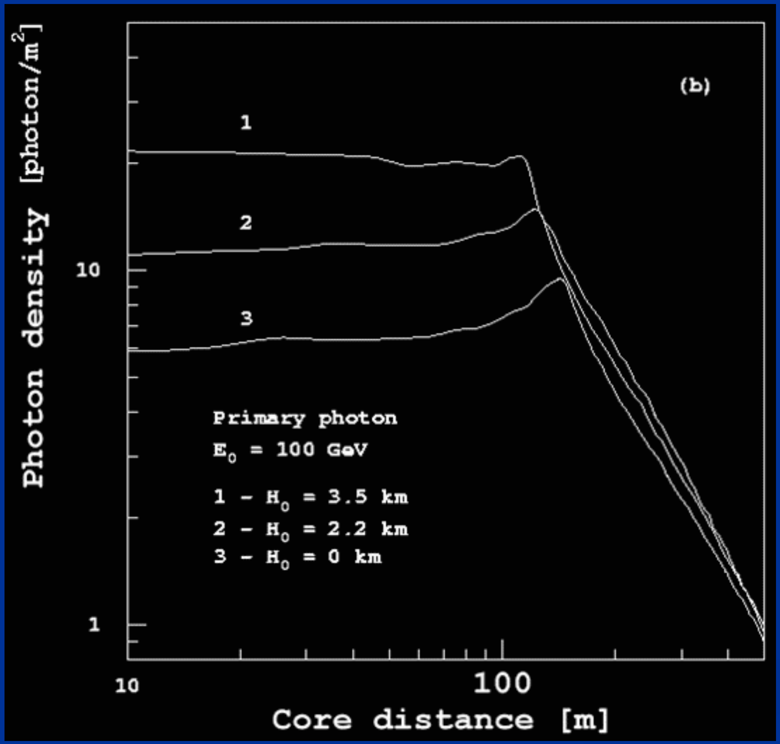

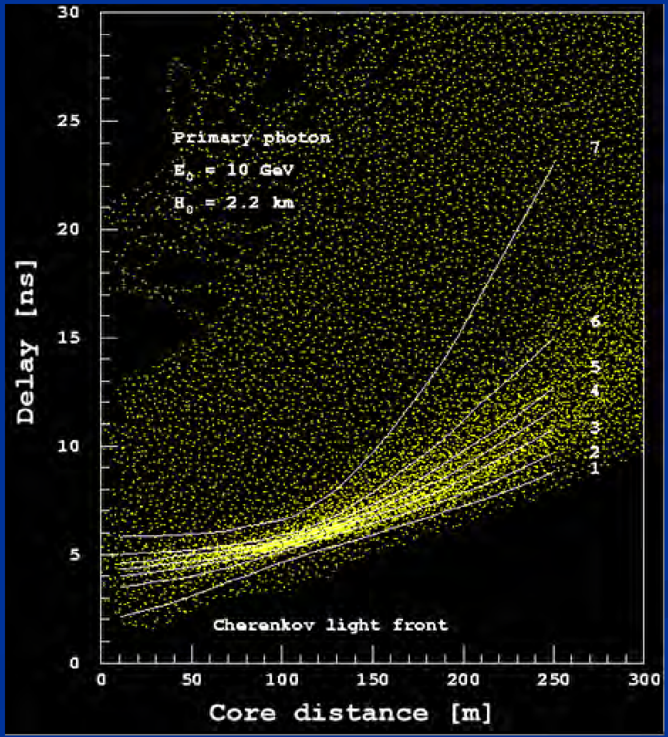

Atmospheric transmission

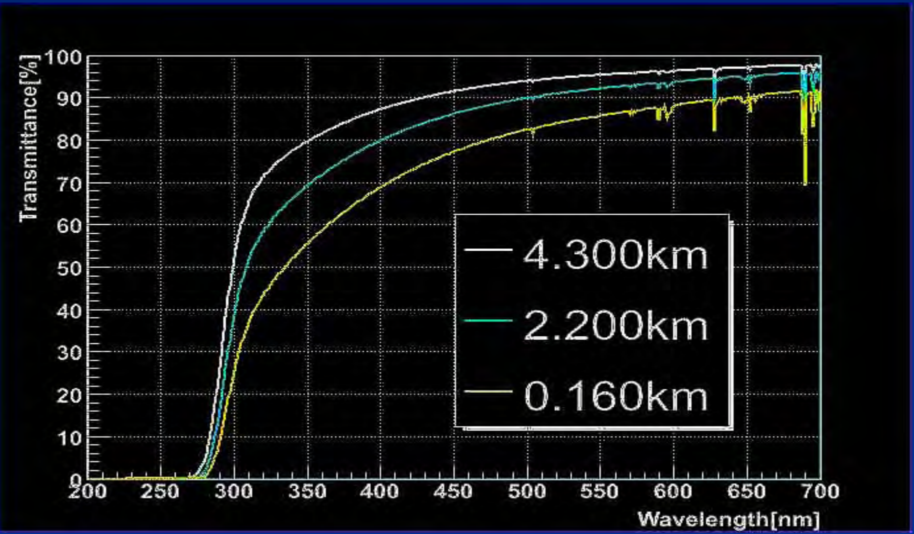

MODRAN4 calculation by M.Yuasa (2006)

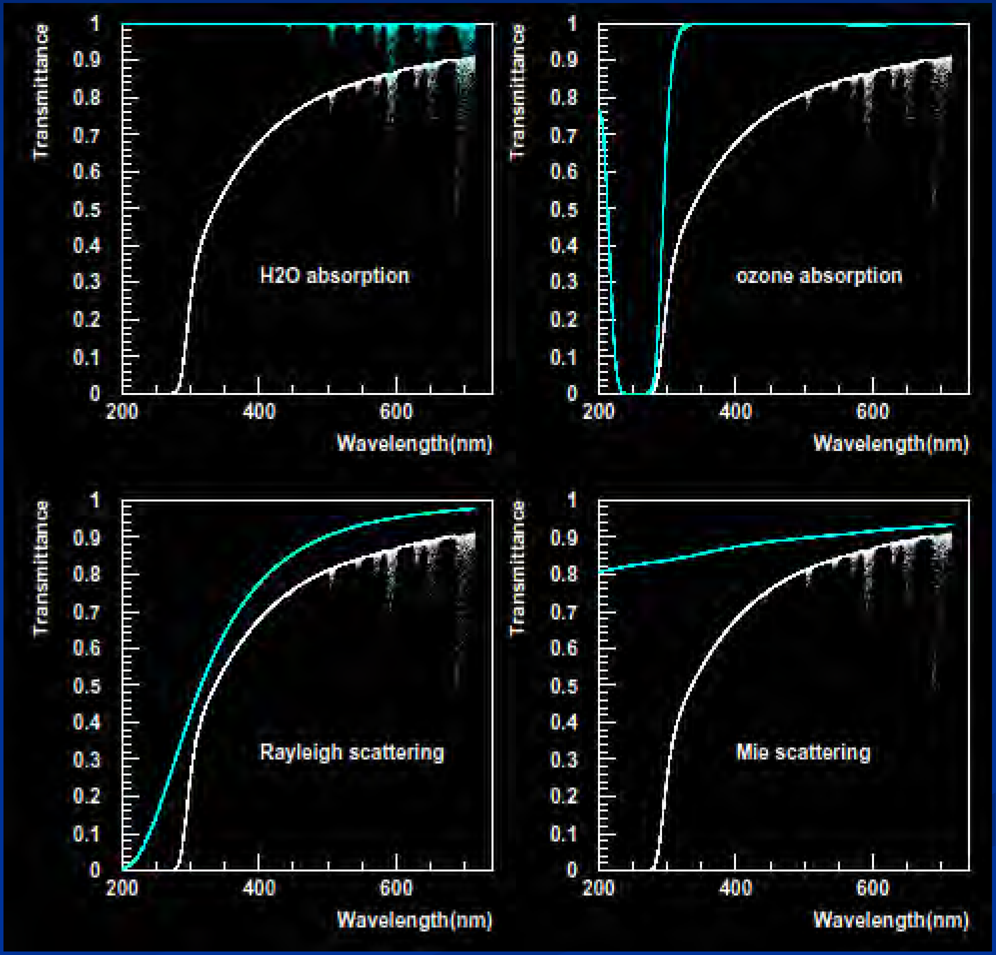

MODRAN4 calculation by H. Tsunoo (2002)

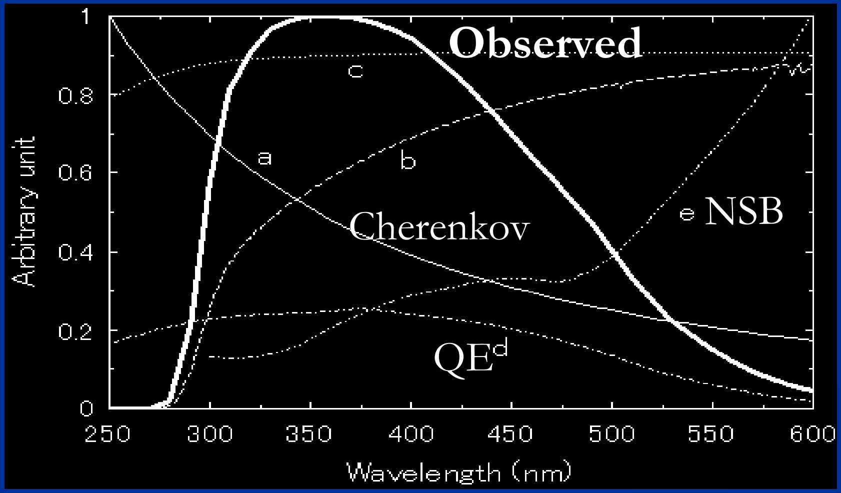

Imaging Cherenkov Telescopes

Shower profile

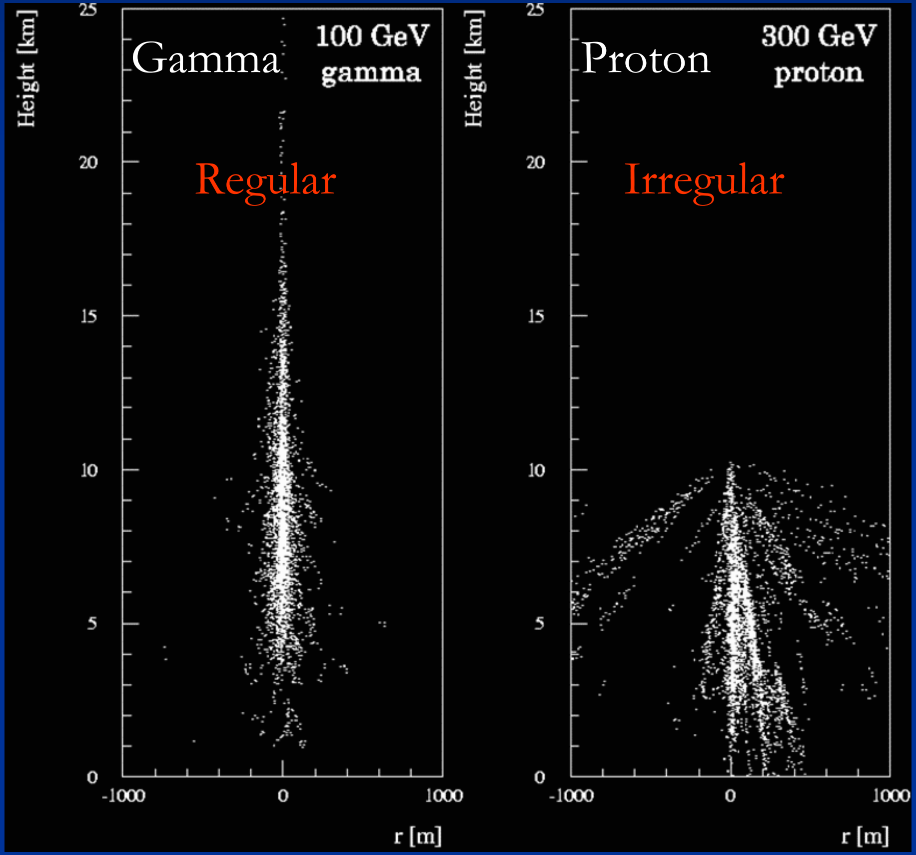

Focal plane image

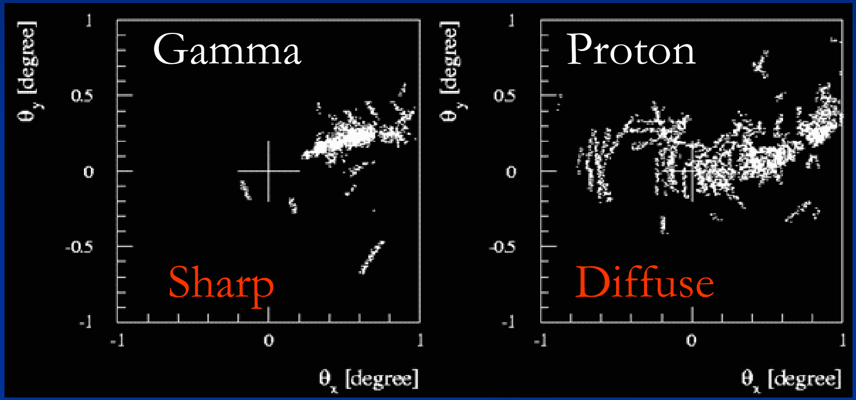

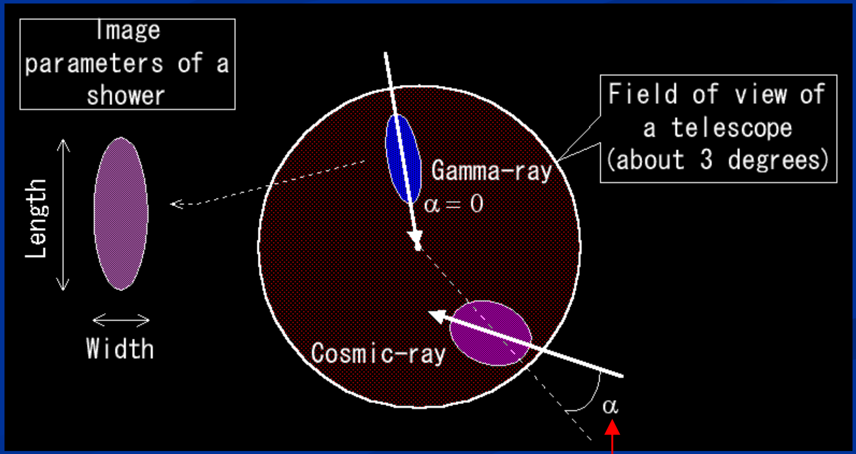

α (image orientation angle)

Imaging analysis

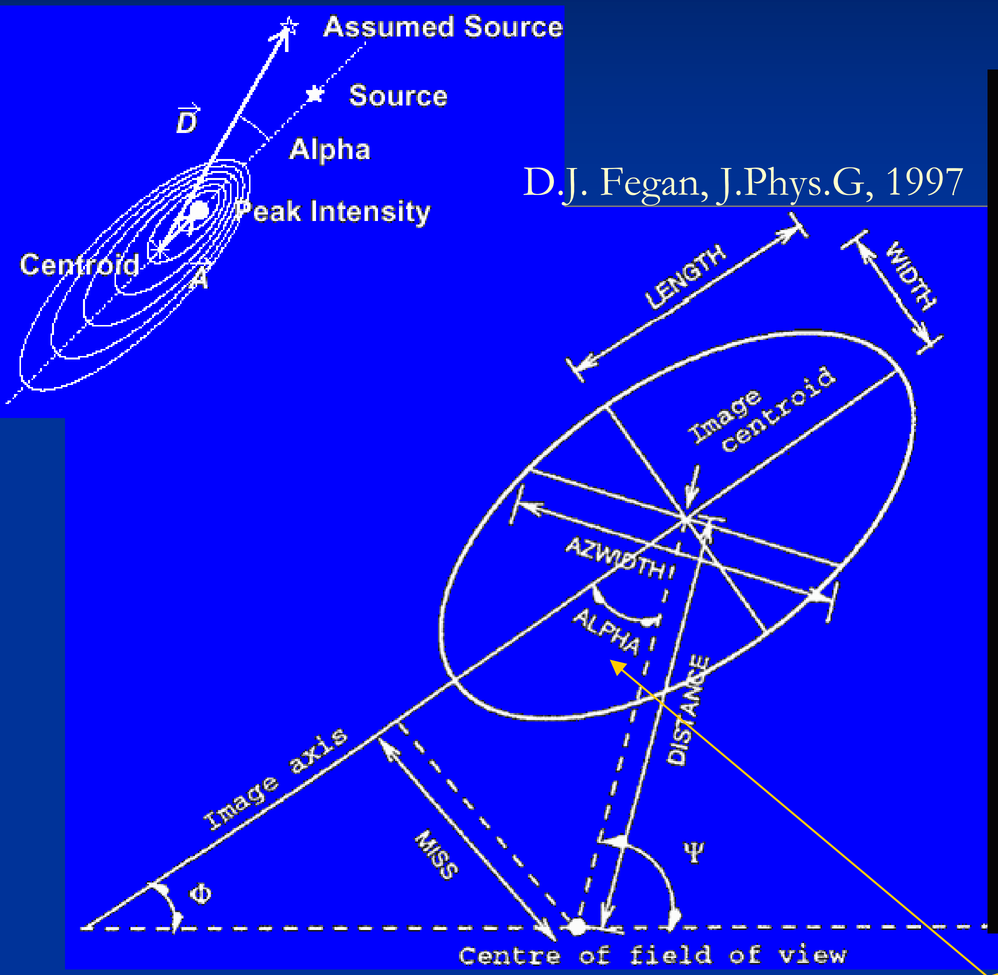

D.J. Fegan, J.Phys.G, 1997

Distribution of imaging parameters

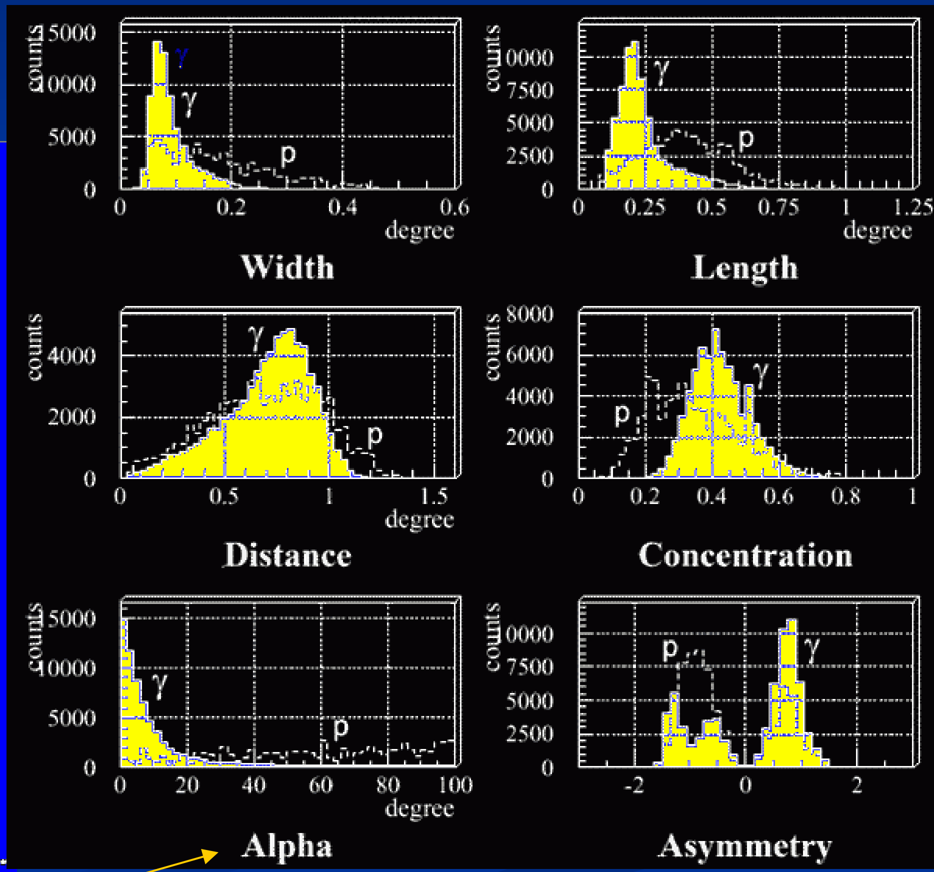

(Simulation)

α (image orientation angle)

"Image parameters": A.M. Hillas, 1983 ICRC

"Alpha": A.V.Plyasheshnikov and G.F.Bignami, N.C. 1985

WhippleによるCrabの検出

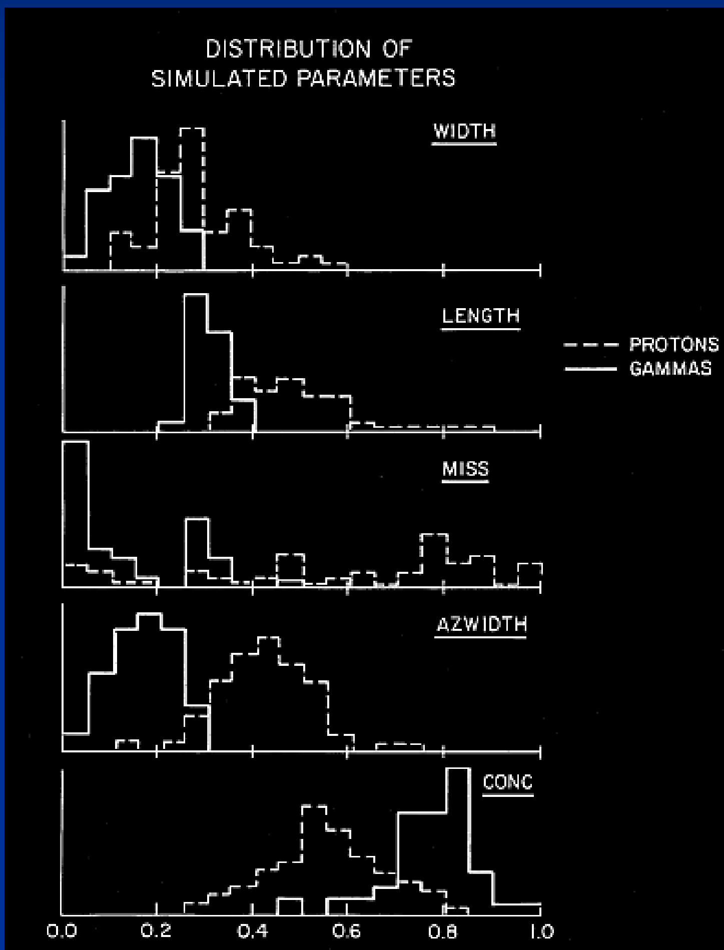

ガンマ線信号

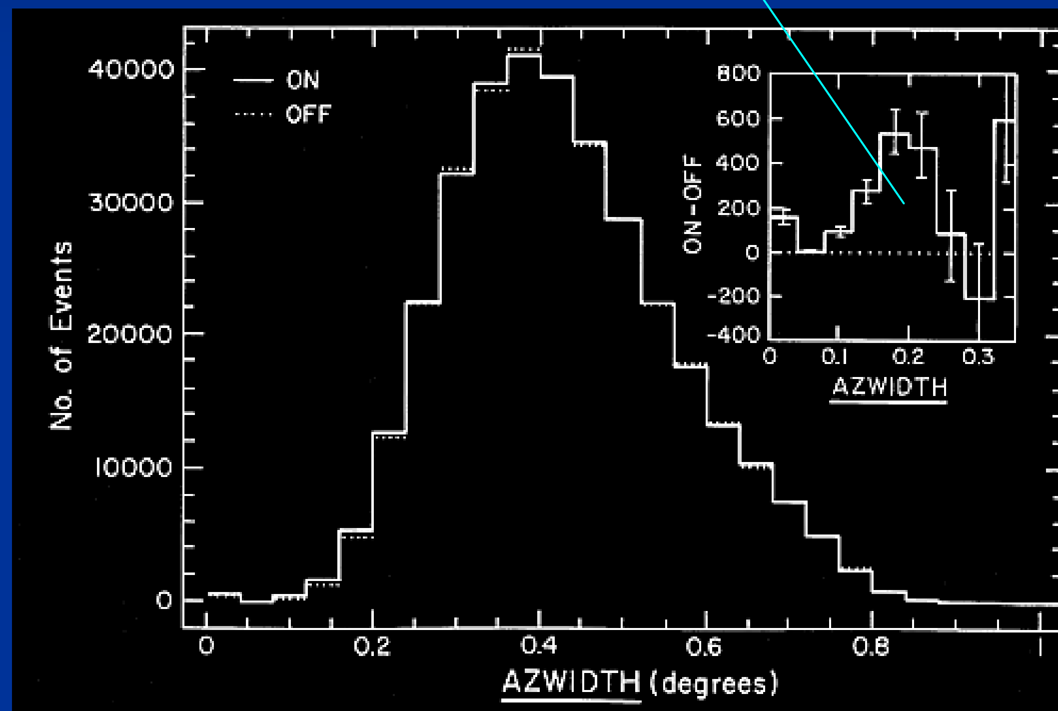

82hrs, 0.24γ/min

Weekes et al. ApJ 342 (1989) 349

WhippleによるMrk421の検出

ガンマ
線信号

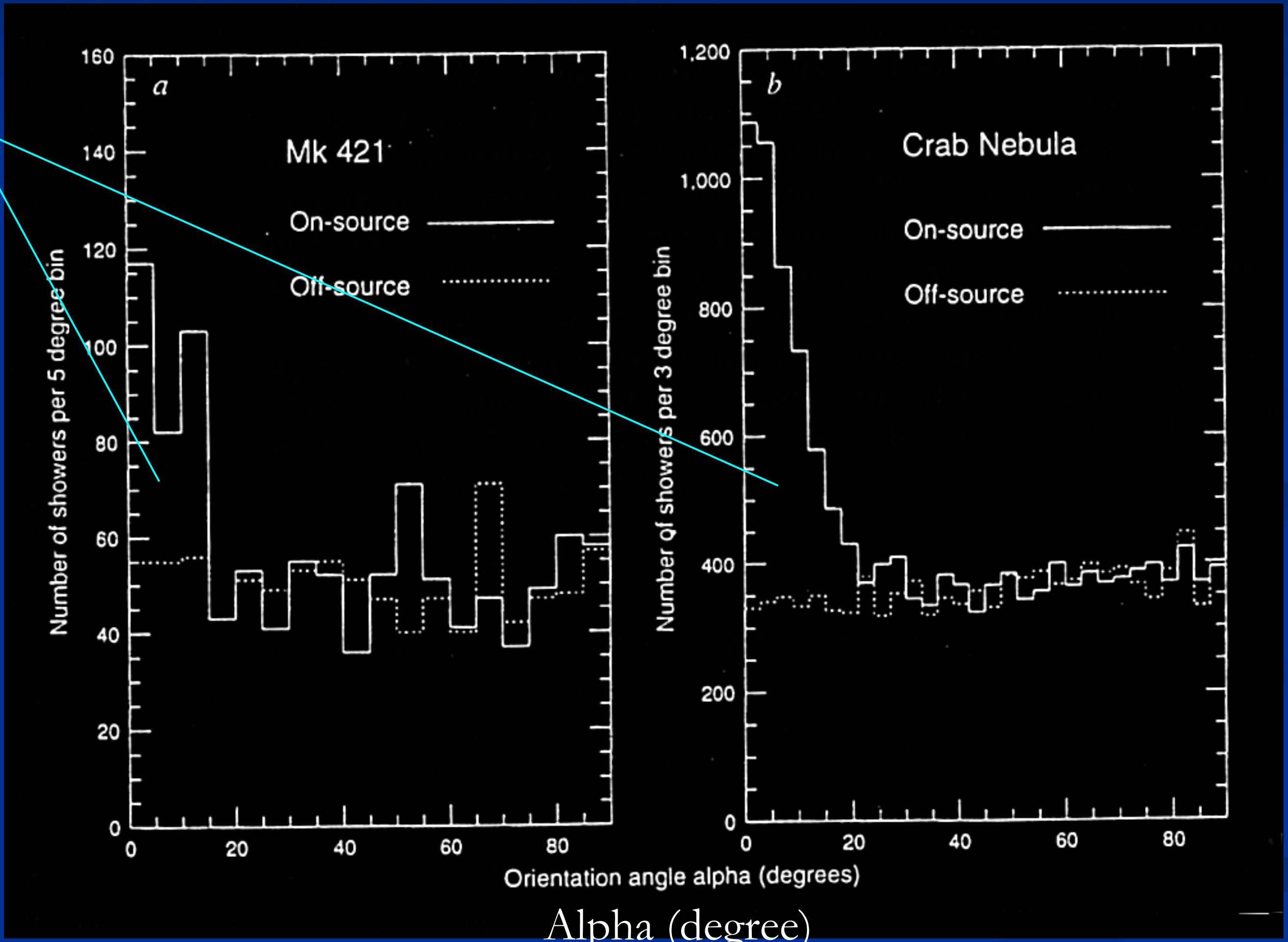

Alpha (degree)

Punch et al. Nature 358 (1992) 477

Stereo observation

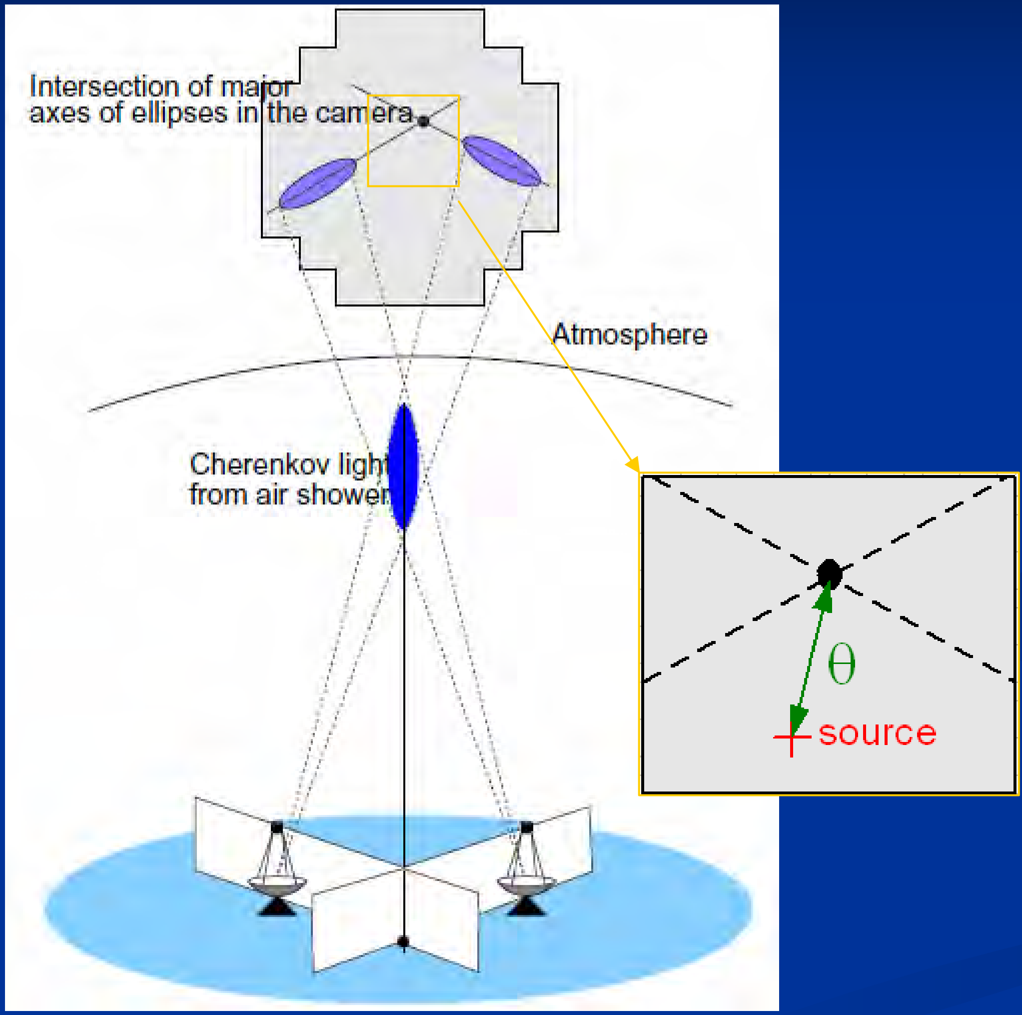

© S.Funk, 2005

Angular resolution

0.25deg → 0.1 deg

Energy resolution

30% → 15%

Better S/N (no local muons)

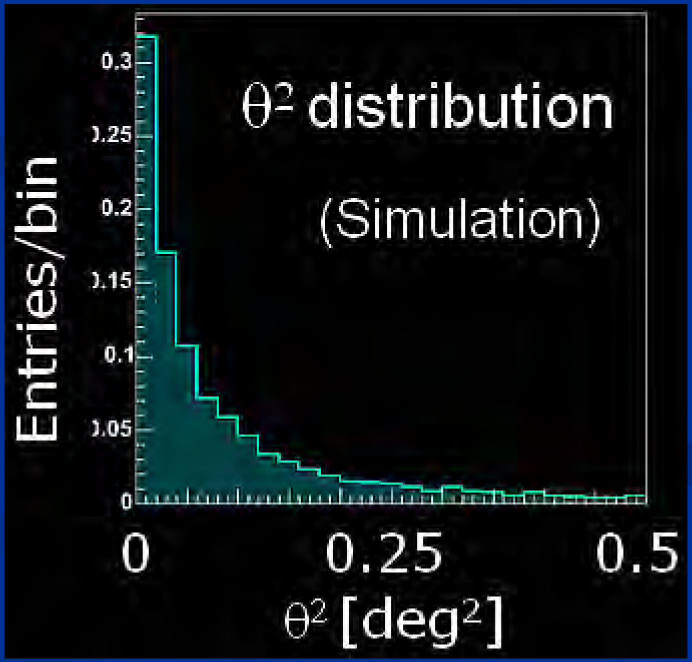

Detection of gamma-rays (2)

Base	Satellite	Ground	Ground
Gamma-ray detection	Direct (pair creation)	Indirect (atmospheric Cherenkov)	Indirect (shower array)
Energy	< 30 GeV (→ 100 GeV)	>100 GeV (→ 50 GeV)	>3 TeV (→ 1 TeV)
Pros	High S/N Large FOV	Large area Good $\Delta\theta$	24hr operation Large FOV
Cons	Small area High cost	Low S/N (CR bkgd.) *(but imaging overcomes this!)* Small FOV	Low S/N (CR bkgd.) Moderate $\Delta\theta$

Rene Ong, ICRC2005 OG2 rapporteur talk

Table 1. Currently operating VHE gamma-ray telescopes. The name of each telescope is given, along with its type (AC=Atmospheric Cherenkov), location, altitude, specifications, and reference at this meeting. The specifications list the currently installed detector area (mirror area for atmospheric Cherenkov and instrumented detector area for air shower). There is no reference at this meeting for the CACTUS telescope.

Experiment	Type	Location	Altitude	Specifications	Ref.
CACTUS	AC-Sampling	Barstow, USA	640 m	144 x 42 m^2	
CANGAROO-III	AC-Imaging	Woomera, Australia	165 m	4 x 57 m^2	[5]
HESS	AC-Imaging	Gamsberg, Namibia	1800 m	4 x 110 m^2	[6]
MAGIC	AC-Imaging	La Palma, Spain	2250 m	1 x 226 m^2	[7]
PACT	AC-Sampling	Pachmarhi, India	1075 m	25 x 4.5 m^2	[8]
SHALON	AC-Imaging	Tien Shan, Kazakhstan	3338 m	1 x 11 m^2	[9]
STACEE	AC-Sampling	Albuquerque, USA	1700 m	64 x 37 m^2	[10]
TACTIC	AC-Imaging	Mt. Abu, India	1400 m	1 x 9.5 m^2	[11]
VERITAS	AC-Imaging	Mt. Hopkins, USA	1275 m	2 x 110 m^2	[12]
Whipple	AC-Imaging	Mt. Hopkins, USA	2250 m	1 x 78 m^2	[13]
ARGO-YBJ	Air Shower	Yangbajing, Tibet	4300 m	4000 m^2	[14]
GRAPES-III	Air Shower	Ooty, India	2200 m	288 x 1 m^2	[15]
Milagro	Air Shower	Los Alamos, USA	2630 m	4800 m^2	[16]
Tibet	Air Shower	Yangbajing, Tibet	4300 m	761 x 0.5 m^2	[17]

H.E.S.S.

- 107 m² mirror area
  - 380 individual facets
- 15 m focal length
- 60 t structure
- Alt-Az mount

- 4 x 960 x 0.16° PMTs→ 5° field of view
- Integrated readout electronics
- 2-telescope coincidence

MAGIC-I & MAGIC-II

576-
pixel
Camera

17m diameter largest dish
High resolution camera
Ultra fast read out system 300M → 2GHz
Analogue signal fiber transmission

MAGIC-II is under construction and will be completed in the fall of the next year

CANGAROO-III

- Location:
  - 31°06'S, 136°47'E
  - 160m a.s.l.
- Telescope:
  - 114× 80cmϕ FRP mirrors (57m^2, Al surface)
  - 8m focal length
  - Alt-azimuth mount
- Camera:
  - T1: 552ch (2.7° FOV)
  - T2,T3,T4: 427ch (4° FOV)
- Electronics:
  - TDC+ADC

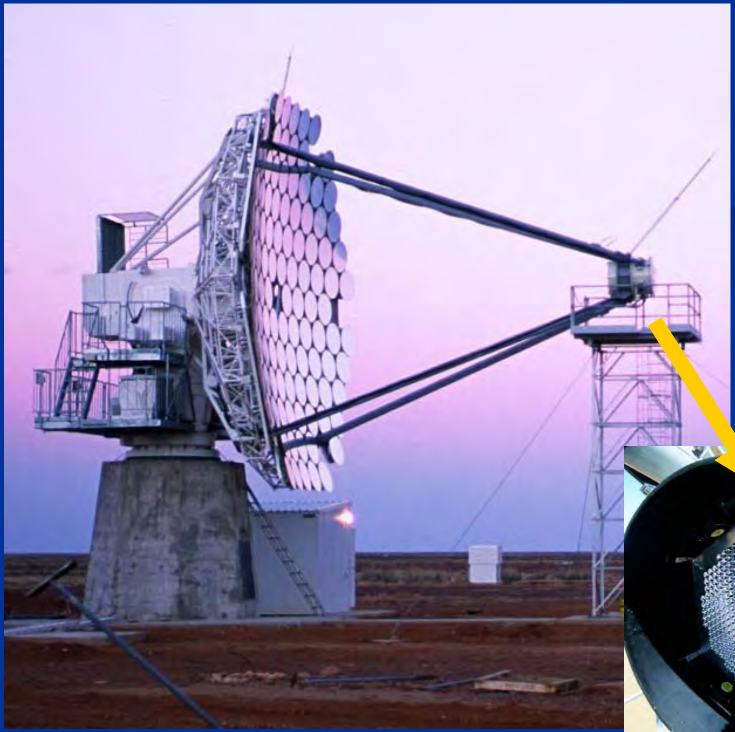

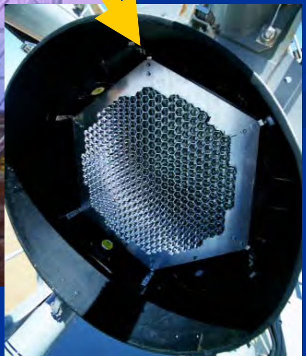

427-pixel Camera

Galactic sources: basics

- Supernova remnants = Origin of CR?
  - Energetics – OK (if 10% of E_{SN} goes to CR)
  - Maximum energy – Up to "Knee region"
  - How much of them?
  - Some evidences, which can be ascribed to HE electrons: where are HE protons?
- Pulsar and pulsar wind nebula (plerions)
  - Crab – "The standard candle"
    - Up to a few 10GeV: pulsed+unpulsed
    - Above: unpulsed only
    - - Unpulsed: SSC (Synchrotron-Self-Compton) model
    - - Where is the cutoff?
    - - (Pulsar emission models)
  - Others?

Particle acceleration in SNR

Non-linear kinetic theory

$t_0 = R_0/v_0$; sweep up time

Particle spectrum

Maximum momentum

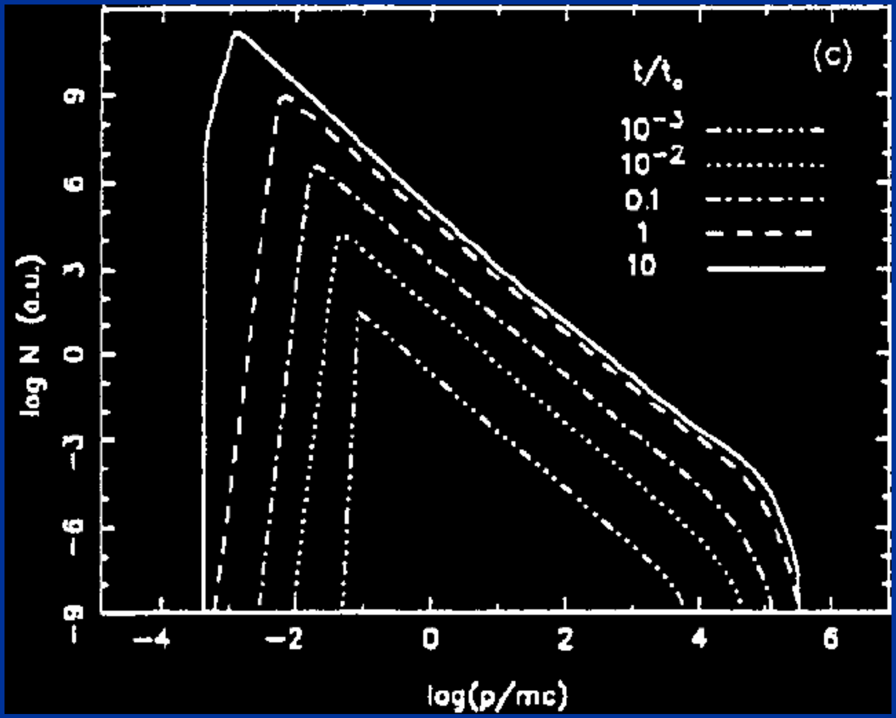

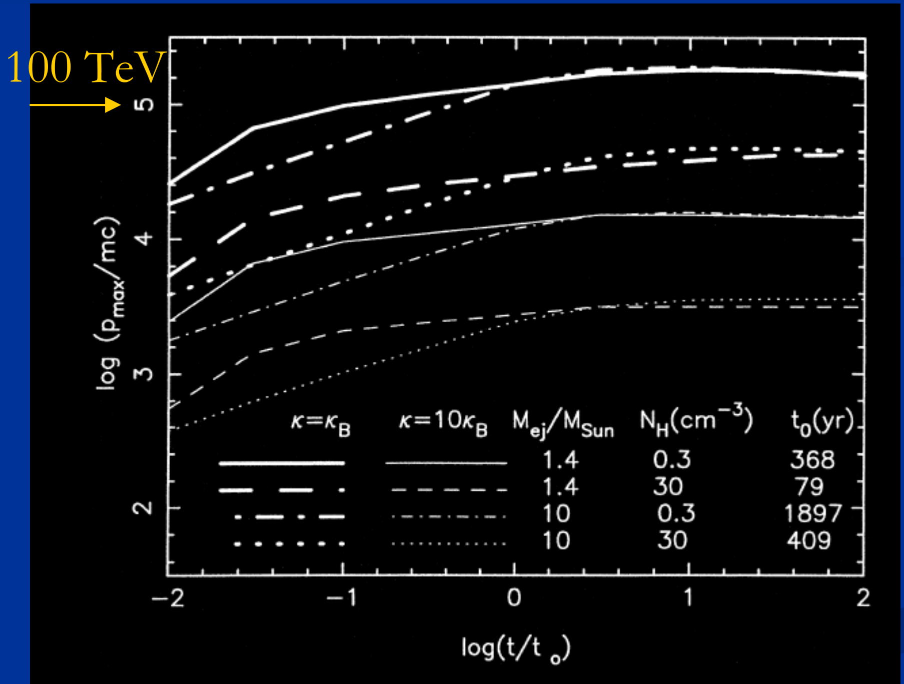

Fig. 2. The maximum CR momentum as a function of time for the same cases as in Fig. 1.

Berezhko & Voelk, APh 1997

Berezhko & Voelk, APh 2000

Cf. Lagage and Cesarsky 1984

Nuclear gamma-ray flux from SNR

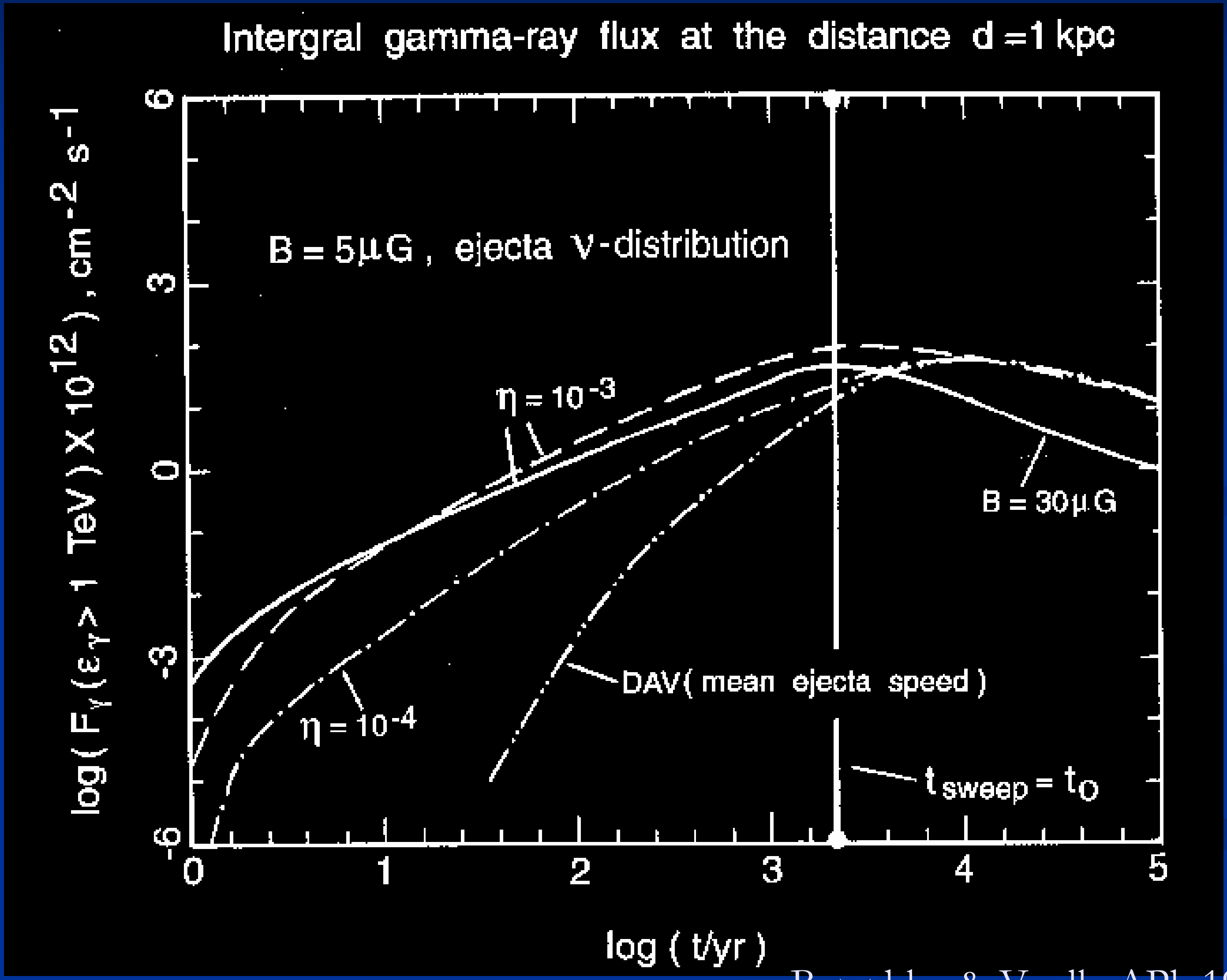

Berezhko & Voelk, APh 1997

Gamma-ray emission from SNR

n=10 cm^{-3}

n=1 cm^{-3}

n=0.1 cm^{-3}

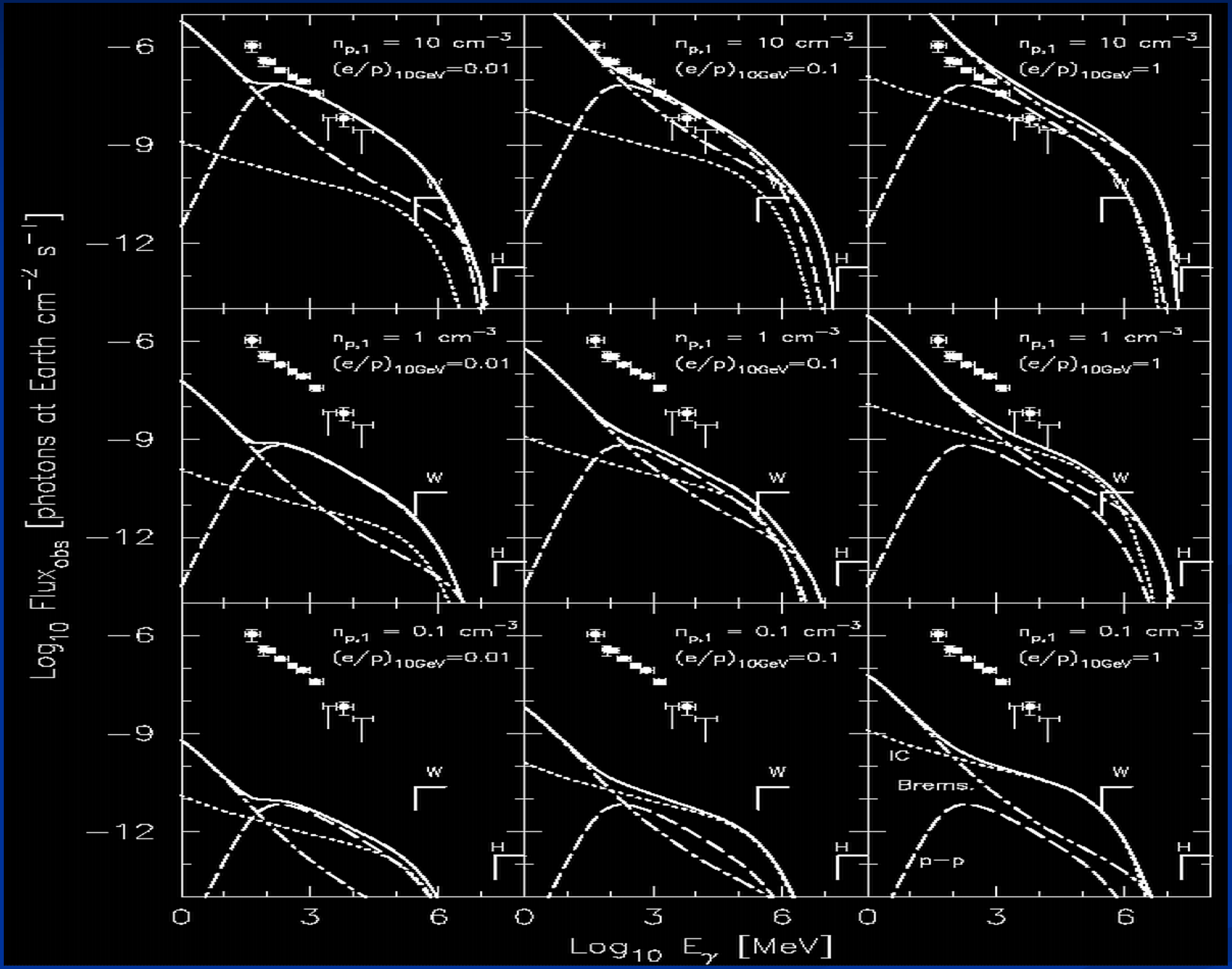

Dot: IC

Dash: π^0

Dot-dash:brems

(Data: EGRET IC443)

e/p = 0.01 0.1 1

Baring et al. 1999 ApJ 513, 311

Pulsar nebula

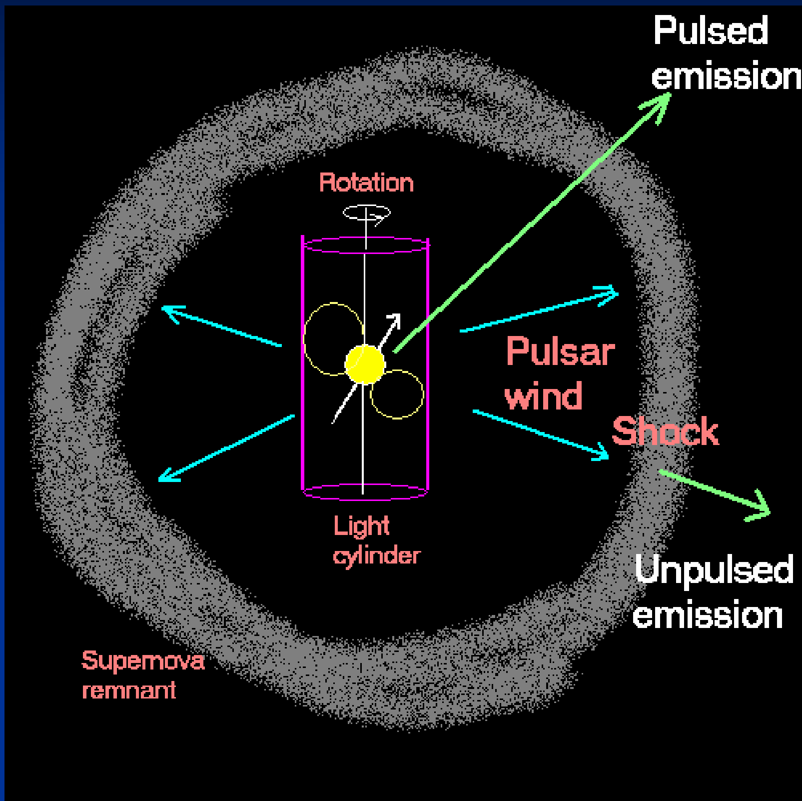

- A shock is formed when pulsar wind balances with ambient gas pressure, and the wind shines by synchrotron emission by thermalization

K.Mori, talk at ICRR, Dec 2003

The Crab

Inner ring
=
Shock front

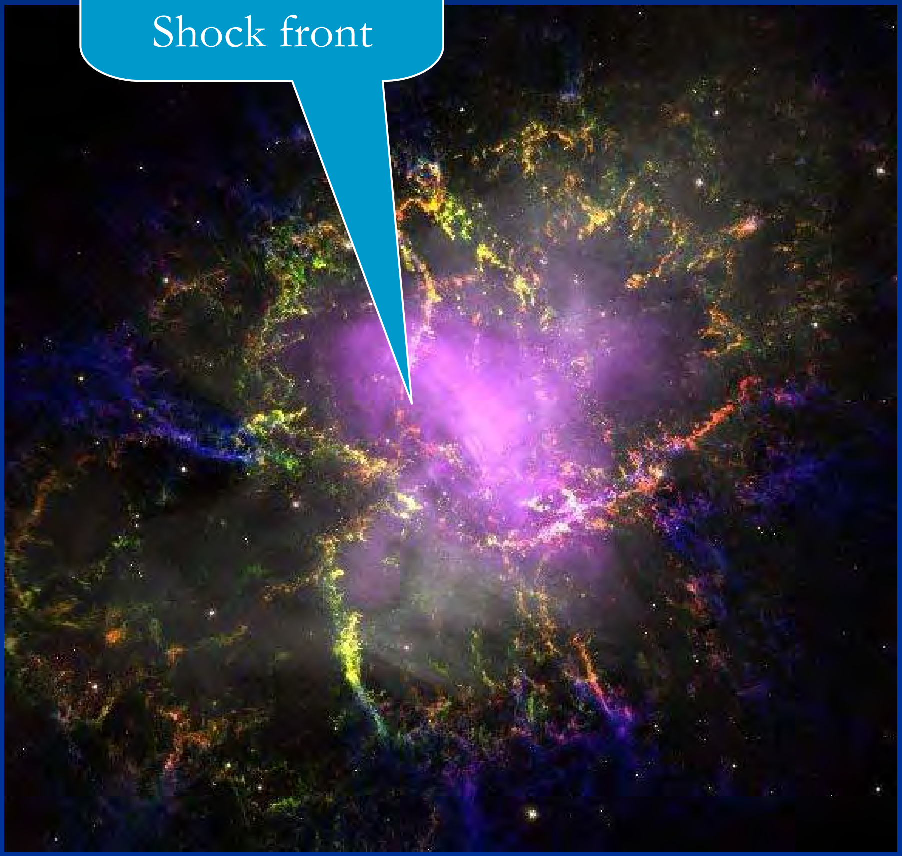

Optical + X-ray image

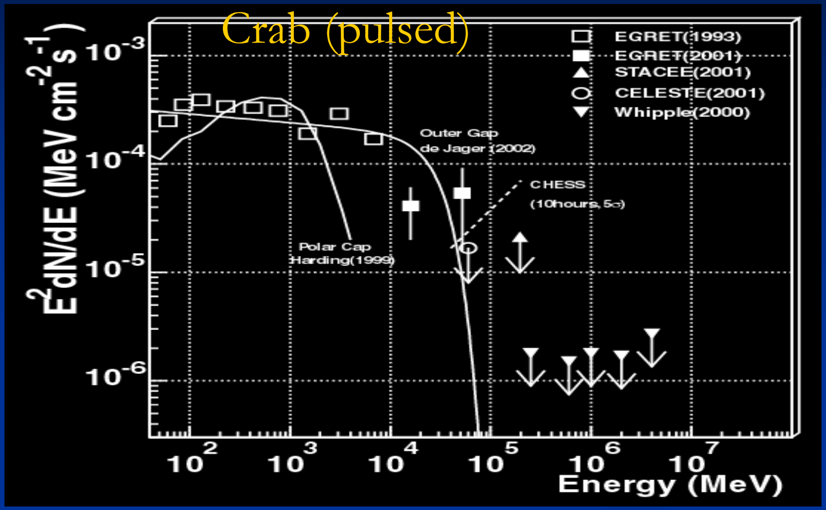

Synchrotron Self Compton

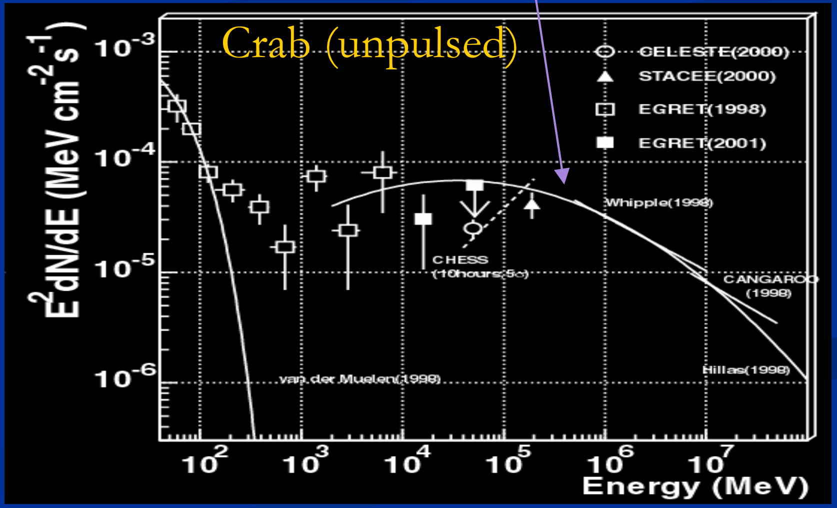

Asahara et al., SPIE 2002

"Known" galactic sources: Supernova remnants

- **Crab** "The standard candle"
  - Well established (many observations since 1989)
- Supernova remnant **RX J1713.7-3946**
  - CANGAROO 2000/2002, H.E.S.S. 2004
- Supernova remnant **Cas A**
  - HEGRA CT system 2001
- Supernova remnant **RX J0852.0-4622**
  - CANGAROO 2005, H.E.S.S. 2005
- Supernova remnant **G0.9+0.1** [H.E.S.S. 2005]
- Supernova remnant **Vela X** [H.E.S.S. 2006, CANGAROO 2006]
- Possible SNRs: G338.3-0.0, G8.7-0.1, G18.0-0.7, G23.3-0.3, G25.5+0.0, AX J1813-178 [H.E.S.S. 2005]
- Pulsar PSR 1706-44, Vela pulsar, SN1006
  - CANGAROO-I claims, but H.E.S.S. upper limits

SNR RX J1713.7-3946 (1)

- Detected in X-rays
- Non-thermal X-ray spectrum

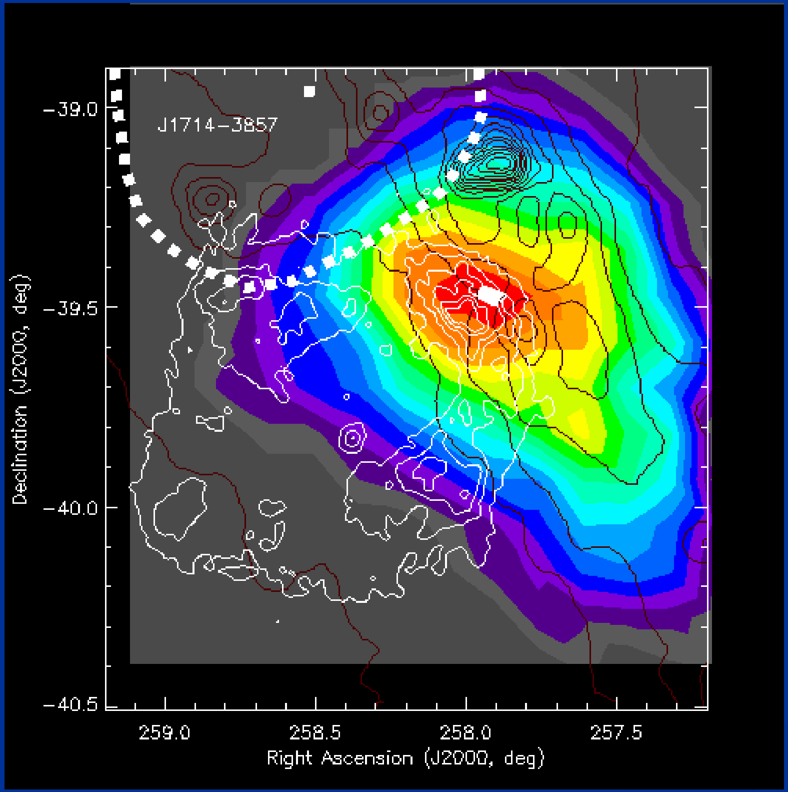

Significance map

Gamma-ray signal = (ON) – (OFF)

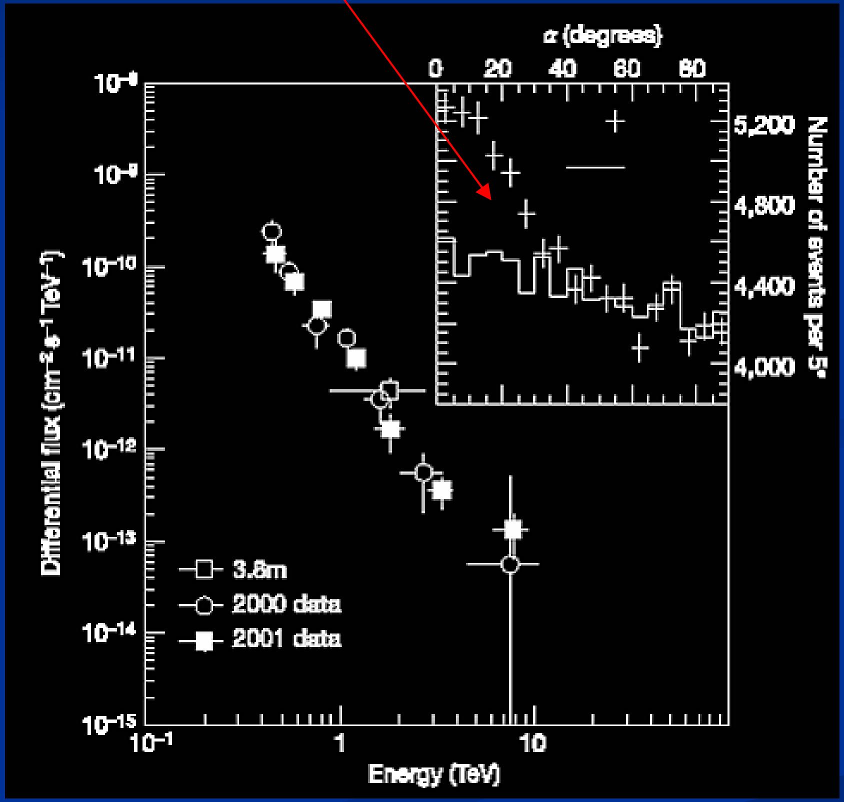

Energy spectrum

Enomoto et al. Nature 416 (2002) 823

SNR RX J1713.7-3946 (2)

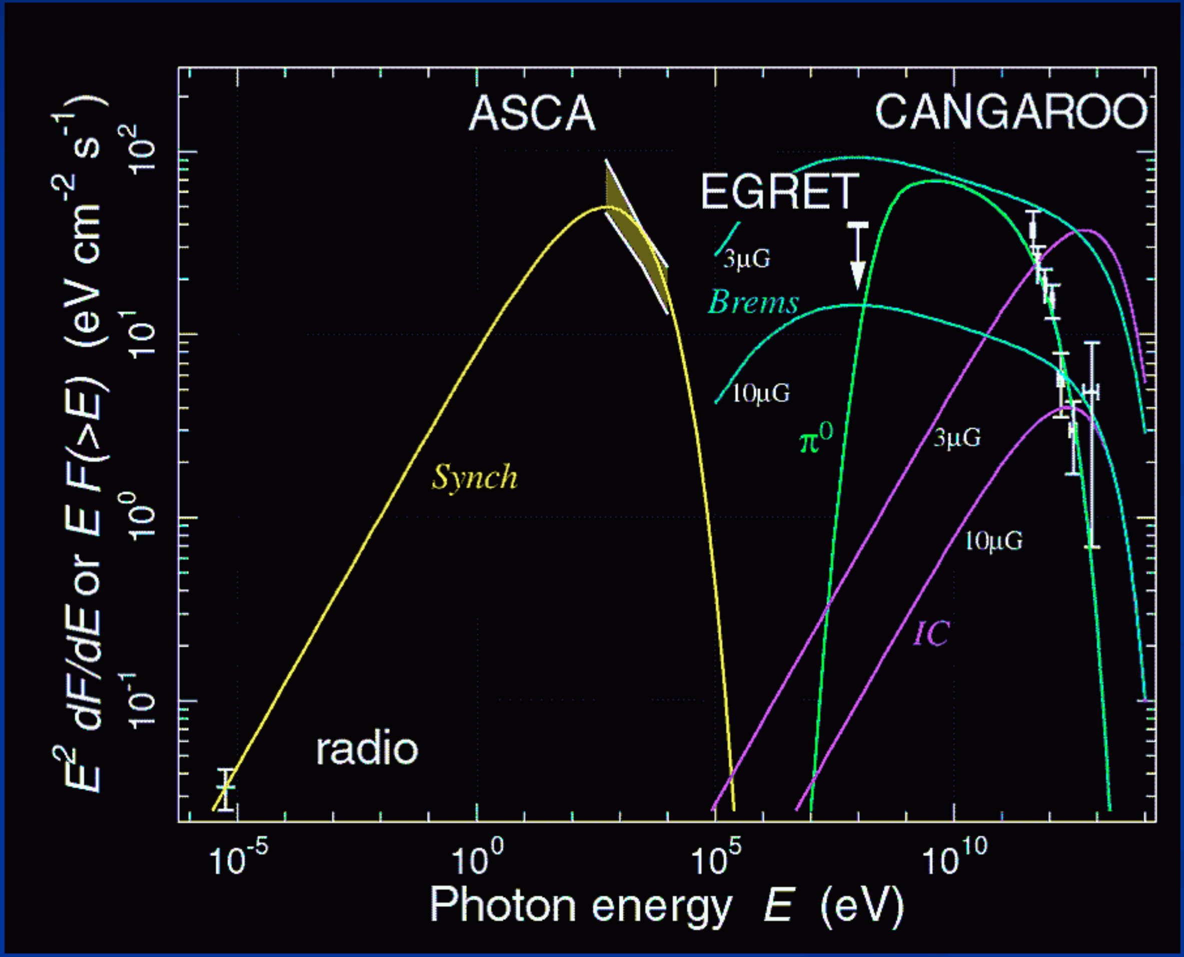

Enomoto et al. Nature 416 (2002) 823

Hard to explain by emission from electrons (Brems, IC)

⇒Emission from protons (π^0)?

⇒ Cosmic ray origin?

NANTEN results :

Distance ~ 1 kpc

Age ~ 1600yr

→ L_p~10^{48}erg ~ $0.001 L_{SN}$

(Fukui et al. PASJ 55, 2003)

SNR RX J1713.7-3946 (3)

Counter arguments

* Reimer & Pohl, A&A 390 (2002) L43

* Butt et al., Nature 418 (2002) 489

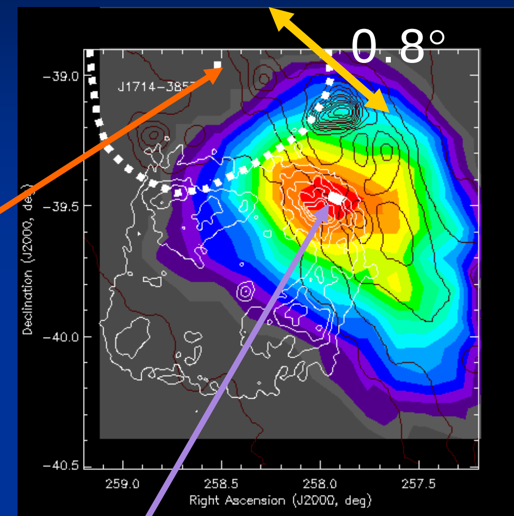

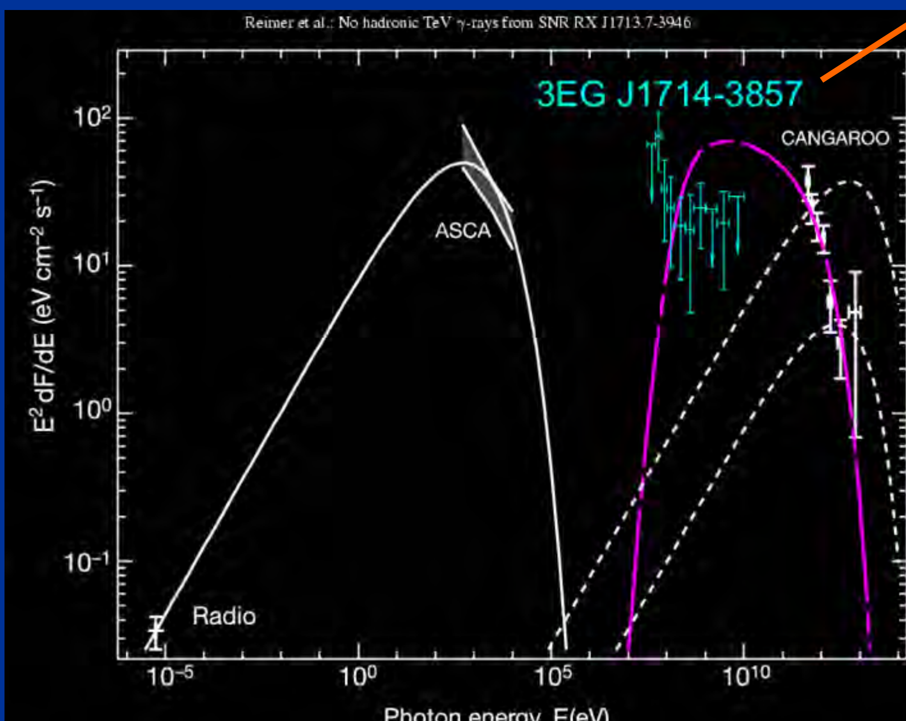

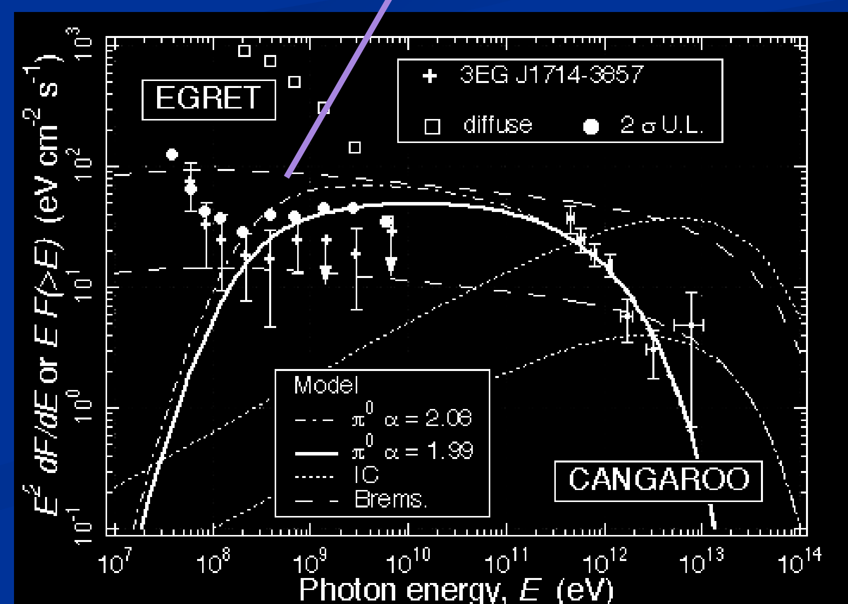

H.E.S.S.: Aharonian et al., A&A 449, 223 (2006)

SNR RX J1713.7-3946 (4)

F. Aharonian et al.: The γ-ray supernova remnant RX J1713.7−3946 9

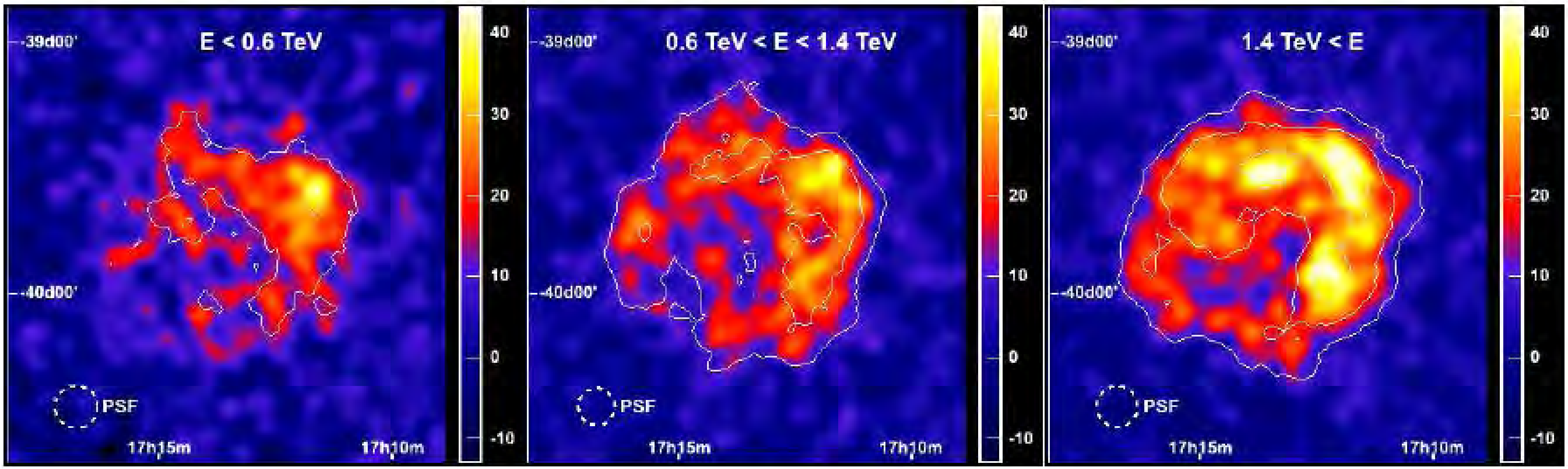

Fig. 9. Morphology of RX J1713.7−3946 as it appears at different energies. Shown from left to right are gamma-ray excess images with energies of $E < 0.6$ TeV, 0.6 TeV $< E <$ 1.4 TeV, and 1.4 TeV $< E$. Drawn additionally as white lines are contours of significance, linearly spaced at 5, 10, 15σ (as in Fig. 7). Note the increase in the signal-to-noise ratio with increasing energy. The energy bands were chosen such that each band represents about a third of the full data set (taking events after cuts). Furthermore, all three images were smoothed with a Gaussian of 2′, which makes them directly comparable to each other, and to Fig. 7. The resolution in each energy band is indicated in the lower left hand corner of the images; the three data subsets have comparable resolutions of $\approx 0.08°$ (the resolution of the intermediate energy band is about 6% better). This might be counter-intuitive, given that at larger energies camera images get bigger and fluctuation effects become negligible thereby improving the energy and direction resolution. However, in this case that effect is compensated by the increasing mean zenith angle of the large-energy events.

H.E.S.S.: Aharonian et al., A&A 449, 223 (2006)

SNR RX J1713.7-3946 (5)

CO

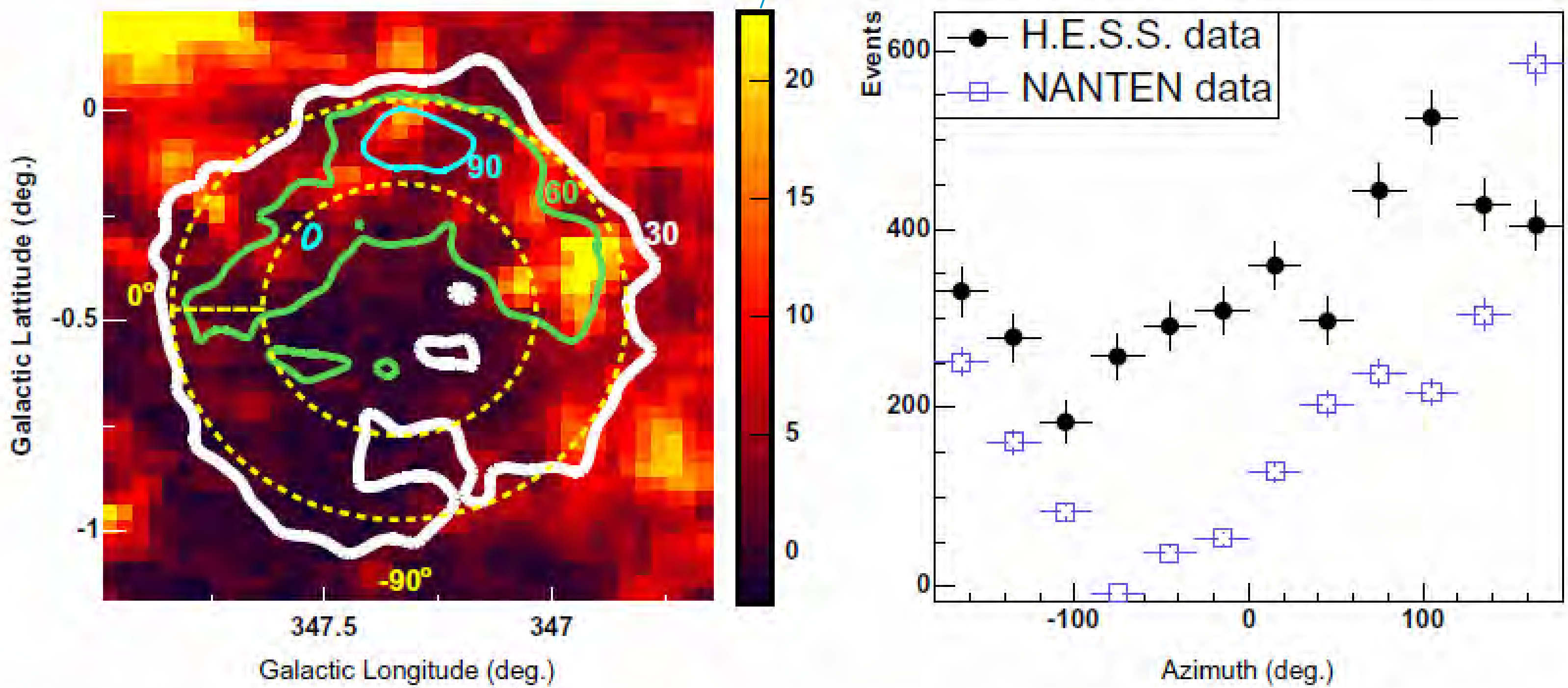

Fig. 17. Left panel: Shown are the intensity distribution of CO ($J = 1-0$) emission (Fukui et al. 2003) (linear colour scale in units of K km s^{-1}, truncated at a value of 23 to highlight important features), derived by integrating the CO spectra in the velocity range from −11 km s^{-1} to −3 km s^{-1} (which corresponds to 0.4 kpc to 1.5 kpc in space). Overlaid are coloured contours of the H.E.S.S. gamma-ray excess image. The levels are labelled and linearly spaced at 30, 60, and 90 counts. Note that the image is shown in Galactic coordinates. **Right panel:** Azimuth profile plot, that is, number of counts as a function of the azimuthal angle, integrated in a 0.2°-wide ring covering the shell of RX J1713.7−3946 (dashed yellow circle in the left-hand panel). Plotted are the H.E.S.S. gamma-ray and the NANTEN data set.

H.E.S.S.: Aharonian et al., A&A 449, 223 (2006)

SNR RX J1713.7-3946 (6)

Electron origin model

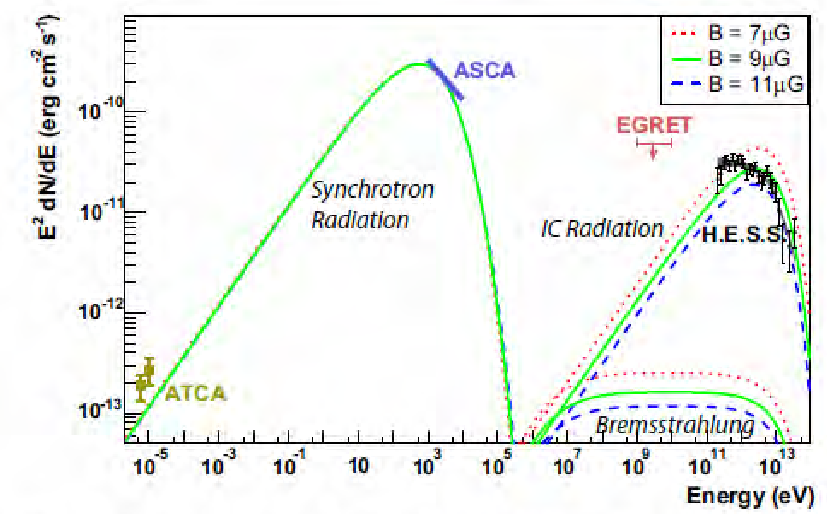

Fig. 19. Broadband SED of RX J1713.7−3946. The ATCA radio data and ASCA X-ray data (Hiraga 2005) for the whole SNR are indicated, along with the H.E.S.S. measurement and the EGRET upper limit. Note that the radio flux was determined in Lazendic et al. (2004) for the northwest part of the shell only and was scaled up by a factor of two here to account for the whole SNR. The synchrotron and IC spectra were modelled assuming a source distance of 1 kpc, an age T of 1000 years, a density n of 1 cm^{-3}, and a production rate of relativistic electrons by the acceleration mechanism in the form of a power law of index $\alpha = 2$ and an exponential cutoff of $E_0 = 100$ TeV. Shown are three curves for three values of the mean magnetic field: 7 μG, 9 μG, and 11 μG, to demonstrate the required range of the B field strength for this scenario. The electron luminosity is adopted such that the observed X-ray flux level is well matched. For the three magnetic field values the luminosity L_e is $L_e = 1.77 \times 10^{37}$ erg s^{-1} (7 μG), $L_e = 1.14 \times 10^{37}$ erg s^{-1} (9 μG), and $L_e = 0.81 \times 10^{37}$ erg s^{-1} (11 μG).

Proton origin model

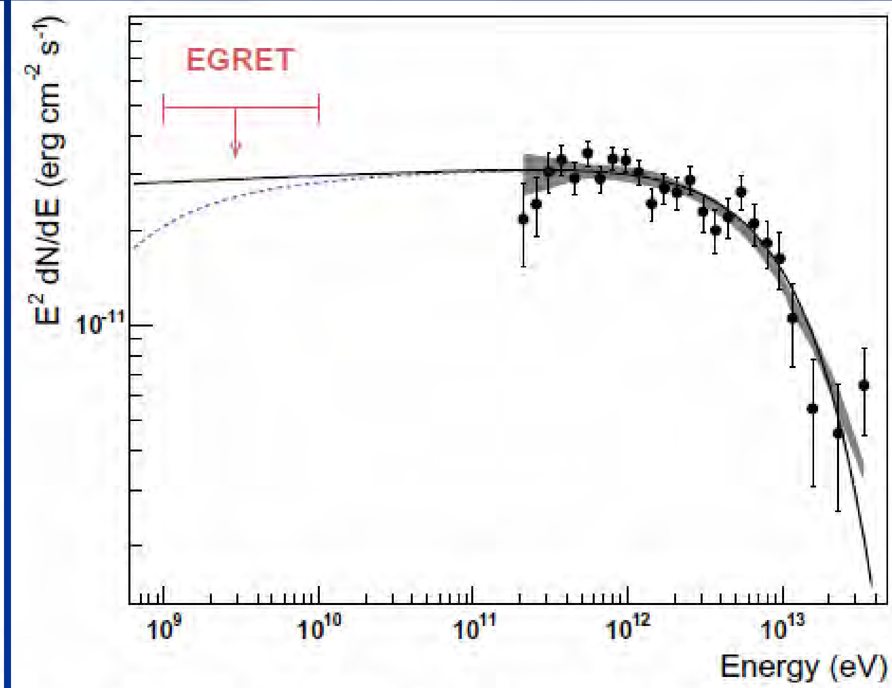

Fig. 20. H.E.S.S. data points plotted in an energy flux diagram. They shaded grey band is the systematic error band for this measurement (see Sect. 3.2). The black curve is the best fit of a power law with exponential cutoff to the data, extrapolated to lower energies. The dashed blue curves is the same function, but it takes the π^0 kinematics into account. The EGRET upper limit from 1 GeV to 10 GeV is plotted as red arrow.

$\Rightarrow$ Protons favored (?)

H.E.S.S.: Aharonian et al., A&A 449, 223 (2006)

SNR RX J1713.7-3946 (7)

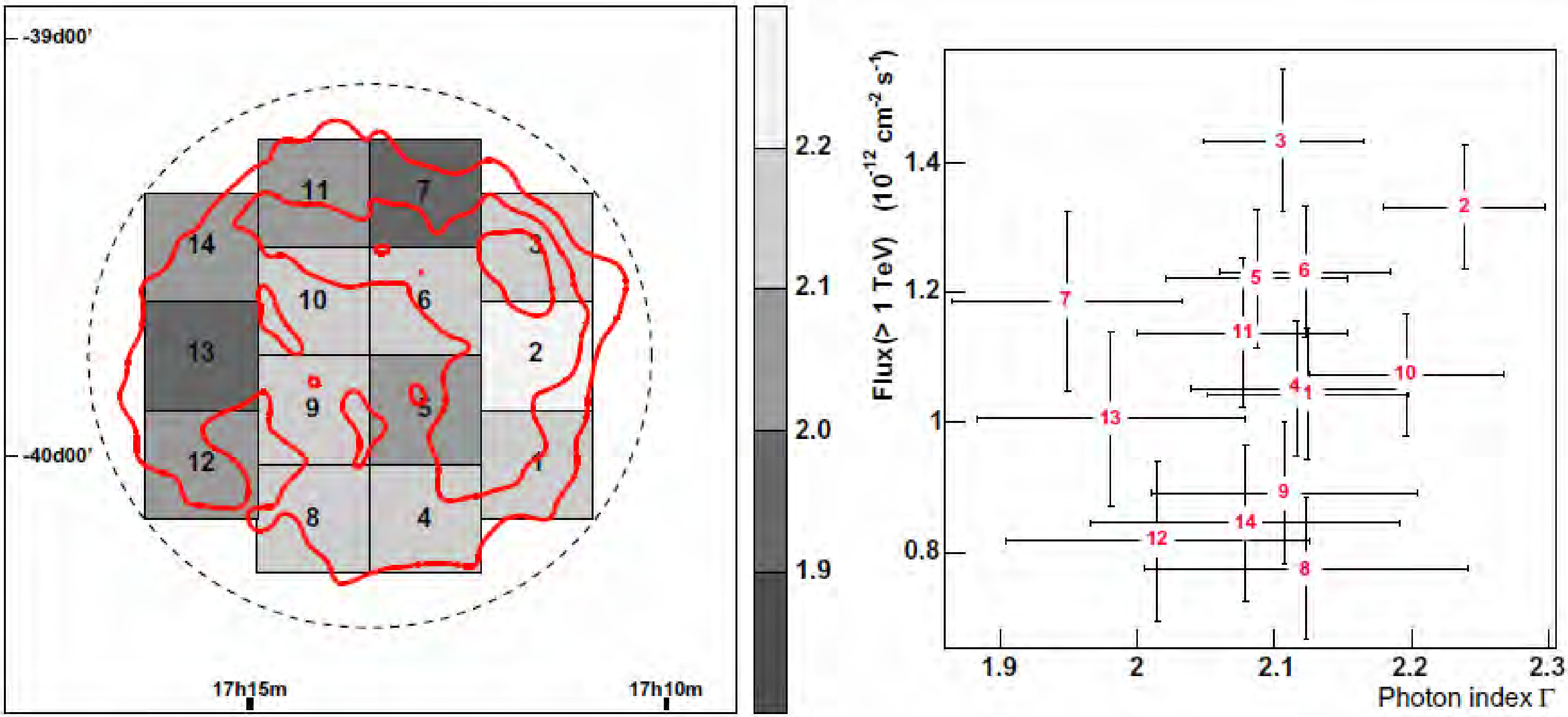

Fig. 14. The image illustrates the results of the spatially resolved spectral analysis. **Left part:** Shown in red are gamma-ray excess contours from Fig. 7, linearly spaced at 30, 60, and 90 counts. Superimposed are the 14 boxes (each $0.26° \times 0.26°$ in dimension) for which spectra were obtained independently. The dashed line is the 0.65° radius circle that was used to integrate events to produce a spectrum of the whole SNR. The photon index obtained from a power-law fit in each region is colour coded in bins of 0.1. The ranges of the fits to the spectra have been restricted to a maximum of 8 TeV (see Table 2). **Right part:** Plotted is the integral flux above 1 TeV against the photon index, for the 14 regions the SNR was sub-divided in. The error bars are $\pm 1\sigma$ statistical errors. Note that systematic errors of 25% on the flux and 0.1 on the photon index are to be assigned to each data point additionally.

B. Aschenbach, Nature, 396, 141 (1998)

SNR RX J0852.0-4622 [G266.2-1.2, Vela Jr.](1)

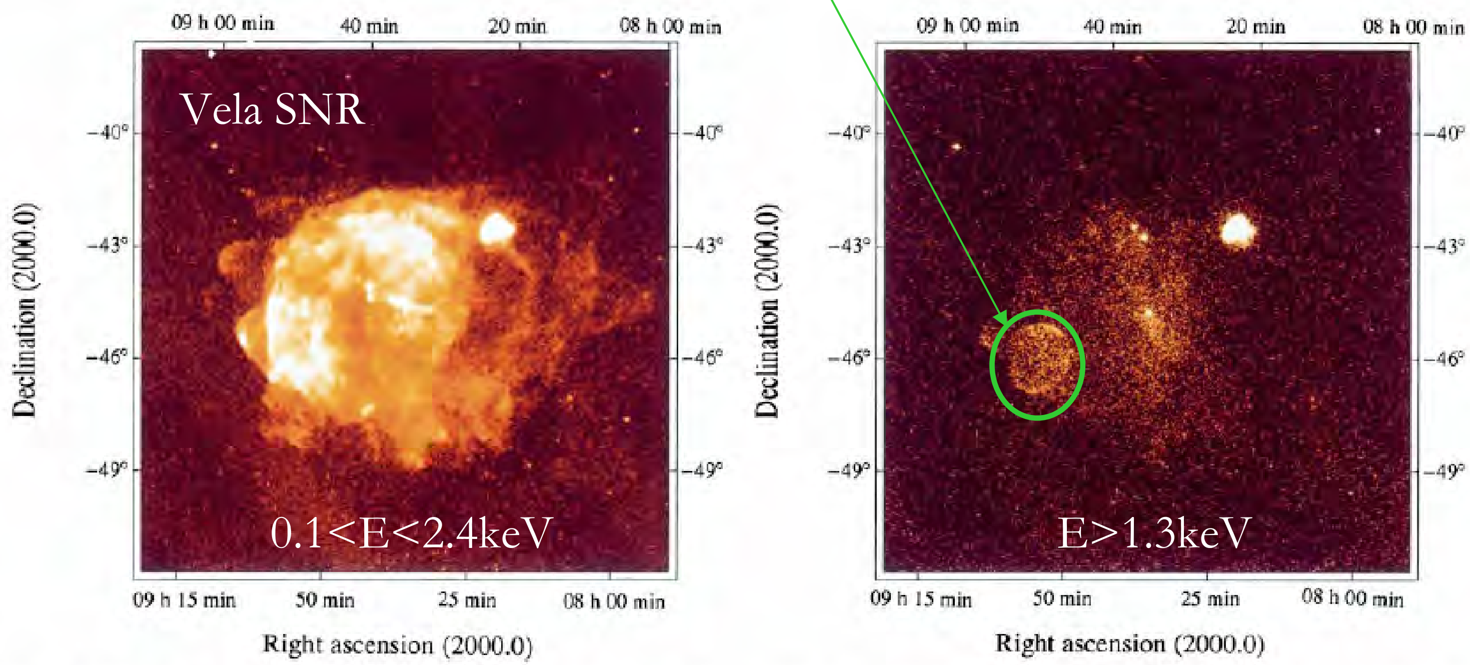

Figure 1 Rosat all-sky survey images of the Vela SNR and its surroundings. Angular resolution is 1 arcmin half-power radius; mean exposure is 993 s. The left-hand image was taken for photon energies $0.1 < E < 2.4$ keV; surface brightness increases from dark yellow to white by a factor of 500. The right-hand image is for photon energies >1.3 keV. Most of the Vela SNR X-ray emission which dominates at low energies had disappeared. At the centre, the synchrotron nebula around the Vela pulsar remains visible as well as the SSW beam-like structure, and at the very northwest (upper right) the bright Puppis-A SNR can be seen. The new shell-type SNR RX J0852.0 − 4622 shows up in the lower left. East of RX J0852.0 − 4622 hard X-ray photons from the D/D′ Vela SNR shrapnels are seen which, however, are associated with a much lower-temperature spectrum than RX J0852.0 − 4622 (ref. 14). For X-ray spectral analysis, RX J0852.0 − 4622 was divided into two regions, one containing the bright northern limb section (l) and the other one (r) excluding the northern and southern limbs. Spectral fits were performed with either power-law models, optically thin thermal emission equilibrium models (Raymond-Smith models) or combinations of both. Solutions with a reduced $\chi^2 < 1$ for region r are obtained only with a two-temperature model with $kT_{r,1} = 0.14^{+0.08}_{-0.03}$ keV, $kT_{r,2} = 2.5^{+4.5}_{-0.7}$ keV. The spectrum of the northern limb can be fitted by either a simple power law with index $\alpha = -2.6^{+0.3}_{-0.4}$ or a two-temperature model with $kT_{l,1} = 0.21^{+0.14}_{-0.09}$ keV, $kT_{l,2} = 4.7^{+4.5}_{-0.7}$ keV. The presence of low-temperature components may partially be due to a residual, uncorrected contribution from the much softer Vela SNR. The total, absorption-corrected flux of the high-temperature components is $F_x(0.1\text{–}2.4\,\text{keV}) = 3 \times 10^{-10}$ erg cm^{-2} s^{-1}.

SNR RX J0852.0-4622 (2)

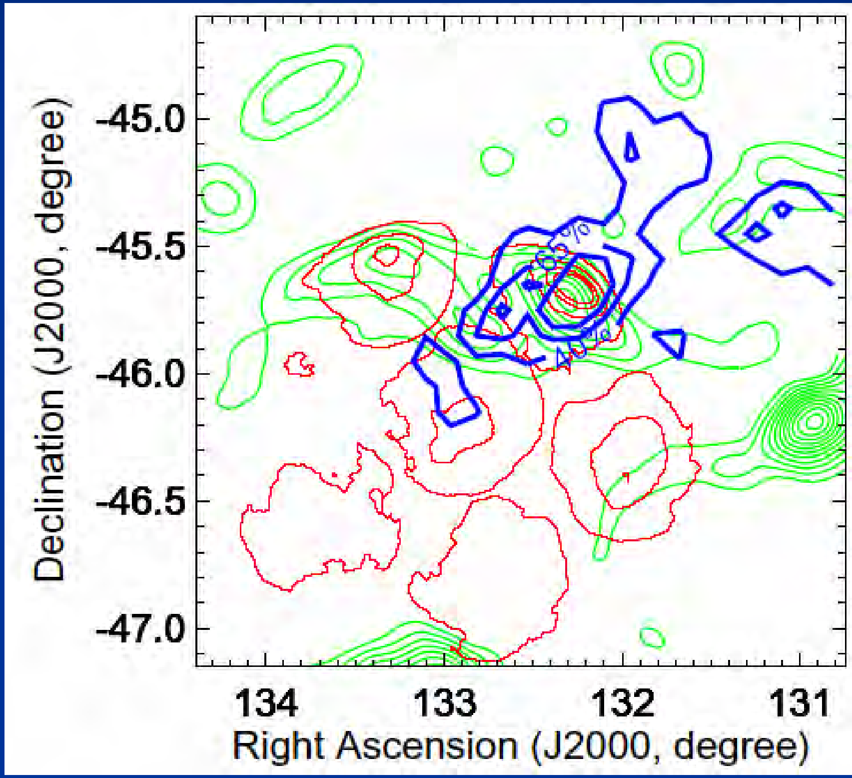

CANGAROO-II: Katagiri et al., ApJ, 619, (2005) L163

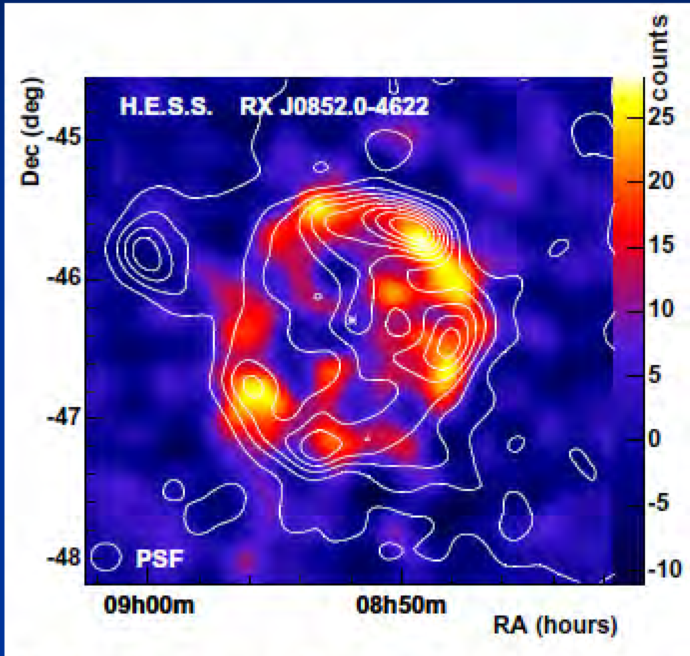

Fig. 2. Count map of γ-rays from the direction of RX J0852.0−4622 after background subtraction. The data are smoothed with a Gaussian ($\sigma = 0.1°$) representing the angular resolution of the instrument. The point spread function (PSF) is indicated by a circle. γ-ray features smaller than the PSF should not be considered as real. The lines denote equidistant contours of smoothed ($\sigma = 0.1°$) X-ray data from the ROSAT All Sky Survey, with energies restricted to above 1.3 keV. The position of the neutron star candidate AX J0851.9−4617.4 is marked with an asterisk. The axes show J2000.0 equatorial co-ordinates.

H.E.S.S.: Aharonian et al., AA 437, L7 (2005)

SNR RX J0852.0-4622 (3)

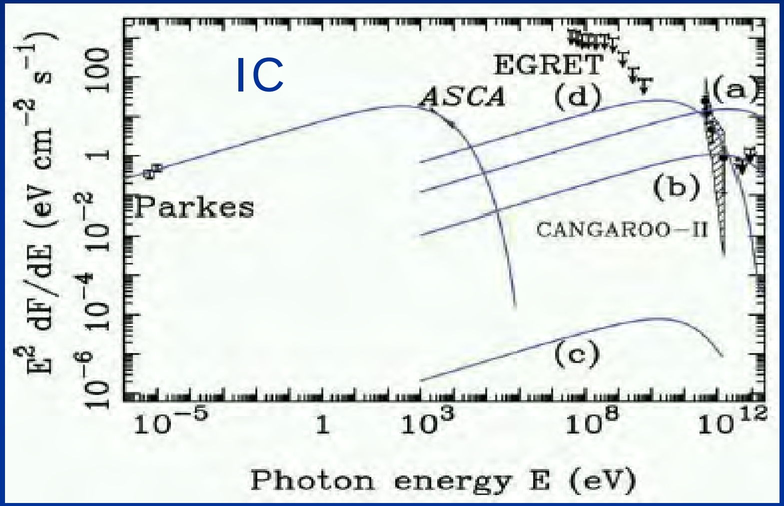

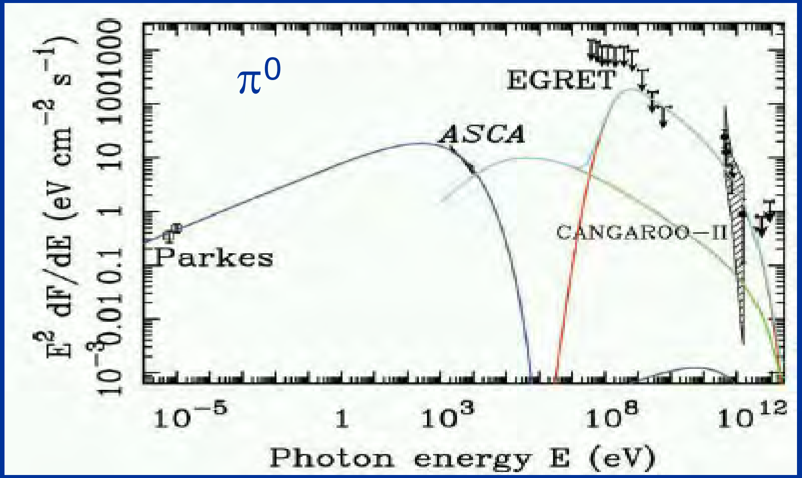

CANGAROO-II: Katagiri et al., ApJ, 619, (2005) L163

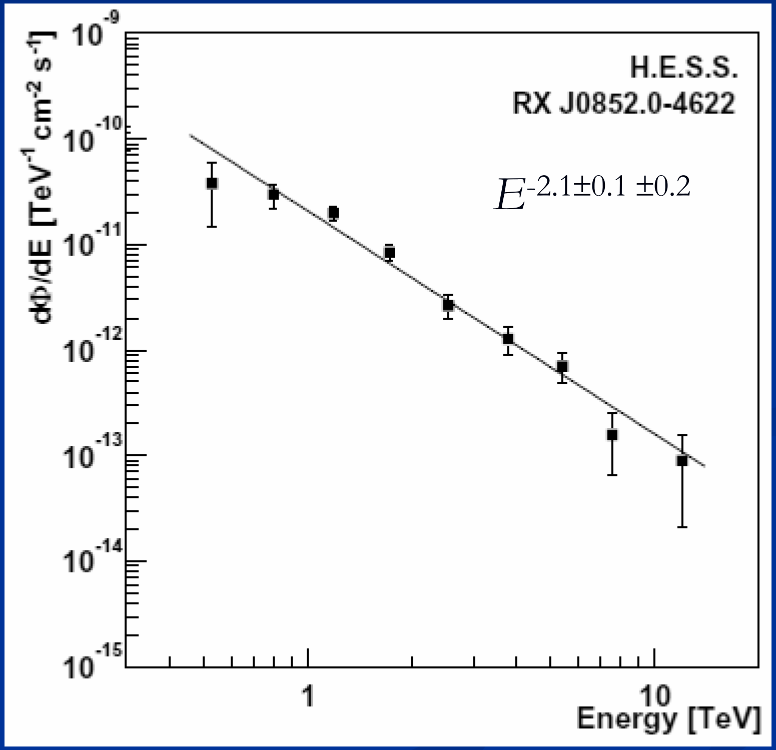

H.E.S.S.: Aharonian et al., AA 437, L7 (2005)

R. Enomoto et al., in press

SNR RX J0852.0-4622 (4)

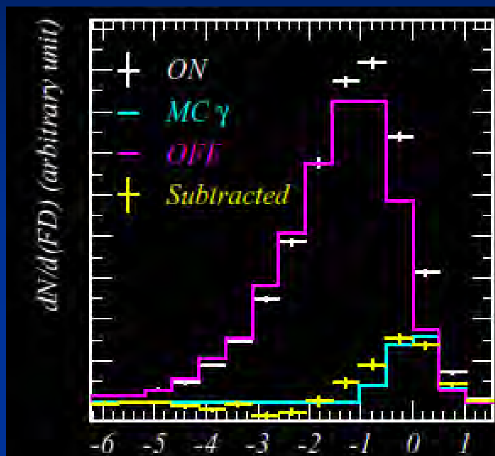

Fisher discriminant

- Distance ~1 kpc
  (NANTEN: Moriguchi et al. ApJ 2005)
- Stereo (T2 & T3 &T4 wobble)
- 1,129 min. ON, 1,081 min OFF
  (2005 Jan/Feb)
- Independent analysis (ICRR, Kyoto)

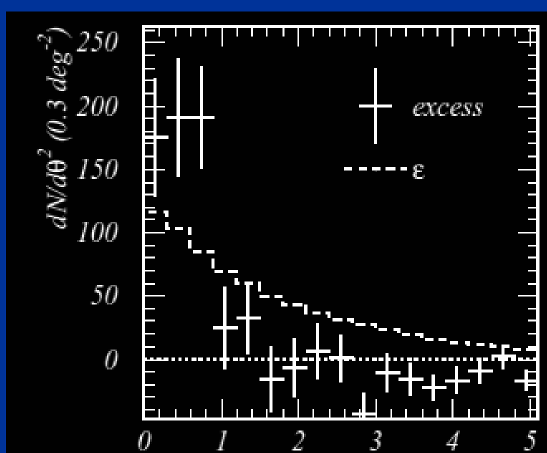

θ^2 from SNR center

Excess event map

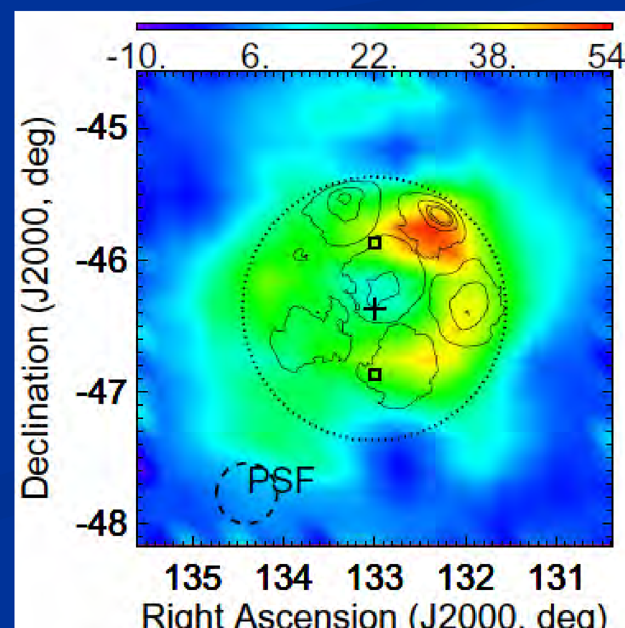

R. Enomoto et al., in press

SNR RX J0852.0-4622 (5)

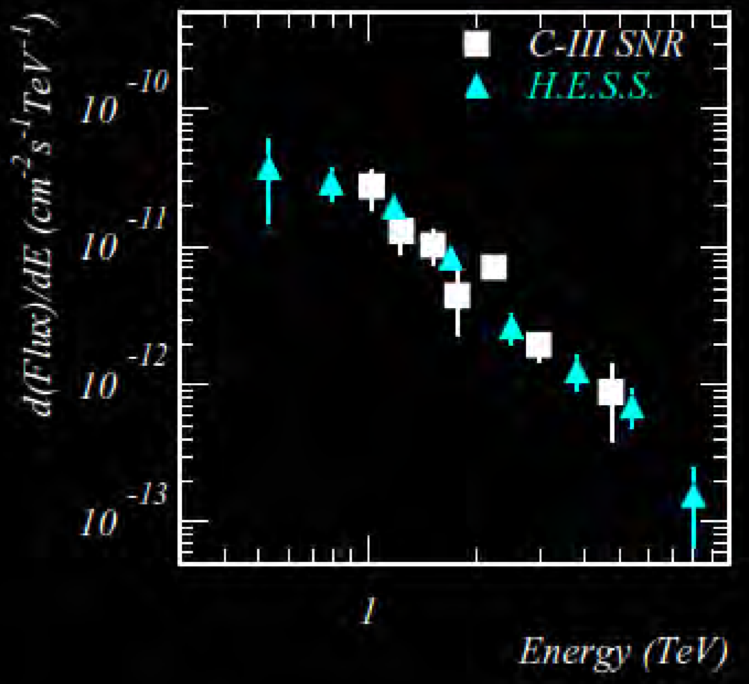

FIG. 7.— Differential energy spectra; the red points by H.E.S.S. are for the whole remnant and the black points from these CANGAROO-III observations are also for the whole remnant. The error bars are statistical.

$$\frac{dF}{dE} = [2.5 \pm 0.6(stat.) \pm 0.6(sys.)] \times 10^{-11} \cdot \left(\frac{E}{1\ \mathrm{TeV}}\right)^{2.2\pm0.3(stat.)\pm0.3(sys.)} [\mathrm{cm}^{-2}\mathrm{s}^{-1}\mathrm{TeV}^{-1}]$$

Comparison with C-II

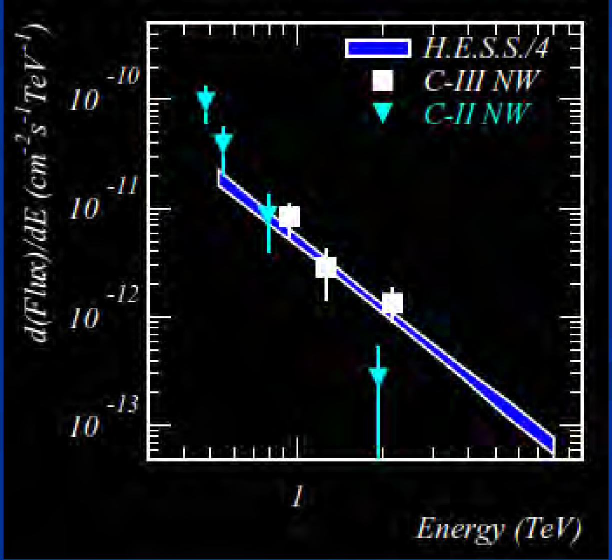

H.E.S.S.: Aharonian et al., A&A 432, L25 (2005)

SNR G0.9+0.1

- Compatible with a point source
- Position compatible with the PWN position
- Emission not consistent with the SNR shell

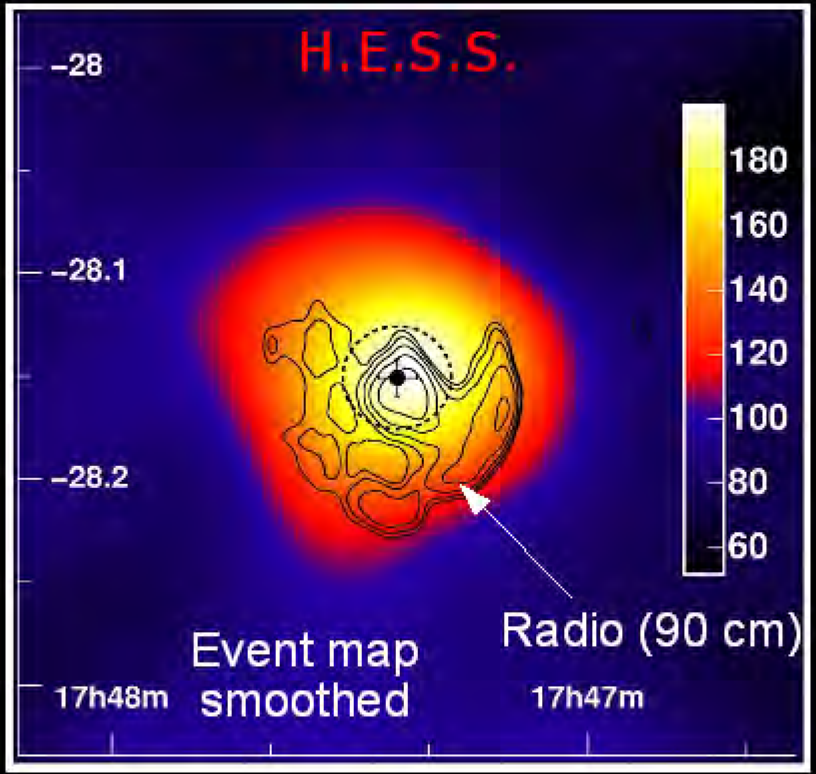

- Composite SNR, but no detected PSR

XMM (1.5-12 keV)
Porquet *et al.*, 2003

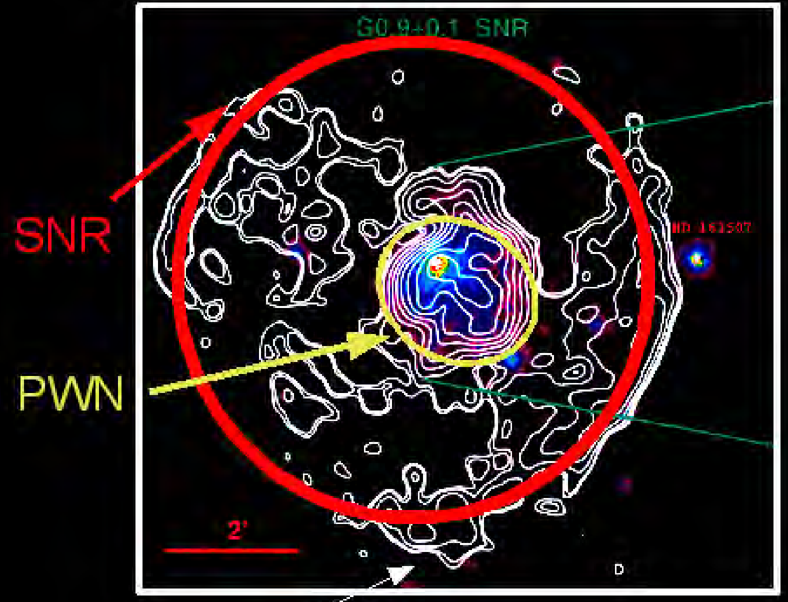

Radio contours (λ=20cm)
Helfand *et al.*, 1987

Aharonian et al., ApJ 636, 777 (2005)

H.E.S.S. Galactic plane survey

230 hr, 500 pointings

14 new TeV sources + 3 known

Scale height

~ 0.3deg RMS

~ molecular gas

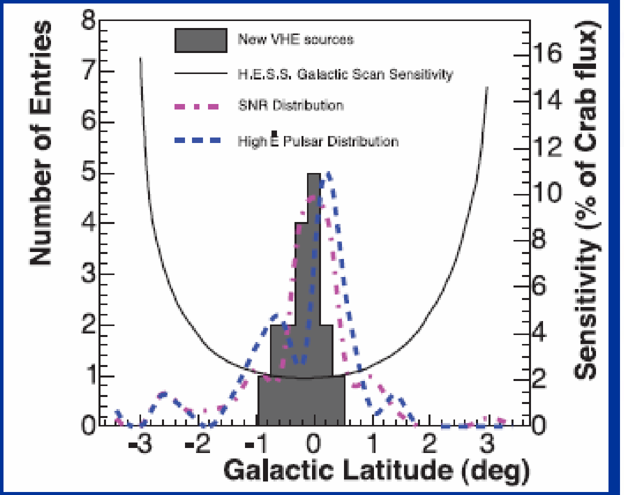

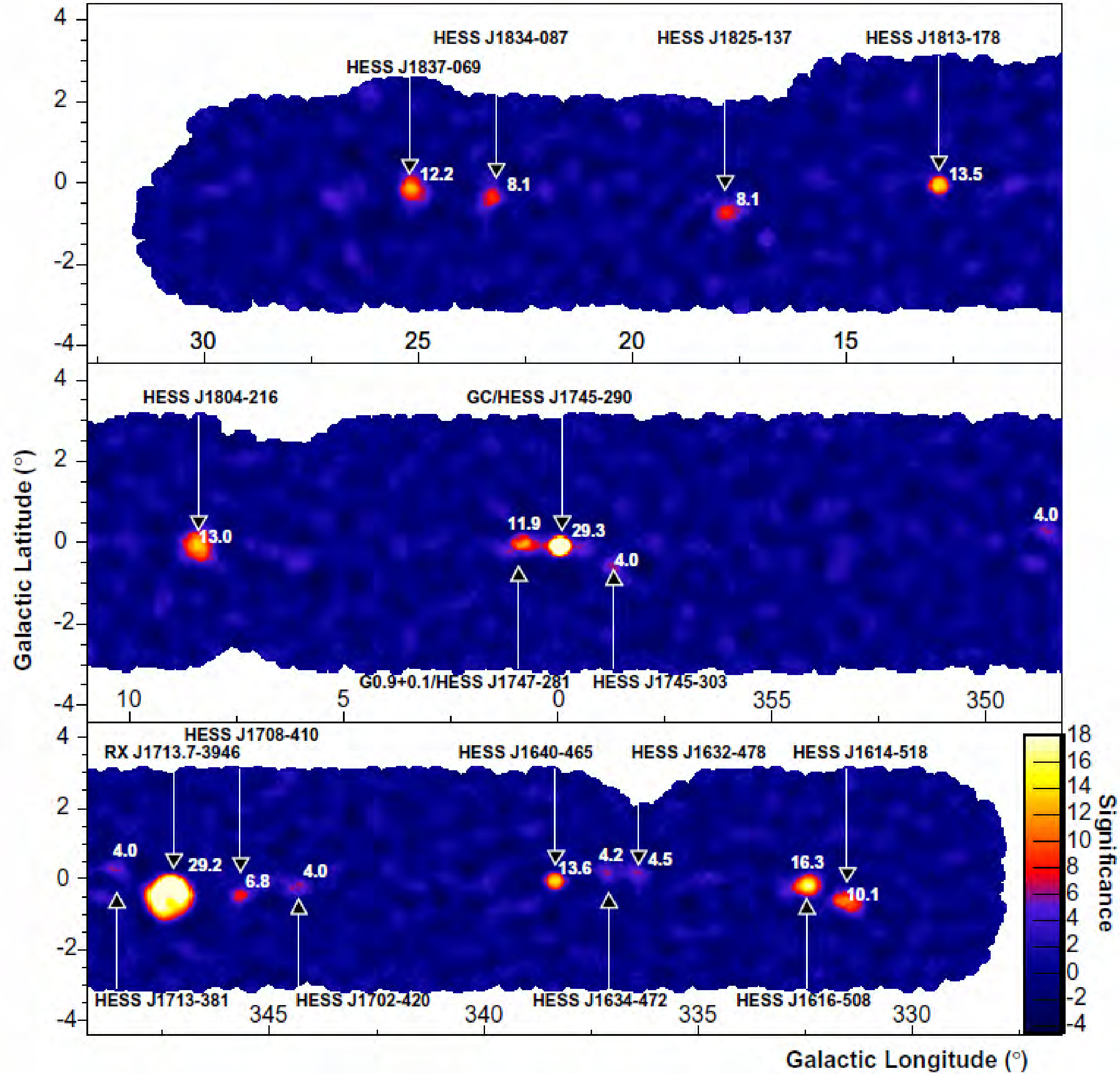

H.E.S.S.: Aharonian et al., ApJ 636, 777 (2005)

Other SNRs?

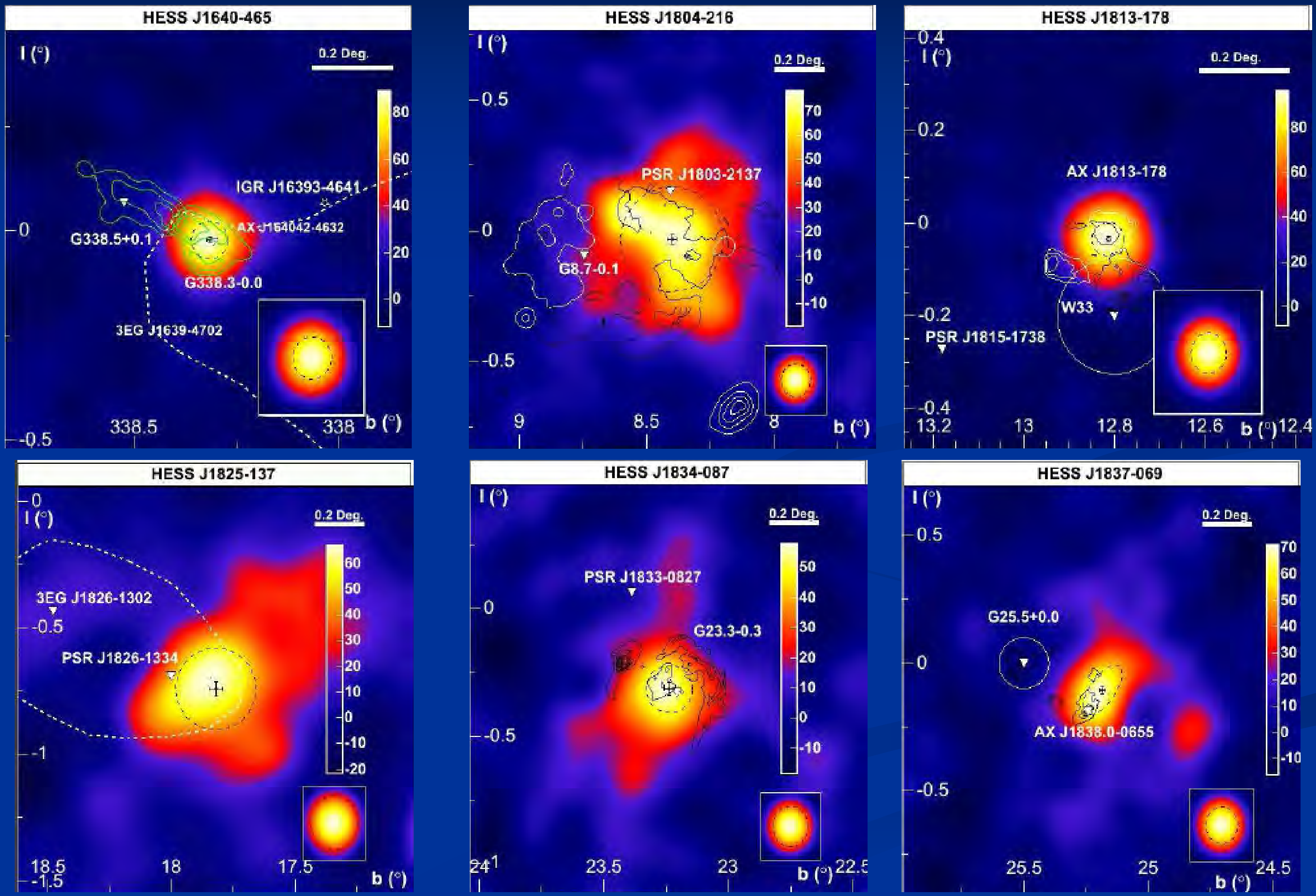

There are many SNRs!

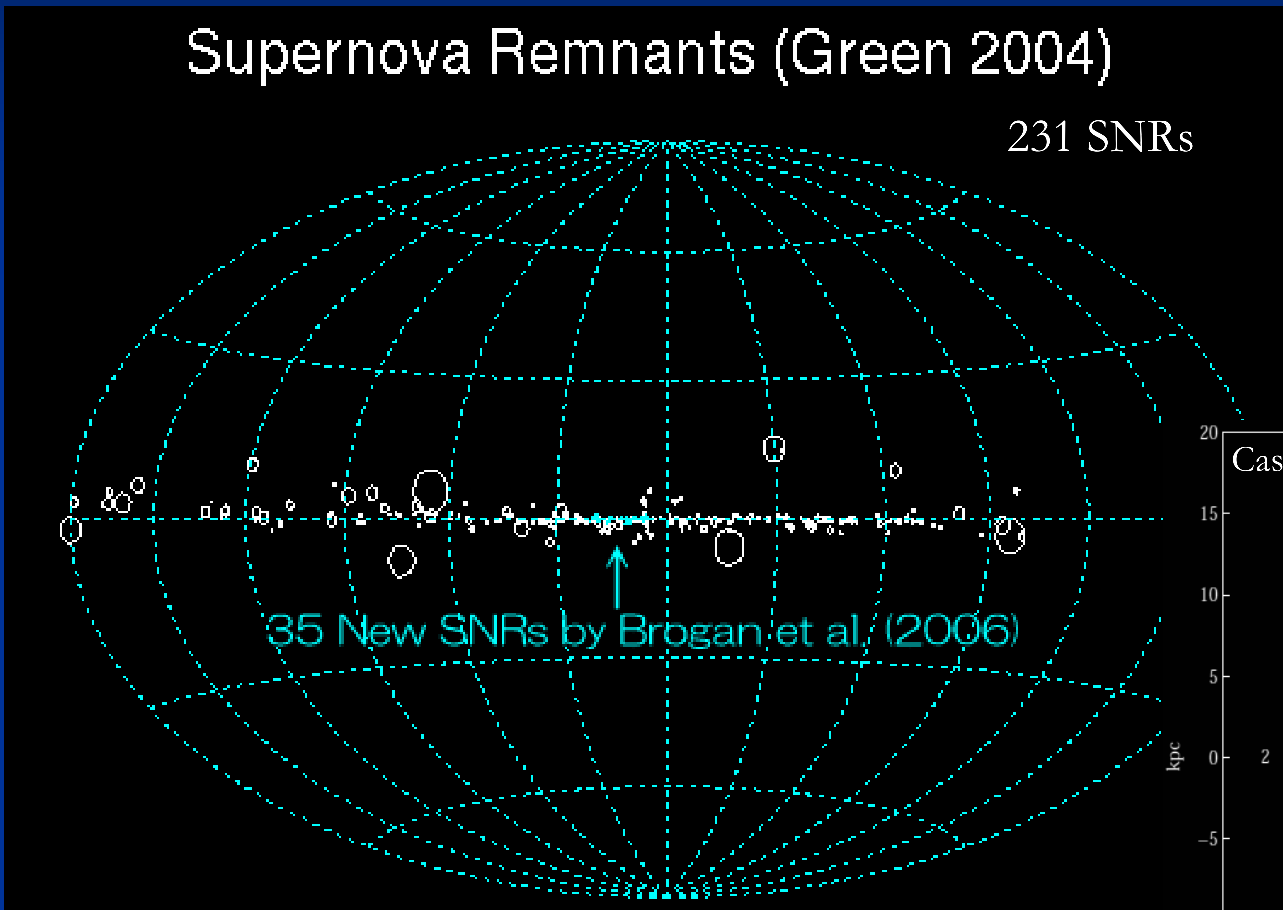

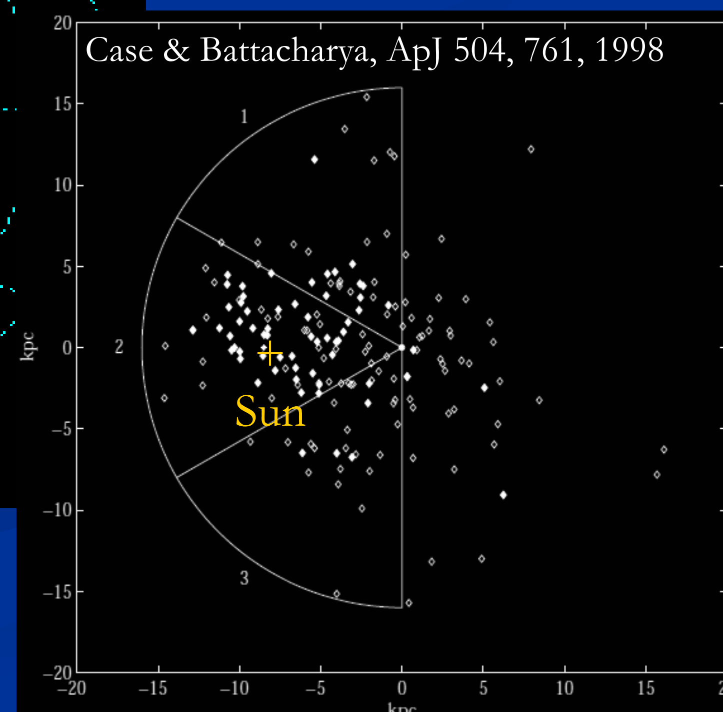

Total >300 SNRs?

"New" galactic sources

- The **Galactic center**
  - Whipple 2004, CANGAROO 2004, H.E.S.S. 2004, MAGIC 2006
- Pulsar wind nebulae
  - **MSH15-52** [CANGAROO 2000, H.E.S.S. 2005]
  - **Vela X** [H.E.S.S. 2005, CANGAROO 2006]
- Pulsar binary **PSR 1259-63/SS2883**
  - H.E.S.S. 2005
- X-ray binary/microquasar
  - **LS5039** [H.E.S.S. 2005, 2006]
  - **LSI +61 303** [MAGIC 2006]
- UnID
  - HEGRA J2032+4130
  - H.E.S.S. J1303-631
  - New H.E.S.S. sources

The Galactic center [Sgr A*]

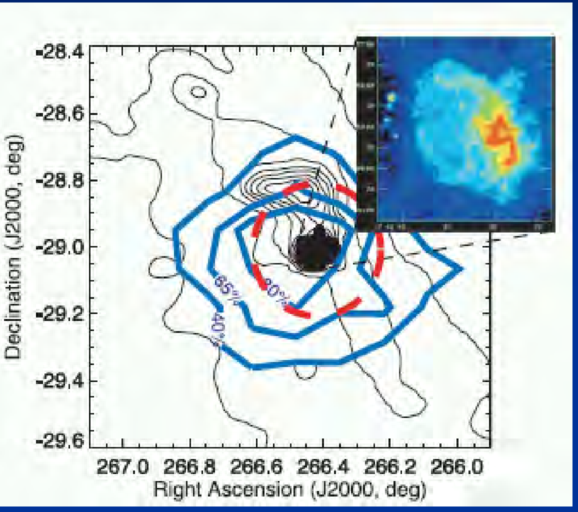

CANGAROO-II (Tsuchiya et al., ApJ 606, L115, 2004)

H.E.S.S.: Aharonian et al., A&A 425, L13 (2004) /ICRC2005

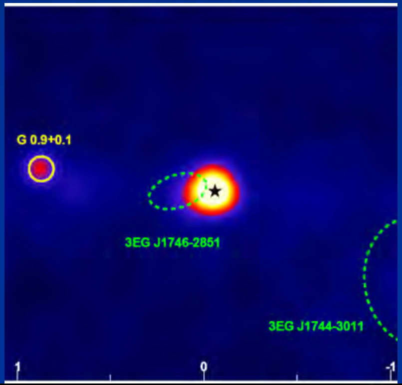

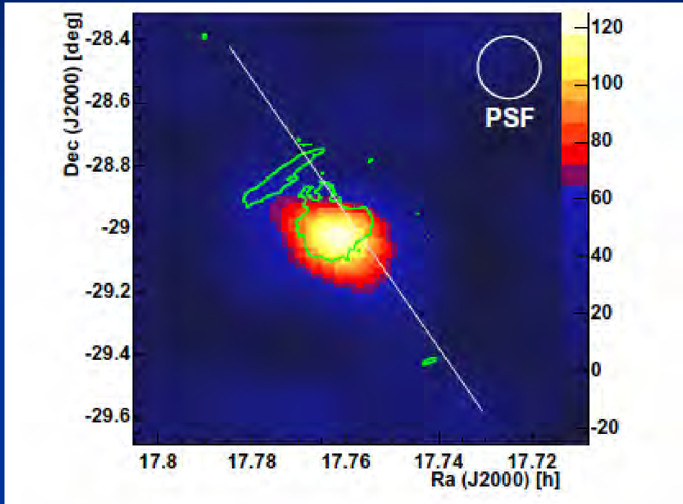

FIG. 1.— Smoothed sky map of γ-ray candidates (background subtracted) in the direction of the Galactic Center for SIZE $\geq$ 300 ph. el. (corresponding to an energy threshold of about 1 TeV). Overlayed are green contours (0.3 Jy beam^{-1}) of 90 cm VLA (BCD configuration) radio data (LaRosa et al. 2000). The white line shows the galactic plane.

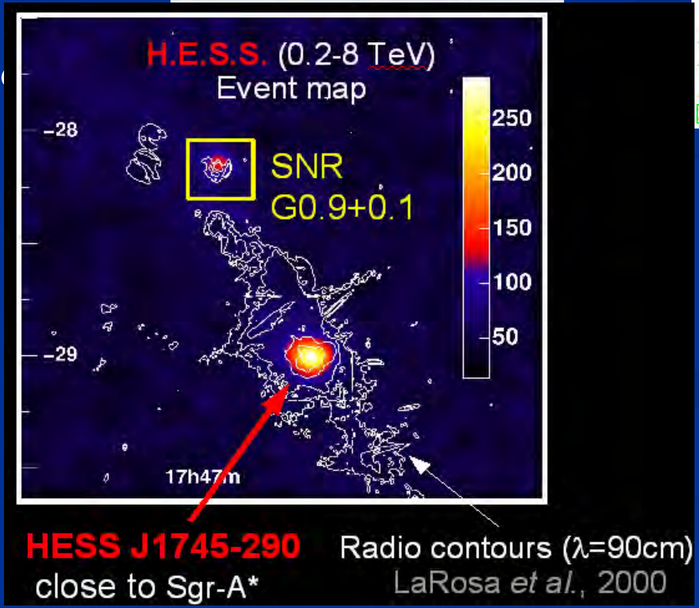

MAGIC, ApJ 638, L101 (2006)

Dark matter signal from Sgr A*?

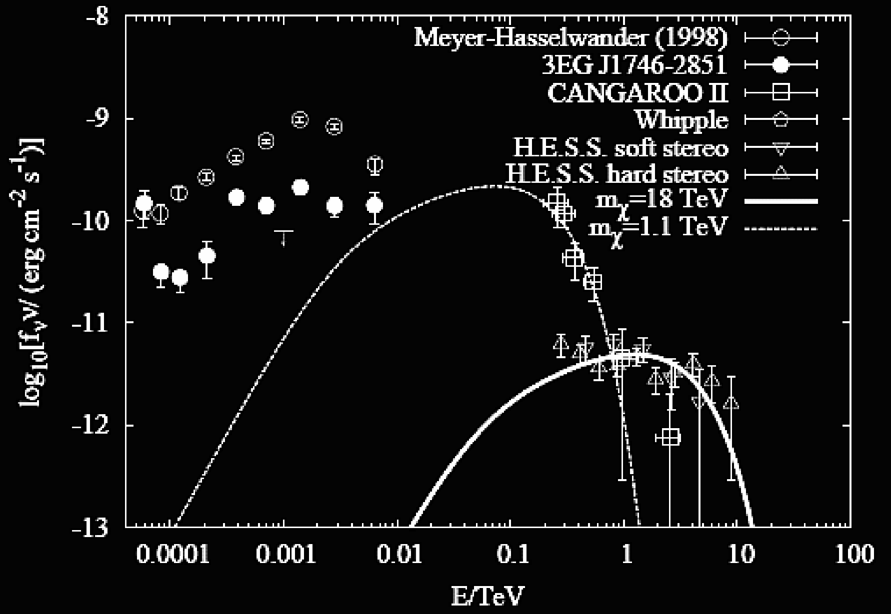

Fig. 2. A summary of data and best-fit models for WIMP annihilation from the Galactic center: H.E.S.S. (open triangles), CANGAROO (open boxes), EGRET (solid and open circles), 10m Whipple telescope of the VERITAS collaboration (solid diamond).

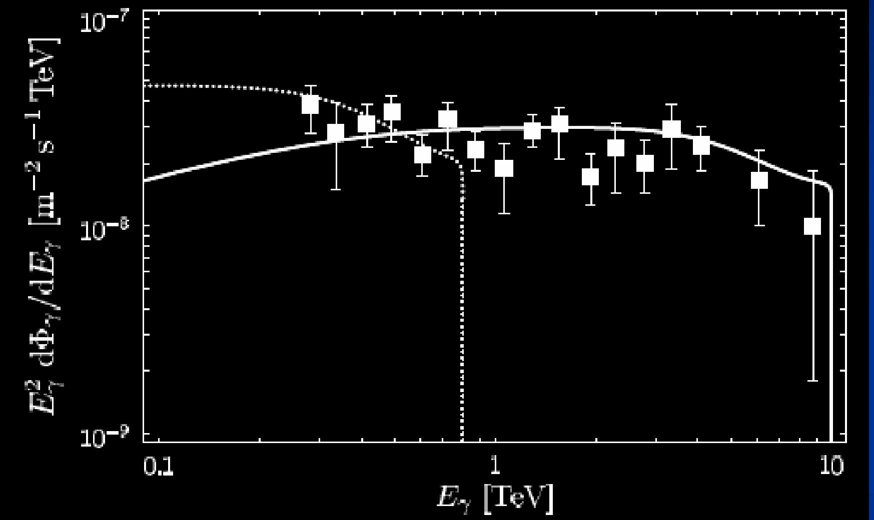

FIG. 3. The HESS data [3] compared to the gamma-ray flux from a region of 10^{-5} sr encompassing the GC, for a $B^{(1)}$ mass of 0.8 TeV, a 5% mass splitting at the first KK level, and a boost factor b around 200 (dashed line). The solid line corresponds to a hypothetical 10 TeV WIMP with similar couplings, a total annihilation rate given by the WMAP relic density bound, and a boost factor around 1000.

Neutralino-type dark matter:

Horns, Phys.Lett. B607 (2005) 225

Kaluza-Klein dark matter:

Bergstroem et al, Phys.Rev.Lett. 94 (2005) 131301

H.E.S.S.: Aharonian et al., astro-ph/0610509

Not dark matter signal from Sgr A*?

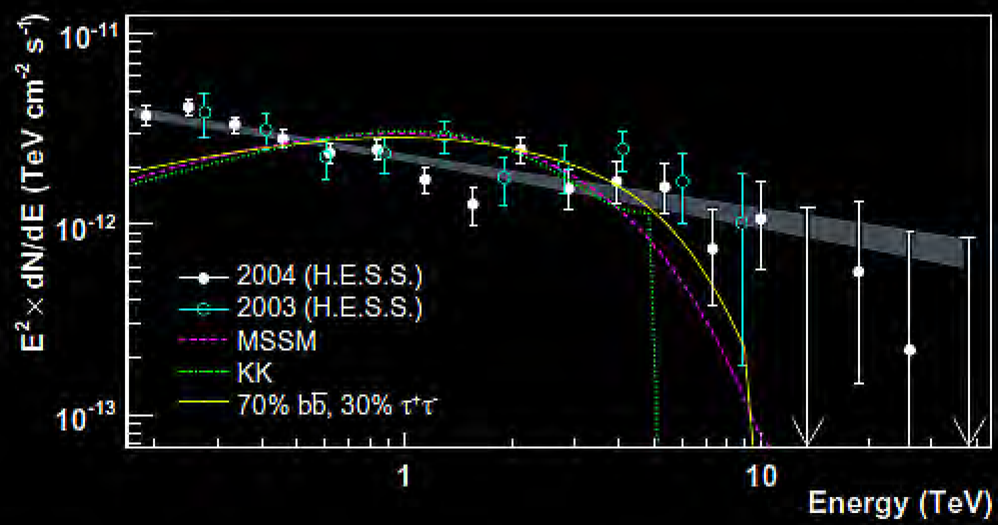

FIG. 2: (Color online) Spectral energy density $E^2 \times dN/dE$ of γ-rays from the GC source, for the 2004 data (full points) and 2003 data [3] (open points). Upper limits are 95% CL. The shaded area shows the power-law fit $dN/dE \sim E^{-\Gamma}$. The dashed line illustrates typical spectra of phenomenological MSSM DM annihilation for best fit neutralino masses of 14 TeV. The dotted line shows the distribution predicted for KK DM with a mass of 5 TeV. The solid line gives the spectrum of a 10 TeV DM particle annihilating into $\tau^+\tau^-$ (30%) and $b\bar{b}$ (70%).

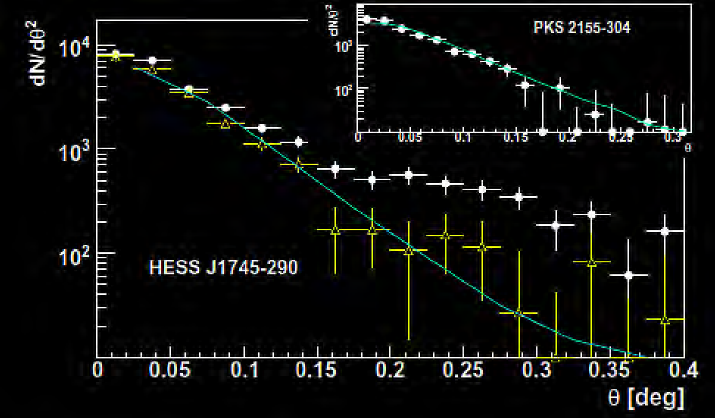

FIG. 1: (Color online) Background-subtracted distribution of the angle θ between the γ-ray direction and the position of Sgr A*. Circles: all detected γ-rays events. Open triangles: central object after subtraction of the γ-ray diffuse emission model (see text). Line: calculated PSF normalized to the number of γ-rays within 0.1° after subtraction is also shown. The distribution of events after subtraction matches the calculated PSF while the initial distribution shows a significant tail. The variation of the PSF related to the source energy spectrum, zenith angle and offset position in the field of view are taken into account. Insert: same distribution for the point-like source PKS 2155-304 [35]. The calculated PSF (line) also matches the data.

Pulsar wind nebula MSH15-52

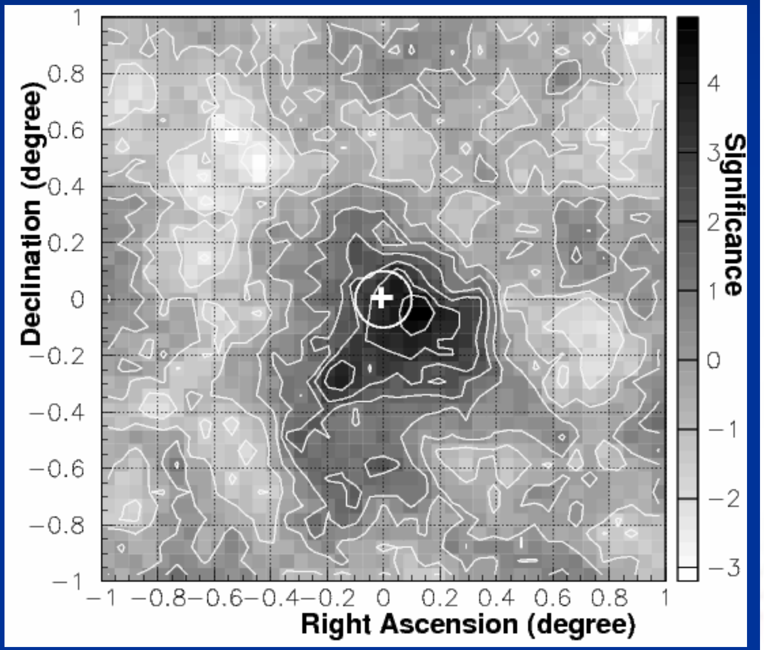

PSR 1509-58

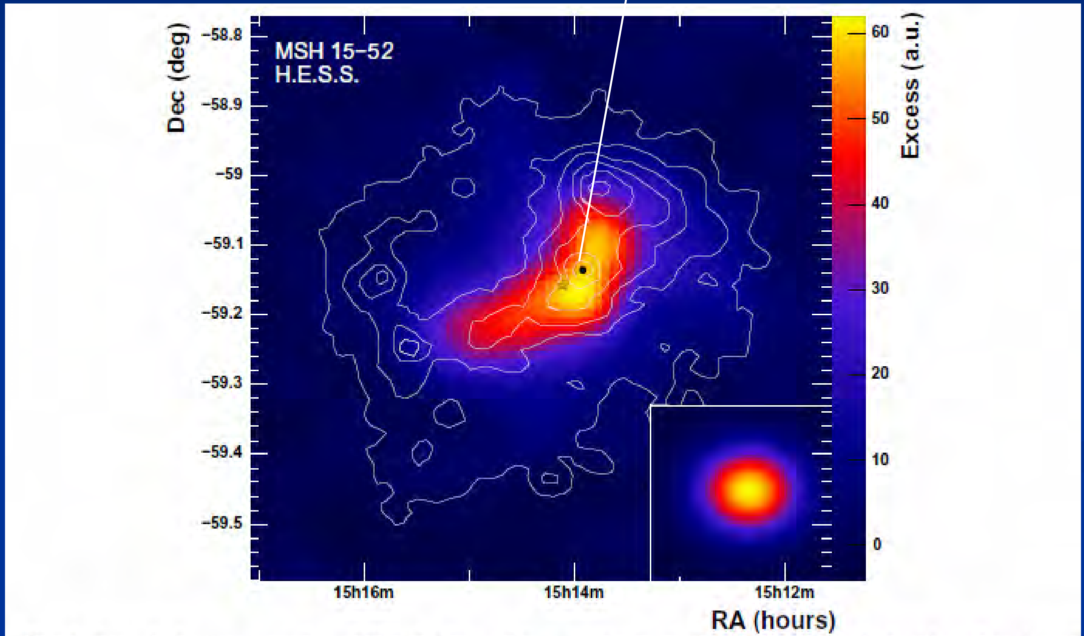

Fig. 1. Smoothed excess map from MSH 15-52 in arbitrary units (a.u.). The map is smoothed with a Gaussian of $\sigma=0.04°$ and only events with image sizes above 400 p.e. are used in order to improve the H.E.S.S. angular resolution. The white contour lines denote the X-ray (0.6–2.1 keV) count rate measured by ROSAT (Trussoni et al. 1996). The black point and black star lie at the pulsar position and at the excess centroid, respectively. The right-bottom inset shows the simulated PSF smoothed identically.

CANGAROO-I.:

Sako et al., ApJ 537, 422 (2000)

H.E.S.S.:

Aharonian et al., A&A 435, L17 (2005)

Vela X nebula

Pulsar position

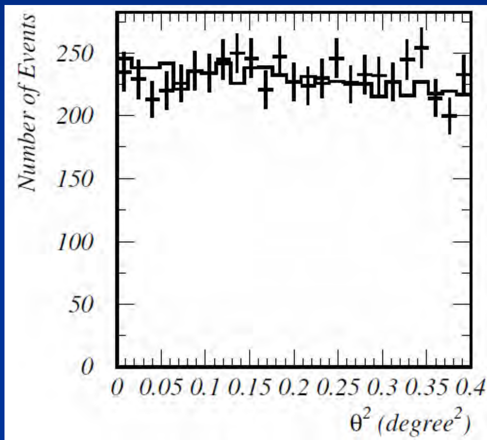

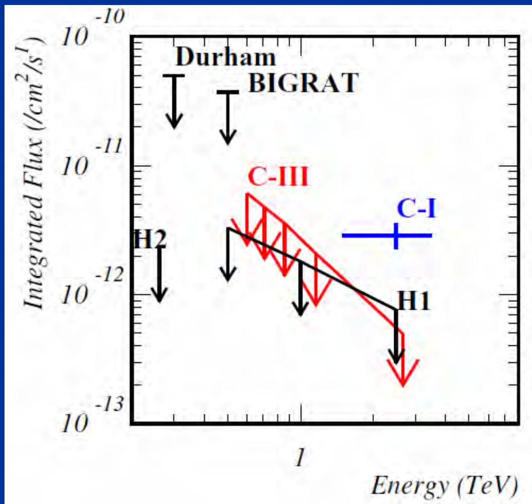

- Pulsar pointing (2004 Jan/Feb)
- Stereo (T2 & T3 wobble)
- 1,311 min.
- Fisher discriminant

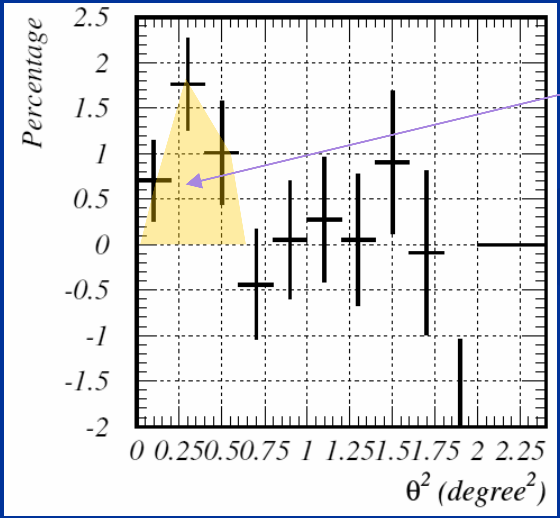

θ^2 from Vela X center

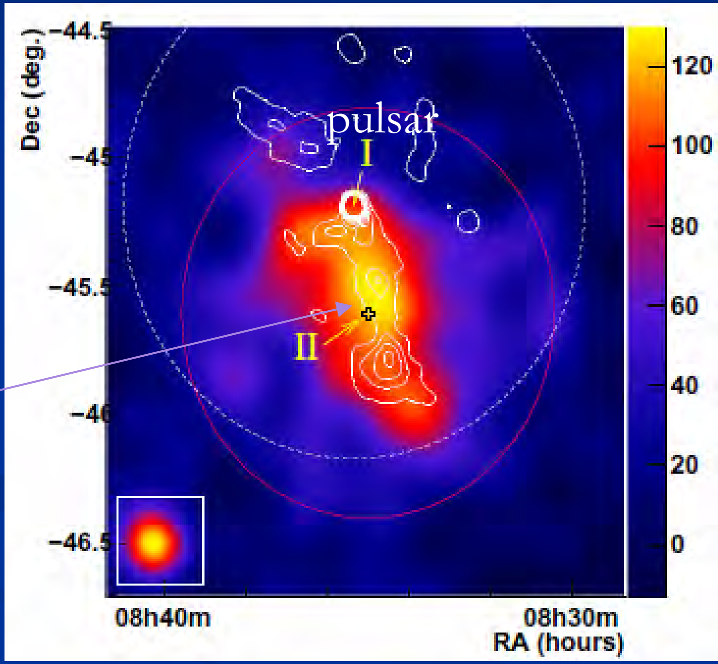

Fig. 1. Gaussian smoothed sky map of region surrounding Vela pulsar, showing significant emission to the south of the pulsar position, coincident with an X-ray feature seen by ROSAT (white contours). The smoothing width used is 0.09°. The contours corresponding to the strong emission close to the pulsar (position I) are truncated. The image inset in the bottom left corner indicates the size of a point source as seen by HESS, for an equivalent analysis. The solid circle represents the HESS integration region for the spectral measurement, while the dashed circle represents the field of view for the ROSAT observations. Position II is marked by a black cross.

H.E.S.S.: Aharonian et al., A&A 448, L43 (2006)

CANGAROO-III: R.Enomoto et al., ApJ 638, 397 (2006)

Pulsar Wind Nebulae

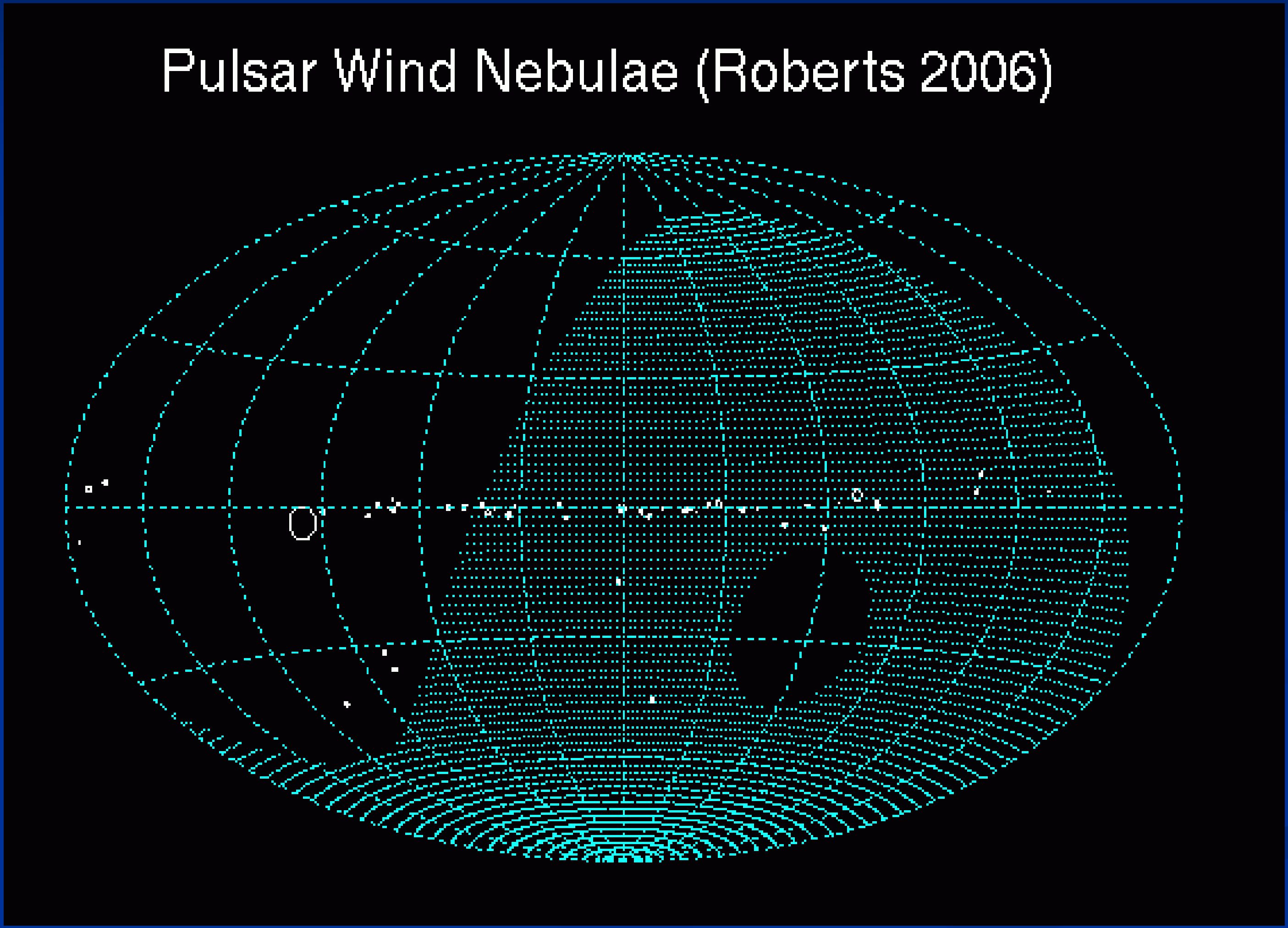

(Hatched: observable from Woomera)

Pulsar binary PSR 1259-63/SS2883 (1)

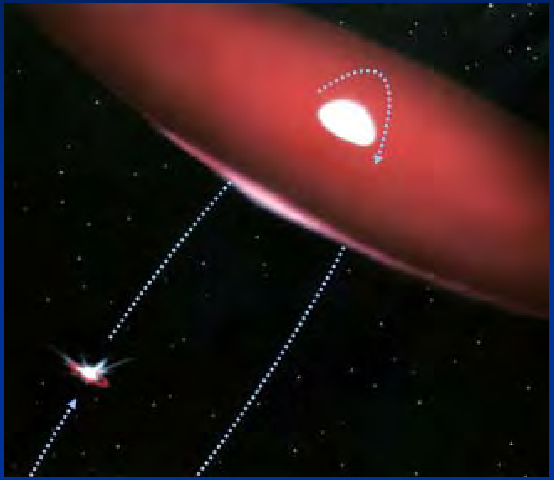

3.4 year highly eccentric orbit around ~10 $M_\odot$ Be star
closest approach ~10^{13} cm or ~20 stellar radii

(i) aligned disc to the orbital plane and interaction throughout the orbit
(ii) mis-aligned disc and interaction in the ~200-day period around periastron (τ), during which the radio emission is depolarized
(iii) mis-aligned disc and interaction in two short periods, [(τ -18 d) ~(τ ~ -8d)] and [(τ +12 d) ~ (τ +22 d)]

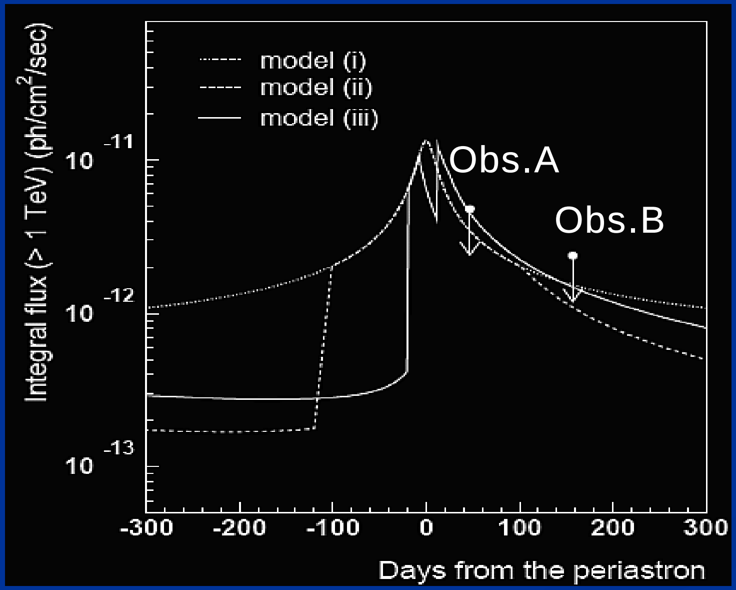

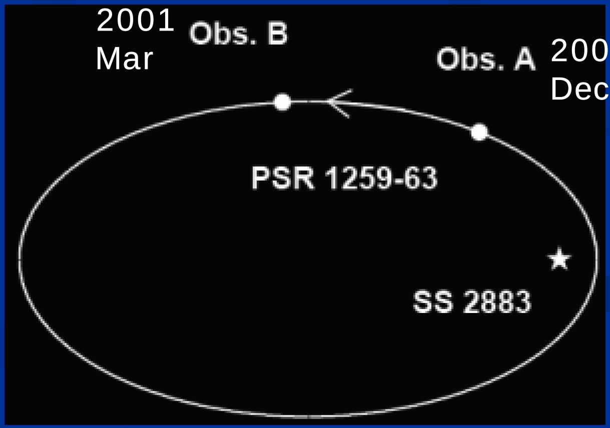

CANGAROO-II: Kawachi et al., ApJ, 607(2004) 949

H.E.S.S.: F. Aharonian et al., Astron. Astrophys. 442 (2005) 1

Pulsar binary PSR 1259-63/SS2883 (2)

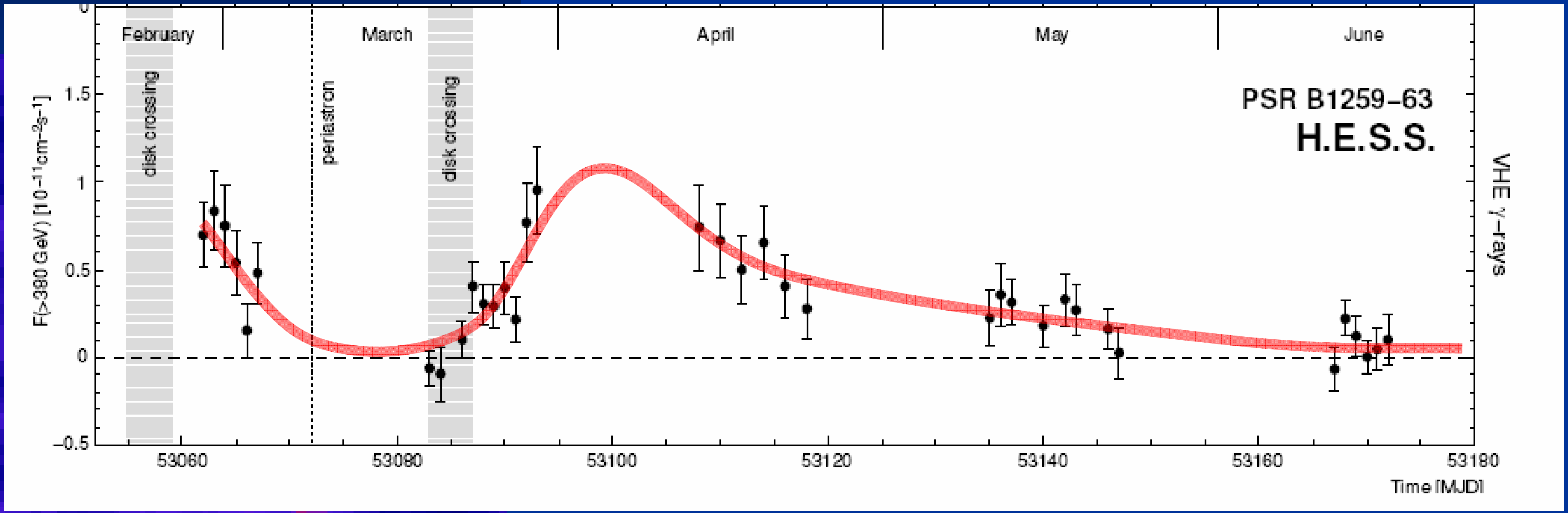

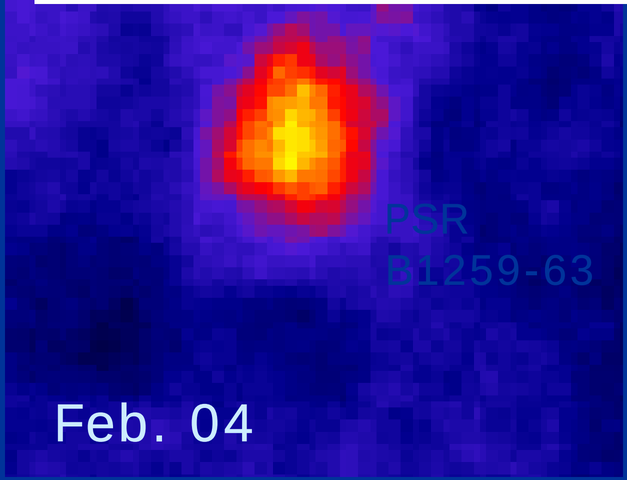

F. Aharonian et al., Science 309 (2005) 746

X-ray binary/microquasar LS5039

- HMXB: compact 4 (?) $M_{\odot}$ object in eccentric 4 day orbit around 20-30 $M_{\odot}$ star
- closest approach ~10^{12} cm or ~2 stellar radii

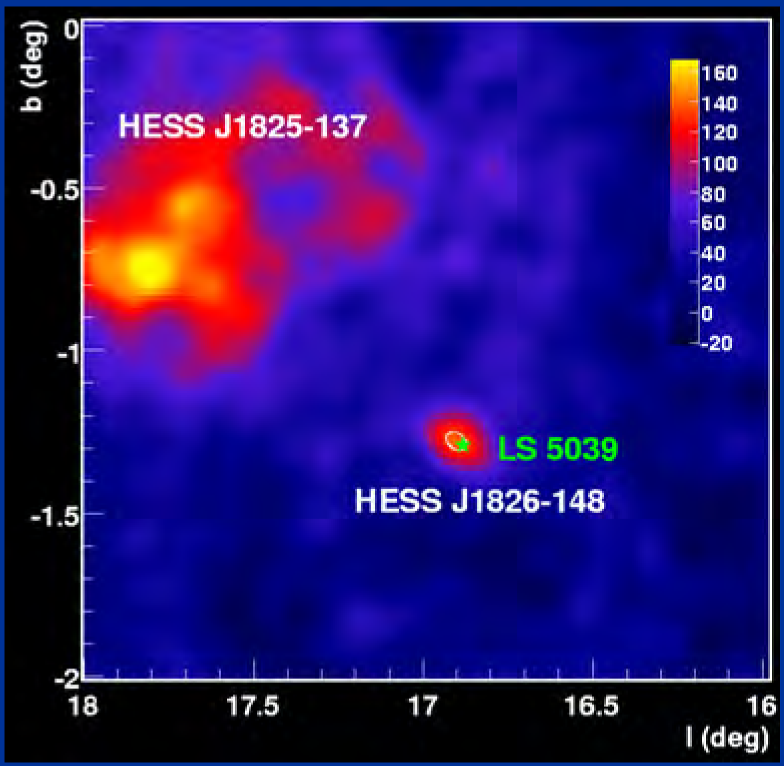

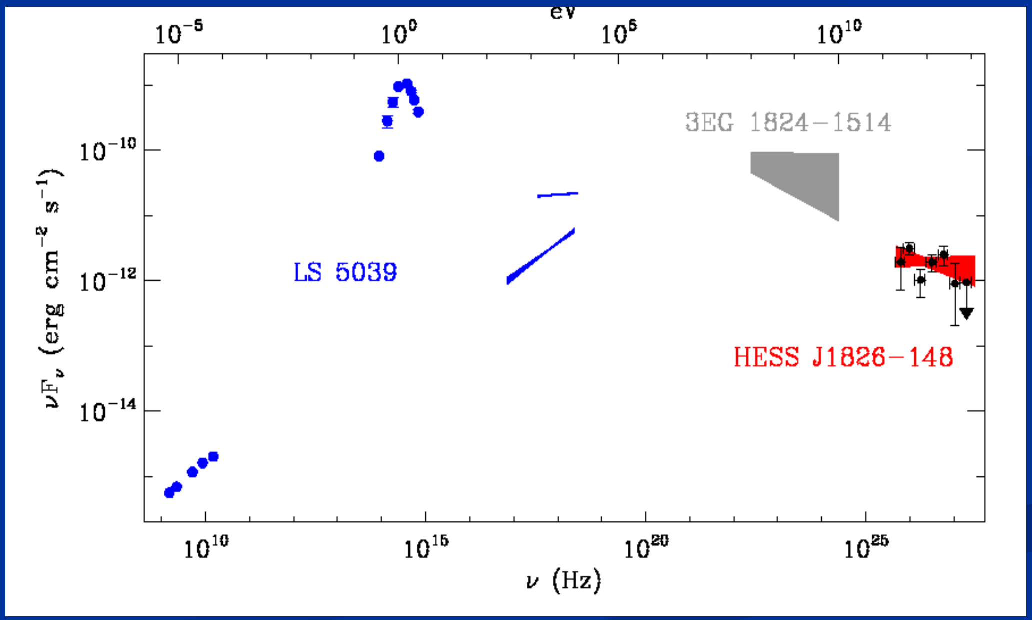

Aharonian et al., astro-ph/0607192

LS5039 modulation

P_{orb}=3.9d

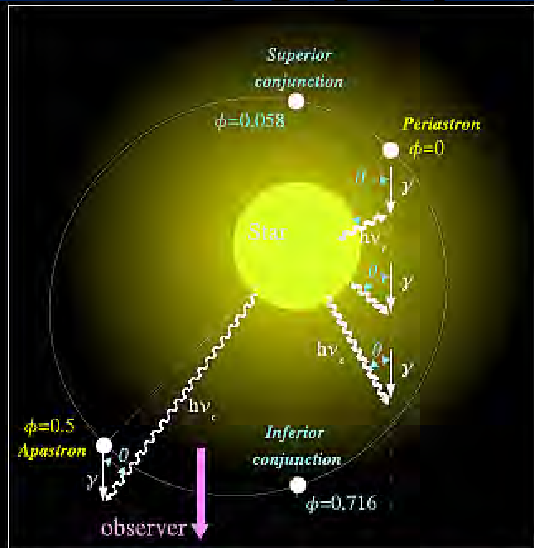

Fig. 4. The orbital geometry (Casares et al. 2005) viewed from directly above LS 5039. Shown are: phases (ϕ) of minimum (periastron) and maximum (apastron) separation between the two components; epochs of superior and inferior conjunctions of the compact object representing phases of co-aligment along our line-of-sight of the compact object and stellar companion. The orbit is actually inclined at an angle in the range $13° < i < 64°$ with respect to the view above. VHE γ-rays (straight black lines with arrows) can be absorbed by optical photons of energy $h\nu_\epsilon$, when their scattering angle θ exceeds zero.

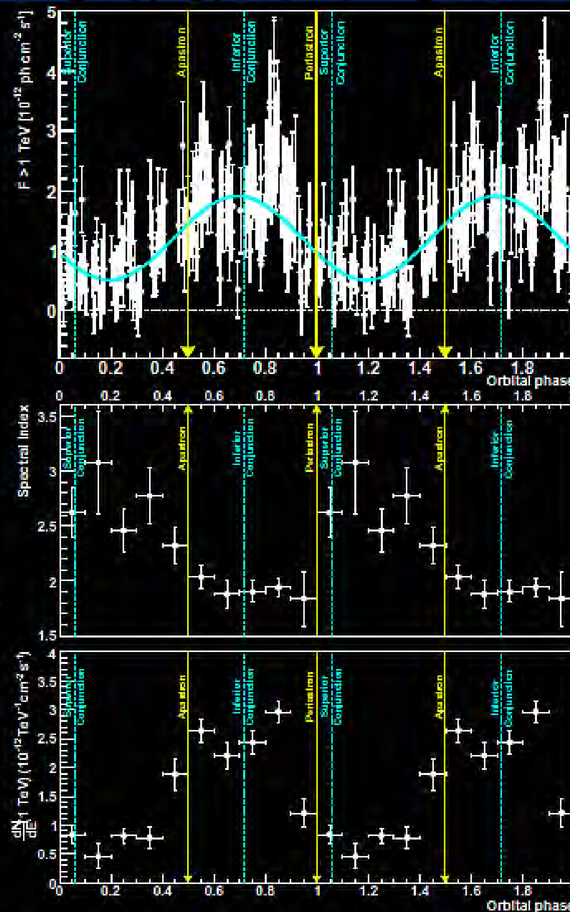

Fig. 5. Top: Integral γ-ray flux ($F > 1$ TeV) lightcurve (phasogram) of LS 5039 from HESS data (2004 to 2005) on a run-by-run basis folded with the orbital ephemeris of Casares et al. (2005). Each run is ~28 minutes. Two full phase (ϕ) periods are shown for clarity. The blue solid arrows depict periastron and apastron. The thin red dashed lines represent the superior and inferior conjunctions of the compact object, and the thick red dashed line depicts the Lomb-Scargle Sine coefficients for the period giving the highest Lomb-Scargle power. This coefficient is subtracted from the light curve in Fig 1 middle panel.

Albert et al., Science 312 (2006) 771

LSI +61 303

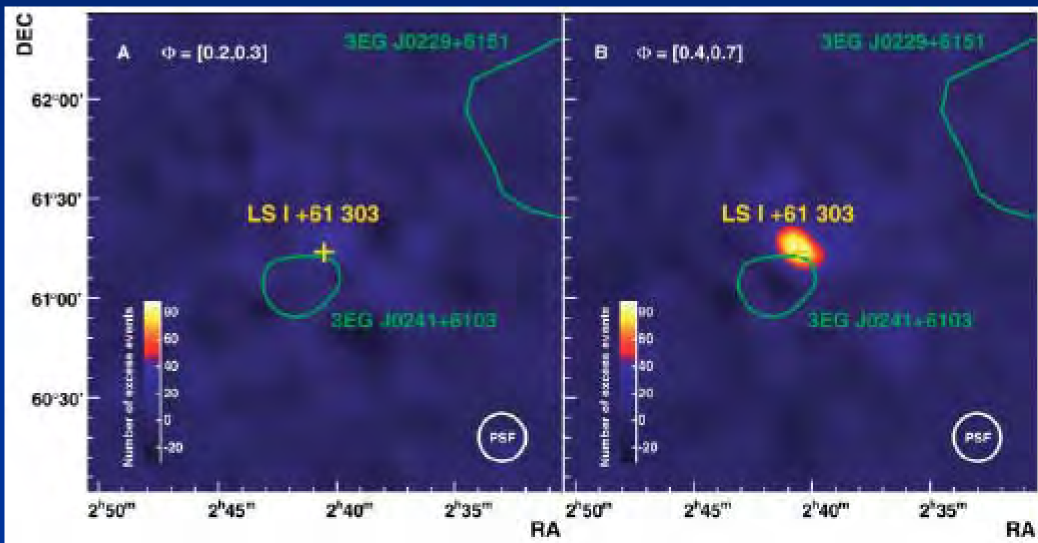

Fig. 1. Smoothed maps of gamma-ray excess events above 400 GeV around LS I +61 303. (**A**) Observations over 15.5 hours corresponding to data around periastron (i.e., between orbital phases 0.2 and 0.3). (**B**) Observations over 10.7 hours at orbital phase between 0.4 and 0.7. The number of events is normalized in both cases to 10.7 hours of observation. The position of the optical source LSI +61 303 (yellow cross) and the 95% confidence level contours for 3EG J0229+6151 and 3EG J0241+6103 (green contours) are also shown. The bottom right circle shows the size of the point spread function of MAGIC (1σ radius). No significant excess in the number of gamma-ray events is detected around periastron passage, whereas it shows up clearly (9.4σ statistical significance) at later orbital phases, in the location of LS I +61 303.

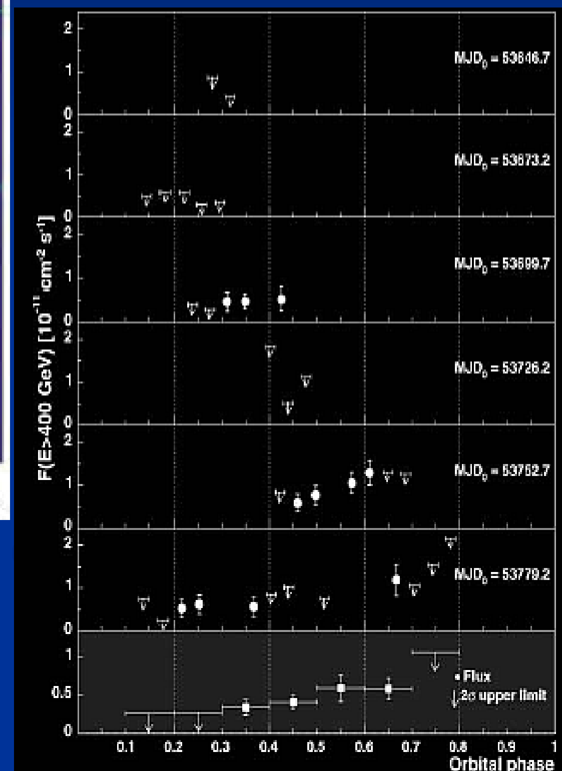

Fig. 2. VHE gamma-ray flux of LS I +61 303 as a function of orbital phase for the six observed orbital cycles (six upper panels, one point per observation night) and averaged for the entire observation time (bottom panel). Vertical error bars include 1σ statistical error and 10% systematic uncertainty on day-to-day relative fluxes. Only data points with more than 2σ significance are shown, and 2σ upper limits (*33*) are derived for the rest. The modified Julian date (MJD) corresponding to orbital phase 0 is indicated for every orbital cycle. The orbital phase is computed with orbital period of 26.4960 days and zero phase at JD 2443366.775 (*9*); periastron takes place at phase 0.23 (*10*). Marginal detections occur between orbital phases 0.2 and 0.4 in different cycles, whereas a significant increase of flux is detected from phase ~0.45 to phase ~0.65 in the fifth cycle, peaking at ~16% of the Crab Nebula flux on MJD 53769 (phase 0.61). During the following cycle, the highest flux is measured on MJD 53797 (phase 0.67). This behavior suggests that the VHE gamma-ray emission from LS I +61 303 has a periodic nature.

F. Aharonian et al., A&A 431 (2005) 197

HEGRA TeV J2032+4130

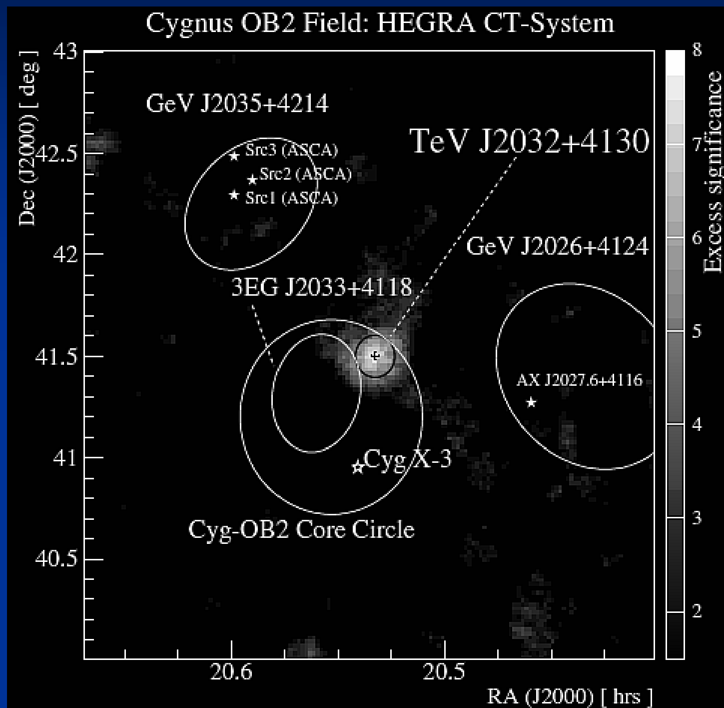

Chandra ACIS-I

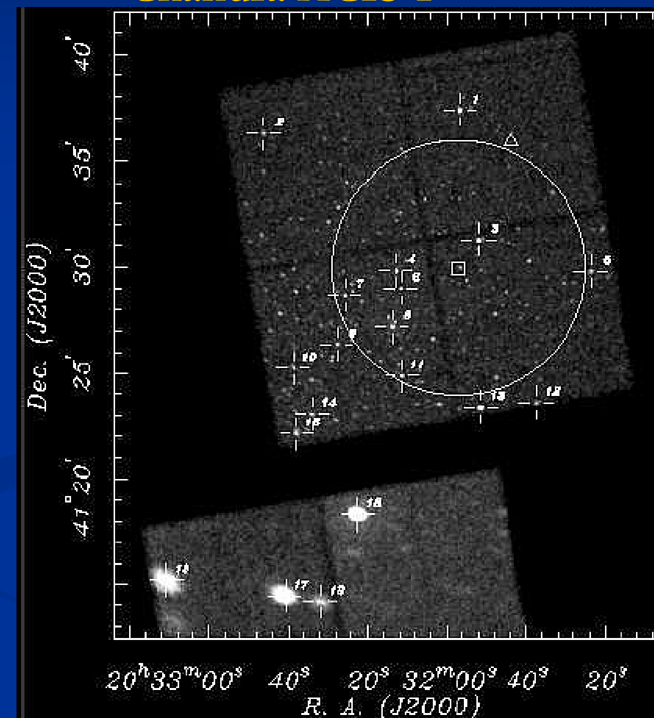

Fig. 1 *Chandra* ACIS-I image of the field of TeV J2032+4130. The positions of the marked sources are given in Table 1. The small square marks the centroid of TeV J2032+4130, and the circle is the estimated Gaussian 1σ extent of the TeV emission [3]. The triangle marks the brightest *Chandra* source in an earlier 5 ksec observation of the region [6], noticeably absent from this image.

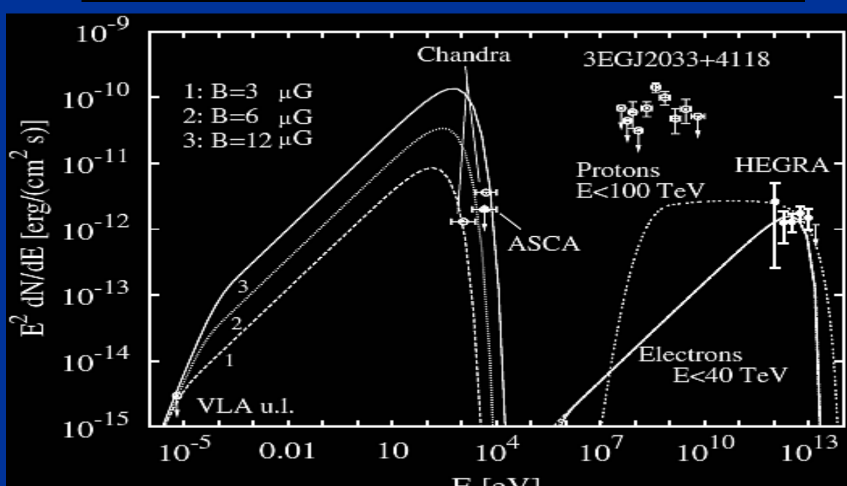

Mukerjee et al., astro-ph/0610299

What are H.E.S.S. unID sources?

- Near the Galactic plane: SNRs, pulsars?
- Hard spectra: marginally compatible with Fermi acceleration?
- Some may be identified with SNRs.
  - J1616-508, J1813-178 , J1825-137
- Old SNRs? [Yamazaki et al., astro-ph/0601704]

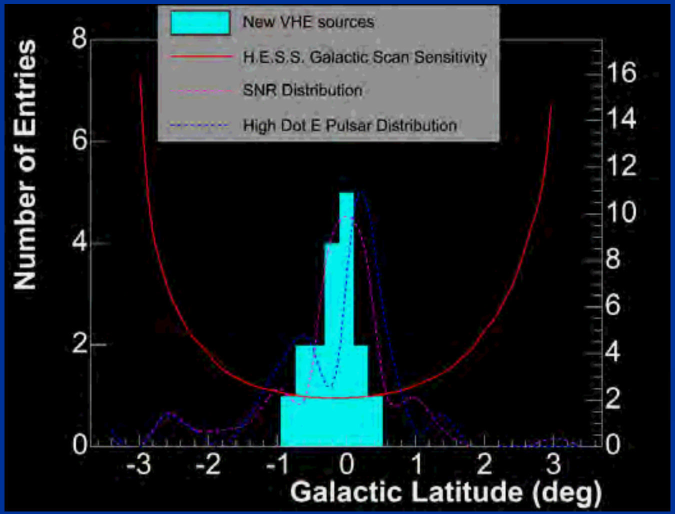

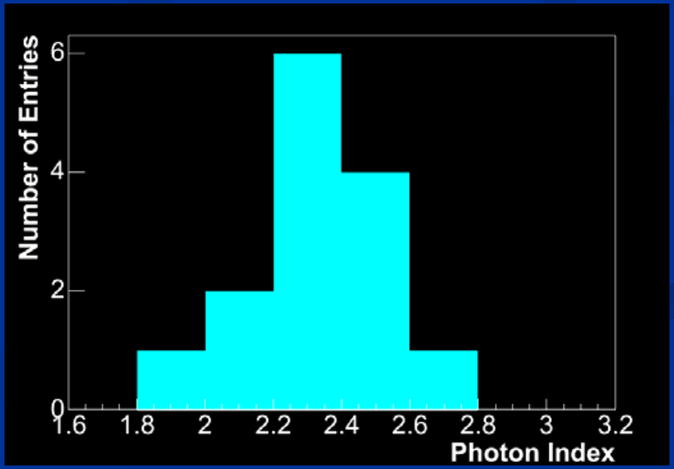

Aharonian et al., ApJ 636, 777 (2005)

H.E.S.S.: Aharonian et al., ApJ 636, 777 (2005)

HESS J1616-508

Young pulsar (69ms)

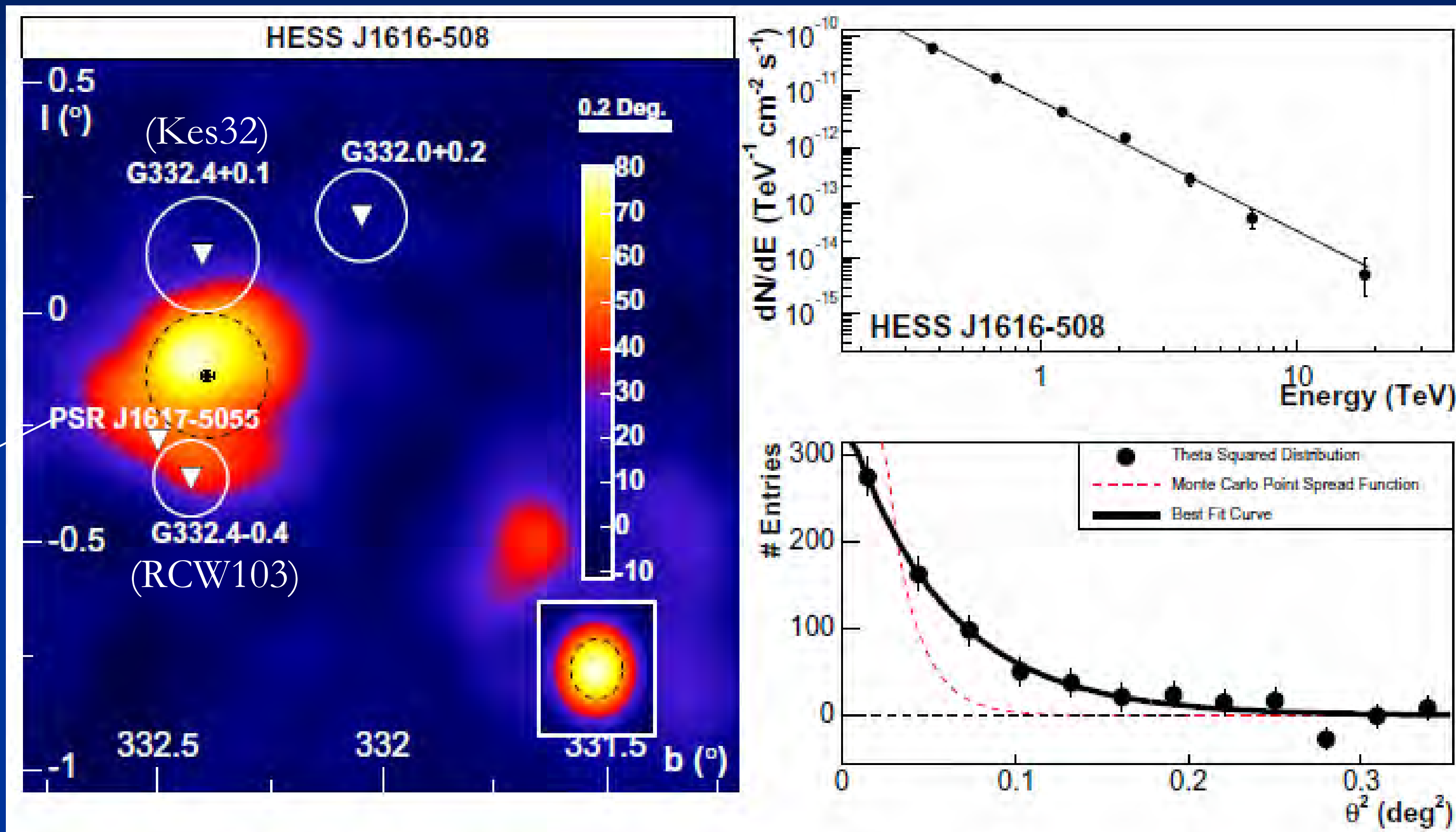

Figure 5.9: Smoothed excess map (left) of the region surrounding HESS J1616–508 (left hand source). HESS J1614–518 is also visible in this map (right hand source), along with nearby pulsars and SNRs which were considered as counterparts (smoothing radius 0.06°). The figures on the right hand side show spectrum (top) and θ^2 (bottom) plot of HESS J1616–508.

HESS J1813-178
= SNR AX J1813-178/G12.82-0.02

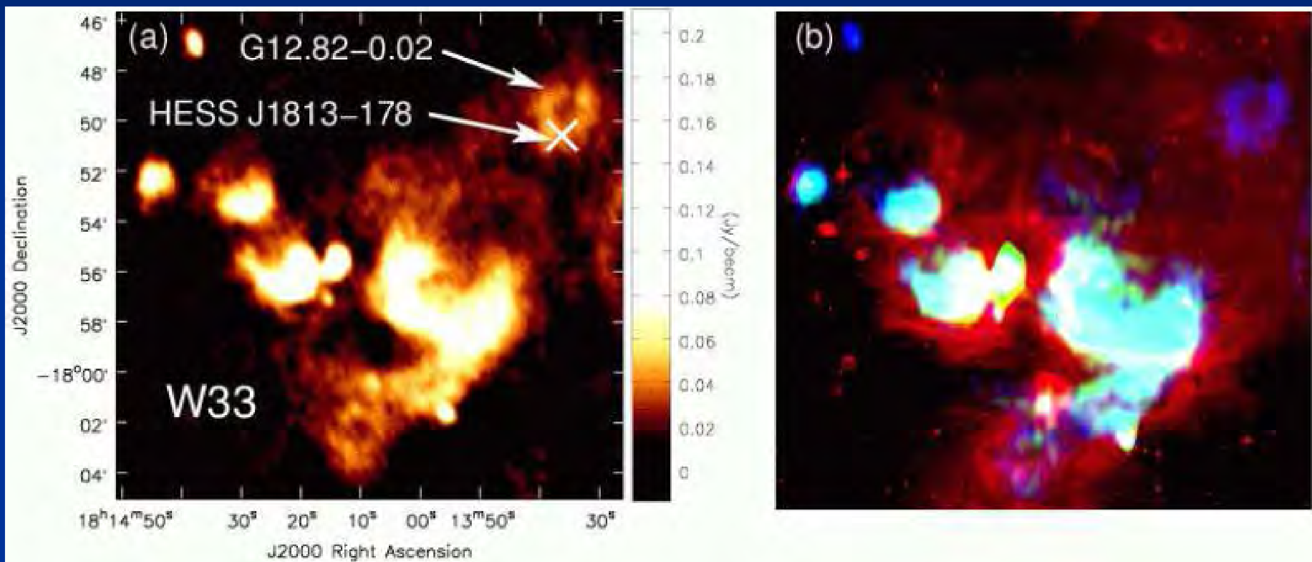

(a) VLA 90cm

(b) Spitzer 8μm /
VLA 20cm /
VLA 90cm

Less IR↔ non-thermal

Brogan et al., ApJ 629, L105 (2005)

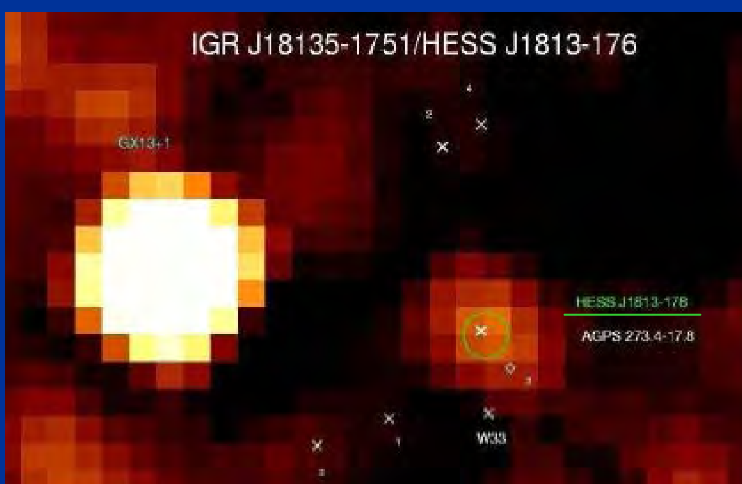

INTEGRAL 20-100 keV

Ubertini et al., ApJ 629, L109 (2005)

HESS J1825-137 = PWN G18.0-0.7?

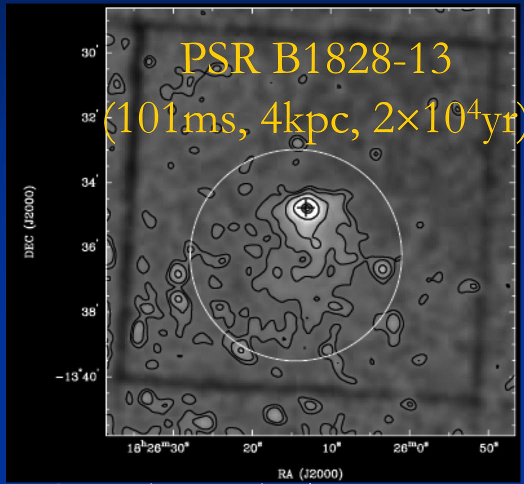

XMM: Gaensler et al., ApJ 588, 441 (2003)

H.E.S.S.: Aharonian et al., A&A 442, L25 (2005)

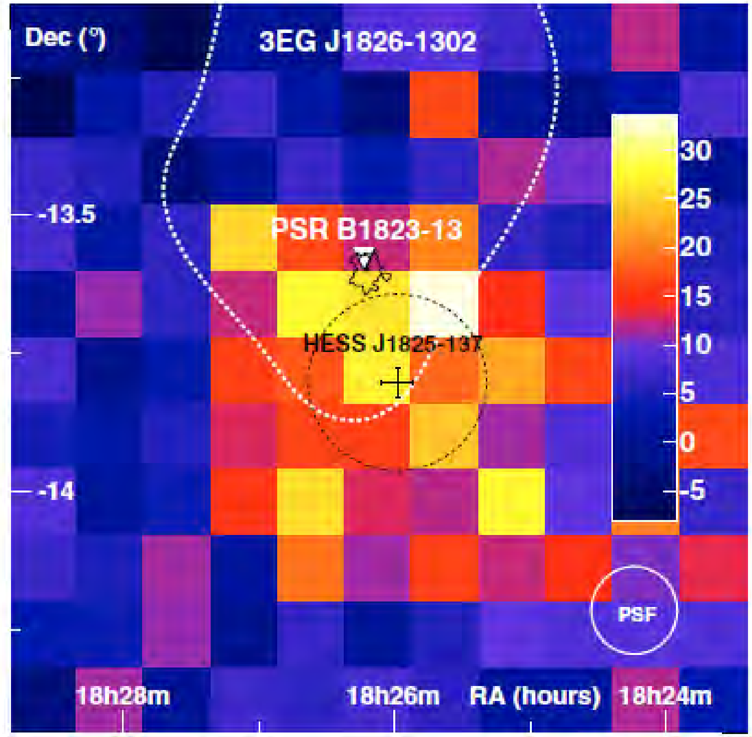

Fig. 1. Excess map of the region close to PSR B1823–13 (marked with a triangle) with uncorrelated bins. The best fit centroid of the γ-ray excess is shown with error bars. The black dotted circle shows the best fit emission region size (σ_{source}) assuming a Gaussian brightness profile. The black contours denote the X-ray emission as detected by *XMM-Newton*. The 95% confidence region (dotted white line) for the position of the unidentified EGRET source 3EG J1826–1302 is also shown. The system acceptance is uniform at the 20% level in a 0.6° radius circle around HESS J1825–137.

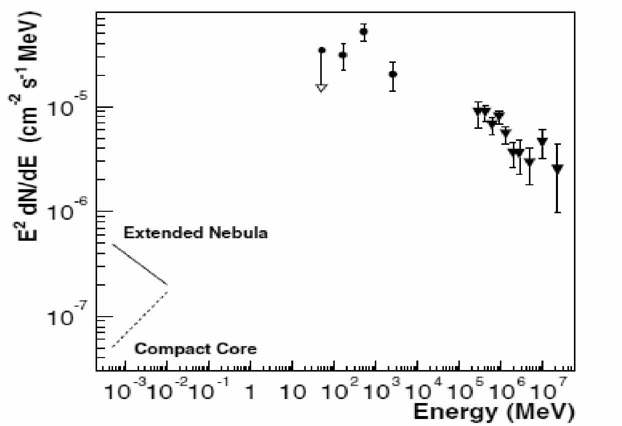

Fig. 3. Spectral energy distribution of HESS J1825–137, assuming that the X-ray emission surrounding PSR B1823–13, the EGRET source 3EG J1826–1302 and the new VHE γ-ray source are related. X-ray data, indicated by lines, are taken from Gaensler et al. (2003) and are shown for the two different regions as described in the text. EGRET data (full circles) are taken from the third EGRET catalog (Hartman et al. 1999). The triangles show the HESS data from this work.

Relation with CO/HI?

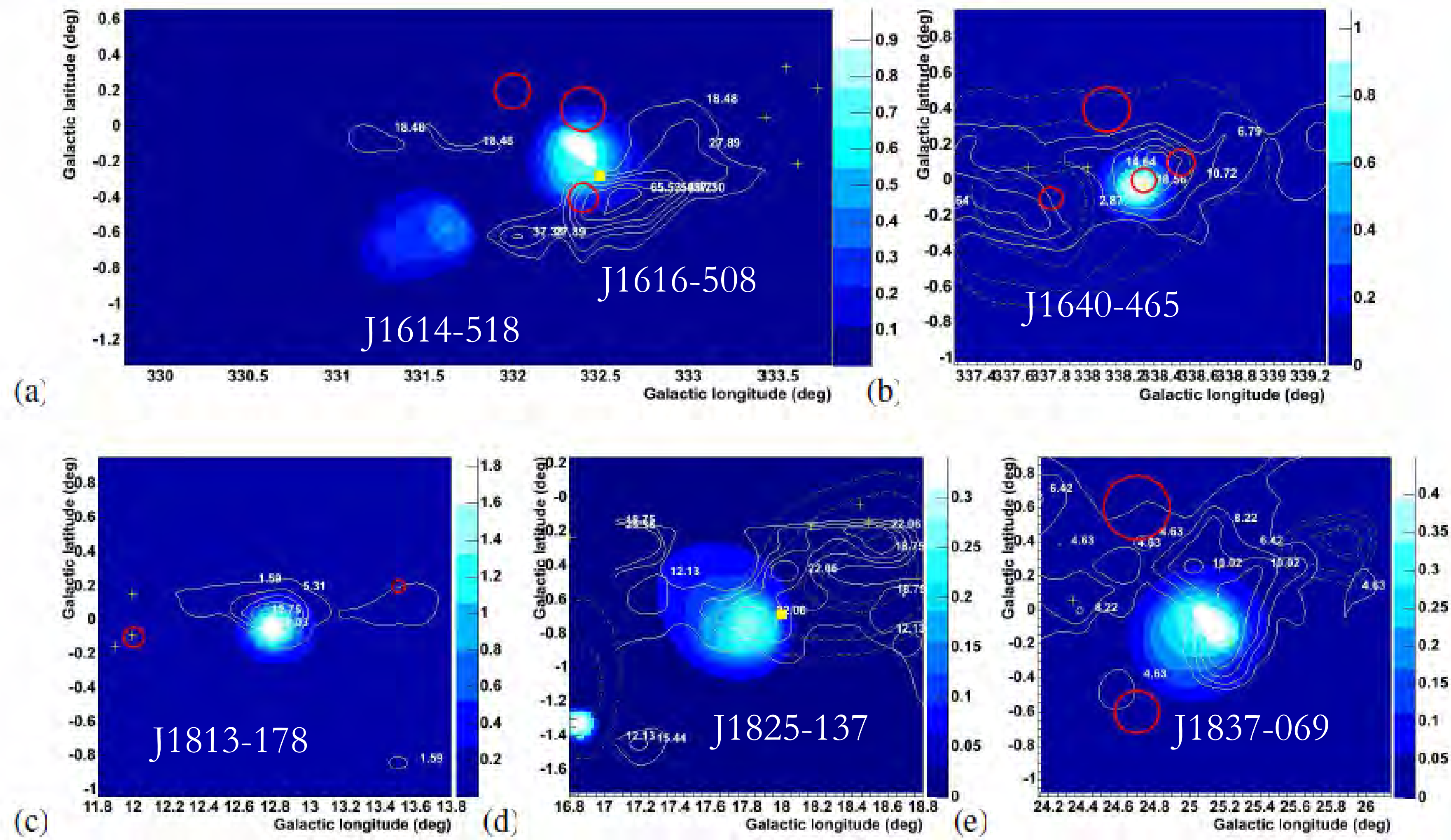

Figure 1. Multi-resolution filtered and reconstructed images of H.E.S.S.survey sources (the colour scale is arbitrary): (a) HESSJ1614-518 and HESS J1616-508 (b) HESSJ1640-465 (c) HESSJ1813-178 (d) HESSJ1825-137 (e) HESSJ1837-069. Possible counterpart are also indicated. The positional confidence contours for EGRET sources are shown in dash Gray (green), ASCA sources are indicated with crosses. The SNRs are indicated as circles (red) and the molecular cloud contours are shown in white, the numbers show column intensity levels in K.kms^{-1} units; the pulsars are shown as light Gray squares.

Lemiere et al., Proc. ICRC2005

H.E.S.S.: Aharonian et al., A&A 456, 245 (2006)

"Kookaburra" region

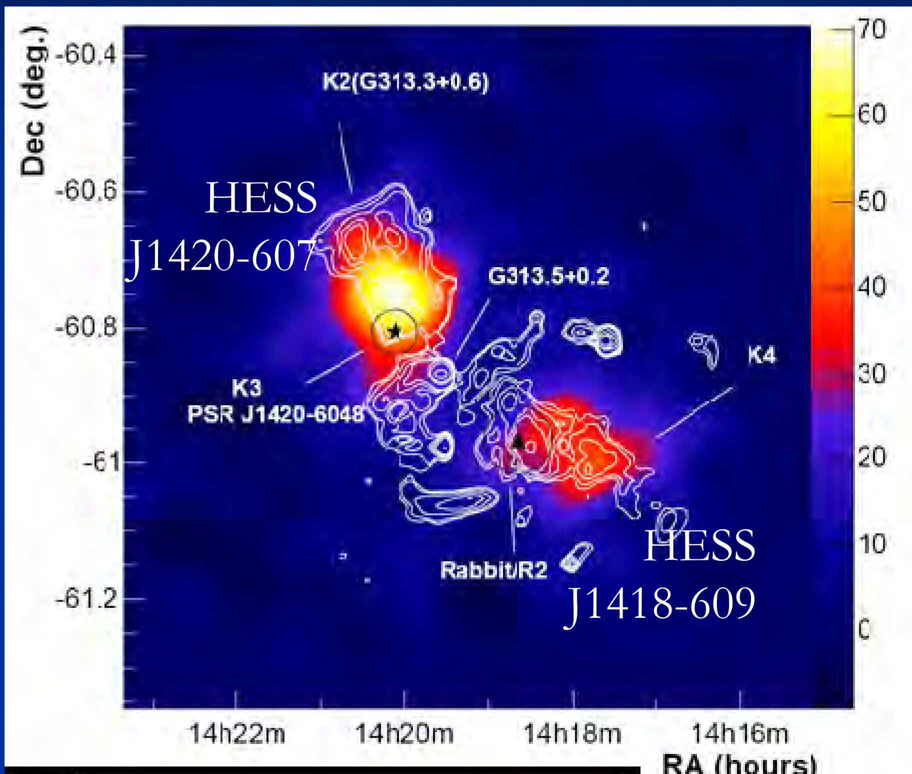

Fig. 2:
TeV emission as shown in Fig. 1, together with the radio contours from Roberts et al. 1999. The TeV emission lines up with the wings of the Kookaburra (labeled K2/K3 and K4) and extends north of the pulsar wind nebula surrounding PSR J1420-6048 (K3) and west of the Rabbit. (Preliminary)

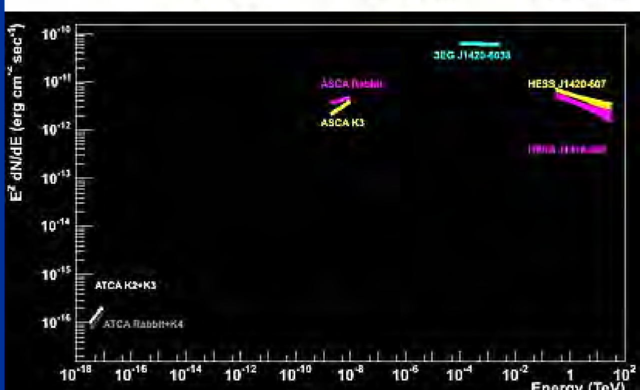

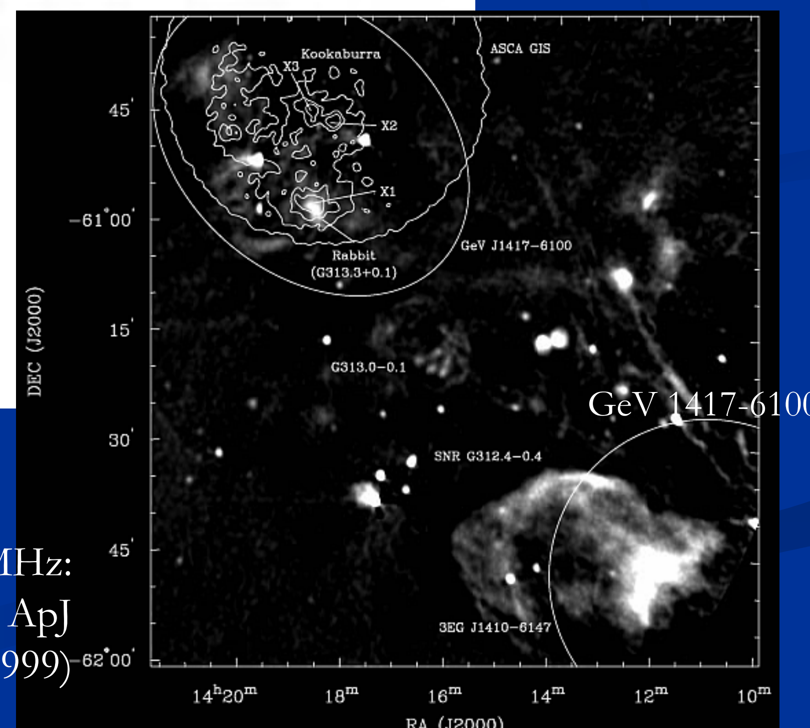

MOST 843MHz:
Roberts et al., ApJ 515, 712 (1999)

R.Yamazaki et al., MNRAS 371, 1975 (2006)

Old SNRs: large $F_{\mathrm{TeV}}/F_{\mathrm{X}}$

Age ~ 10^3 yr

B ~ *10~*100 μG

$E_{p,max}=10^{2\text{-}3}$TeV

$E_{e,max}$~ 10TeV

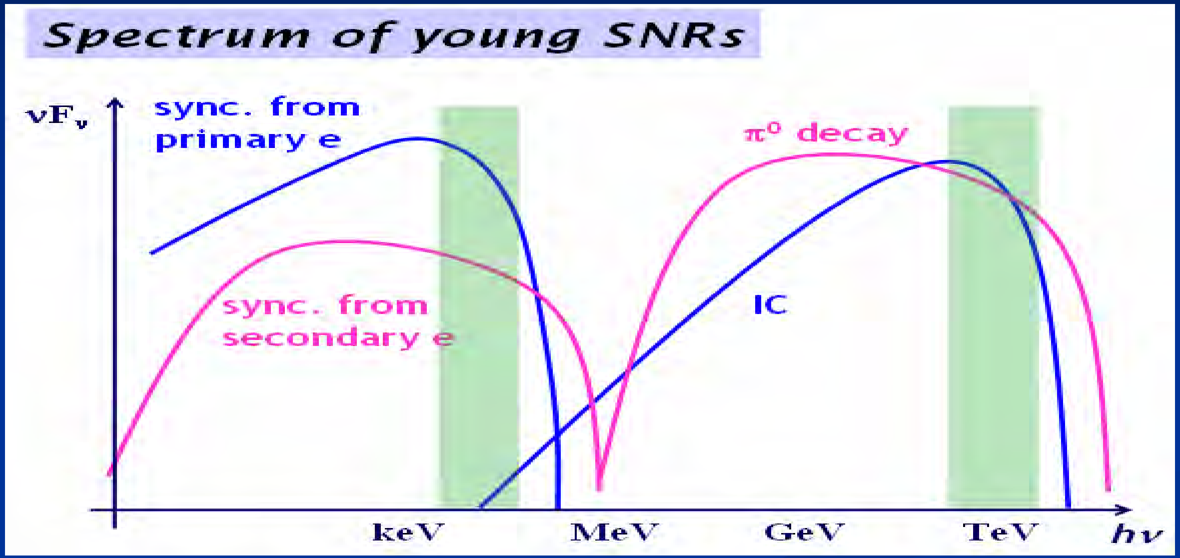

Age ~ 10^5 yr

B ~ 100 μG

$E_{p,max}=10^{1\text{-}2}$TeV

$E_{e,max}$~ 0.1 TeV

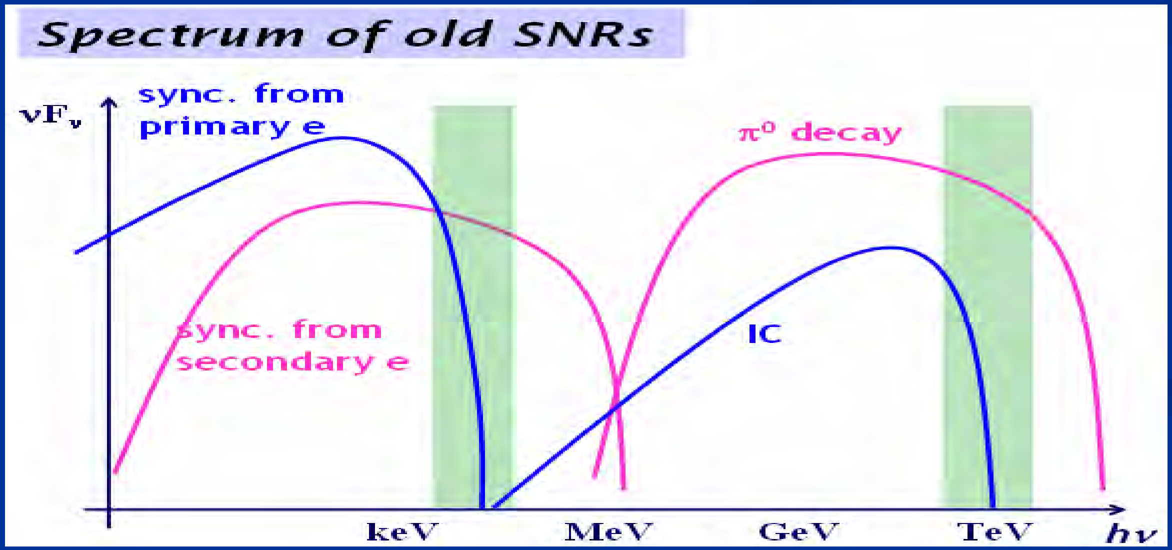

Dim in X:

HESS unID?

Extragalactic sources: basics

- Active galactic nuclei
  - Blazars
    - Wide-band spectrum – nonthermal
    - Quasars – LBL (RBL) – HBL (XBL) sequence
    - Leptonic models
      - SSC or EC (External Compton)
    - Hadronic models
      - Proton-initiated cascades
  - Radio galaxy,…
- Gamma-ray absorption by EBL (Extragalactic Background Radiation)
  - Infrared photon field: uncertain
- Center of galaxies
  - Accumulation of dark matter??
- Extragalactic background radiation

Blazars

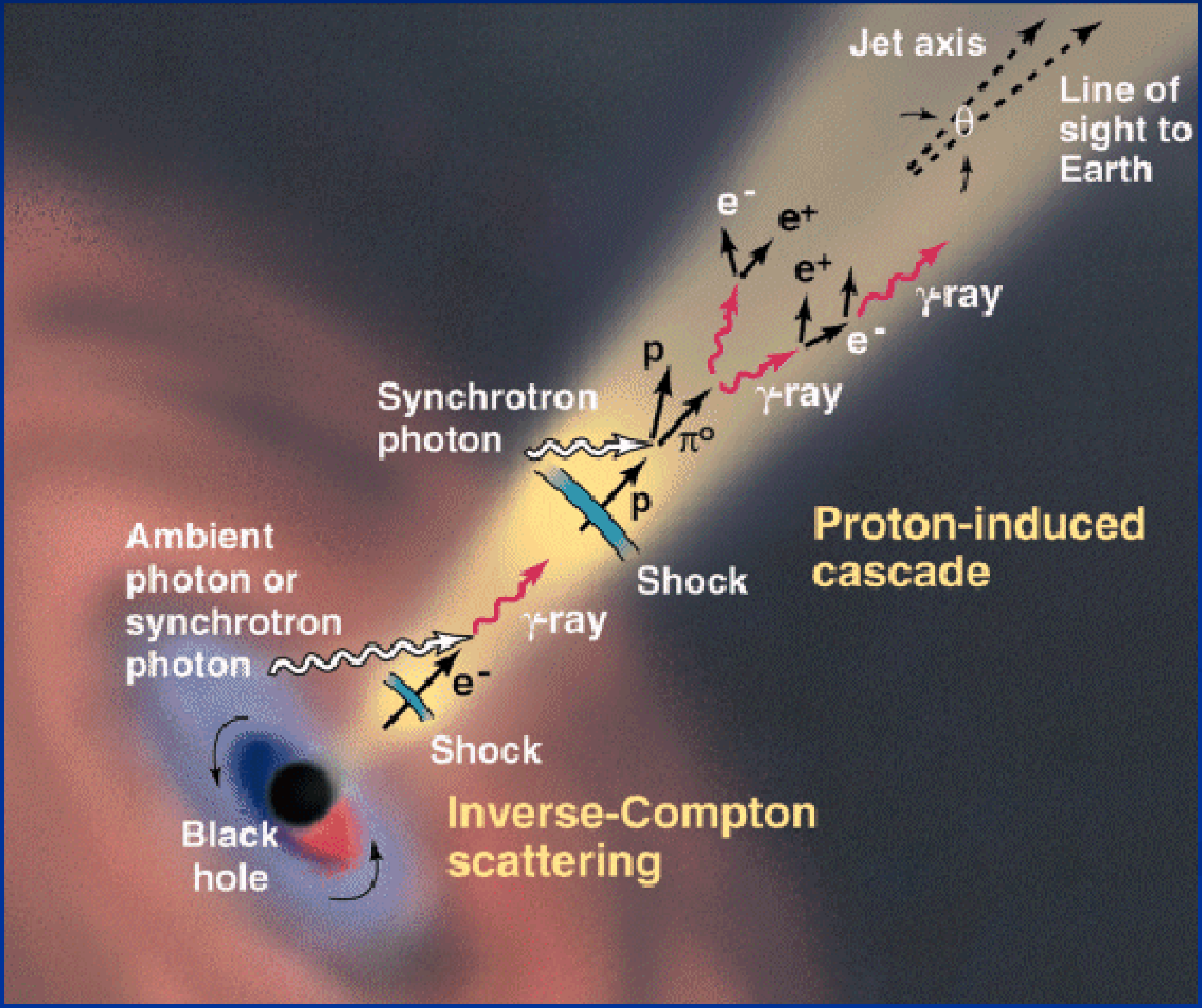

Beaming factor

$\delta \equiv 1/\Gamma\ (1-\beta\cos\theta) > 1$

Observed frequency

$\nu \propto \nu_0 \delta$

Apparent luminosity

$L \propto L_0 \delta^4$

“Known” extragalactic sources

- Mrk421 (z=0.031)
  - First detection in 1992 [Punch et al. Nature 1992]
  - Flares in 1994, 1996, 2001, 2002-3
- Mrk501 (z=0.034)
  - First detection in 1995 [Quinn et al. ApJ 1996]
  - Large flares in 1997
- 1H1426+428 (z=0.129)
  - First detection in 2001 [Horan et al. 5th Compton 2001]
  - Flares in 2001

Multiwavelength spectra of blazars

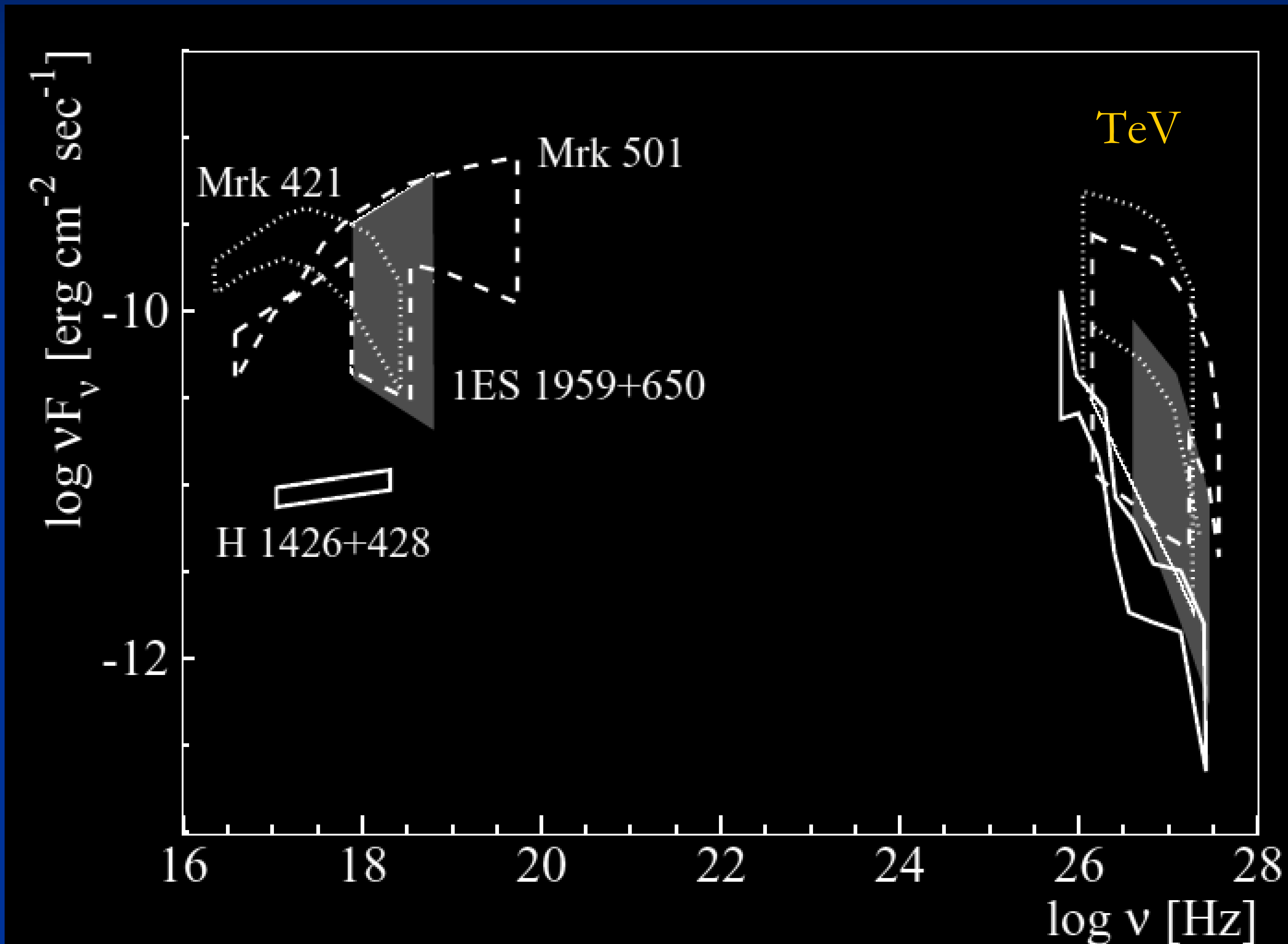

Fig. 1. Simultaneous and non-simultaneous X-ray and TeV γ-ray energy spectra of the 4 TeV blazars with measured TeV γ-ray energy spectra. The regions show the range of values that have been observed with BeppoSAX, RXTE and Cherenkov Telescopes (from ([46])).

Krawczynski, astro-ph/0309443

Synchrotron self-Compton model

- Synchrotron + inverse Compton model works well
  → $e^{\pm}$ origin
  (SSC: Synchrotron Self Compton)

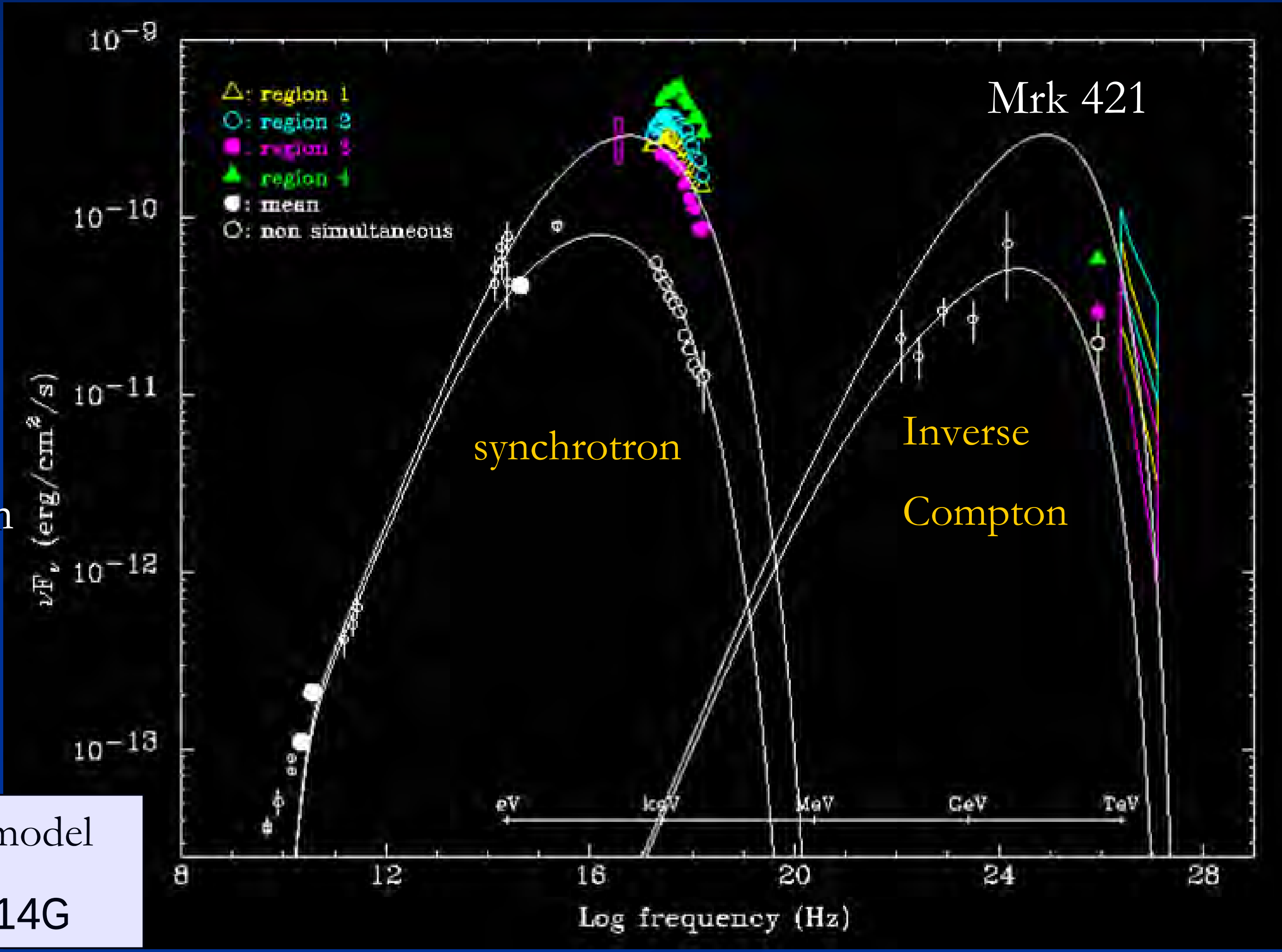

One-zone SSC model

δ =14, B=0.14G

Takahashi et al. ApJ 542, 2000

Synchrotron proton blazar model (1)

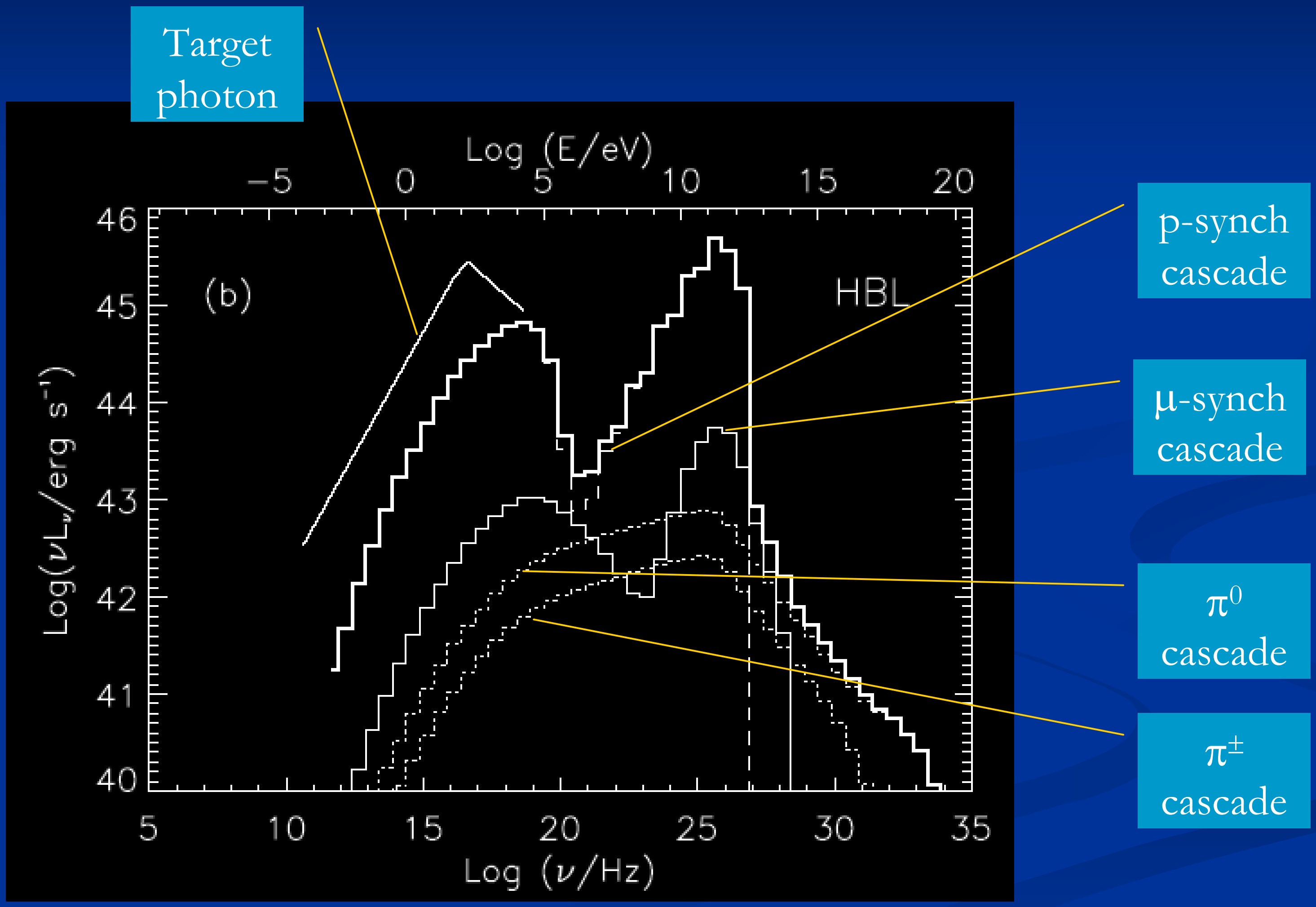

Muecke et al. APh 18, 2003

Synchrotron proton blazar model (2)

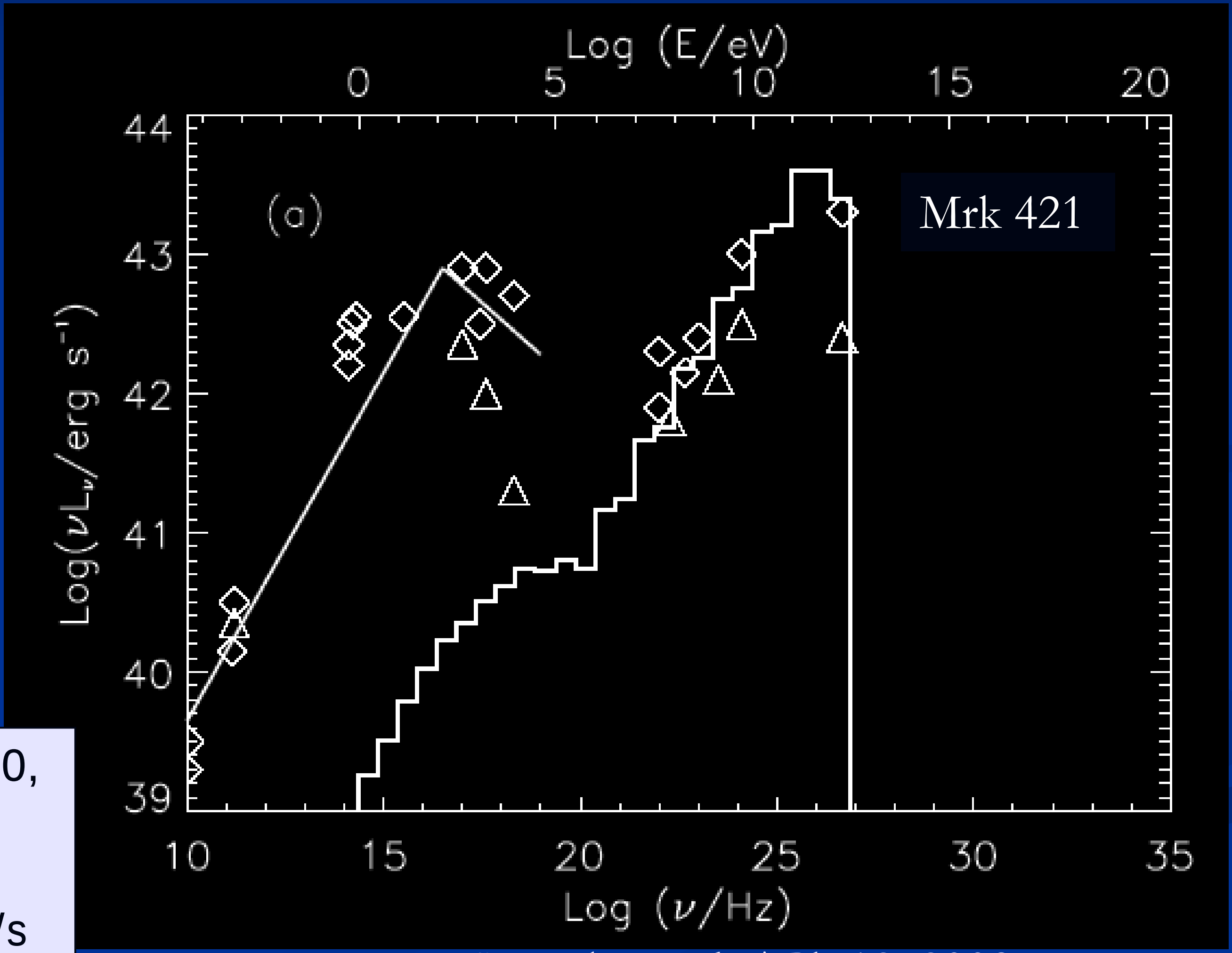

$dF/dE \propto E_p^{-2}$, $\delta=10$,
B=30G,
$\gamma_{max,p}=4\times10^{10}$,
$L_{jet}=9\times10^{44}$erg/s

Muecke et al. APh 18, 2003

AGN summary

Source	Redshift	Type	First detection	Confirmation
M87	0.004	FR I	HEGRA	H.E.S.S.
Mrk 421	0.031	BL Lac	Whipple	Many
Mrk 501	0.034	BL Lac	Whipple	Many
1ES 2344+514	0.044	BL Lac	Whipple	HEGRA
1ES 1959+650	0.047	BL Lac	7TA	Many
PKS 2005-489	0.071	BL Lac	H.E.S.S.	
PKS 2155-304	0.116	BL Lac	Durham	H.E.S.S.
H1426+428	0.129	BL Lac	Whipple	Many
H2356-309	0.165	BL Lac	H.E.S.S.	
1ES 1218+304	0.182	BL Lac	MAGIC	
1ES 1101-232	0.186	BL Lac	H.E.S.S.	

⇒ **Reaching further out in redshift!**

TeV gamma-ray absorption on EBL (1)

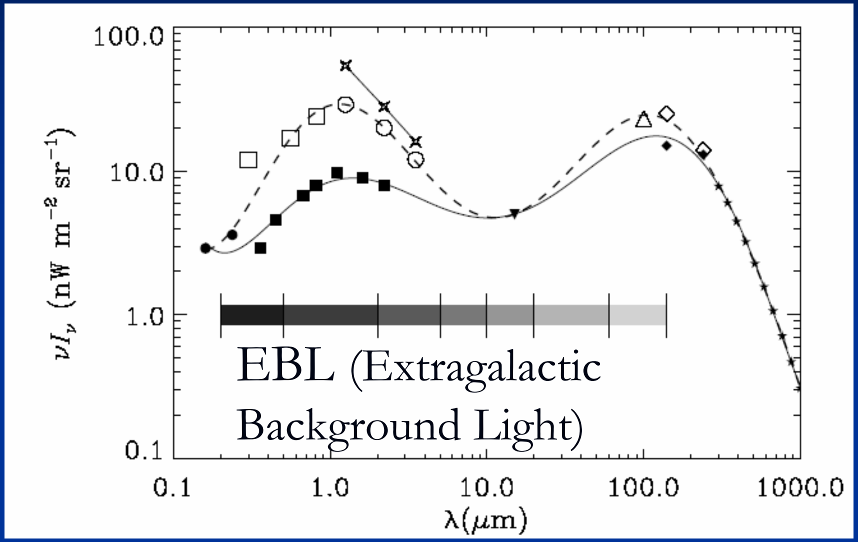

$$\gamma_{TeV} + \gamma_{IR} \rightarrow e^+ + e^-$$

Mean free path for e^+e^- pair production

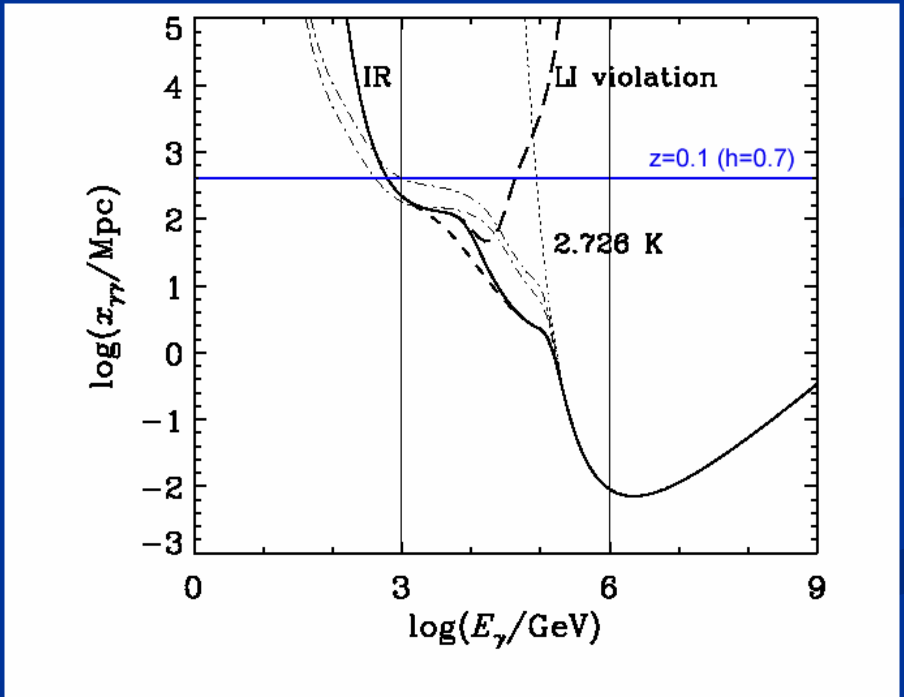

Figure 2: Mean free path for photon-photon pair production in the infrared–microwave background radiation. The curves correspond to those in Fig. 1 except that the effect of Lorentz Invariance violation discussed in Section 4 is shown by the long dashed curve.

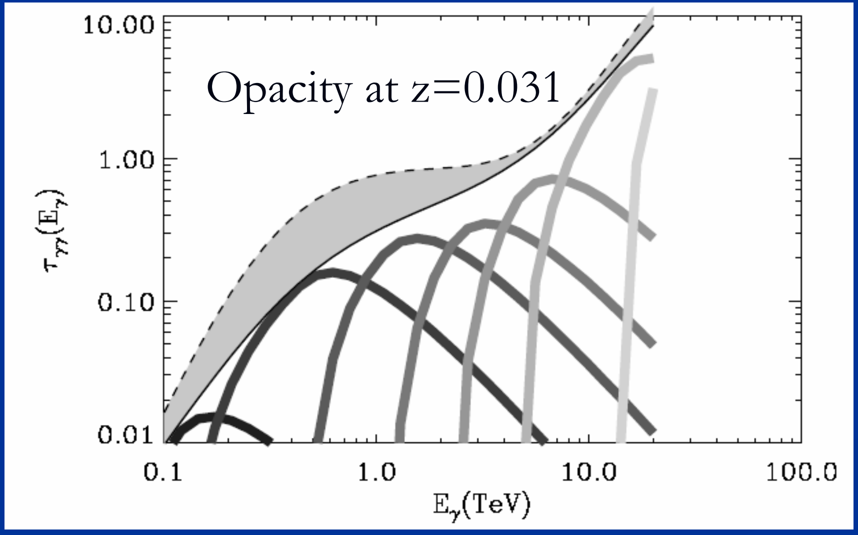

Dwek, "Universe Viewed in Gamma-rays", Kashiwa, 2002

Protheroe & Meyer, Phys.Lett. B493 (2000) 1

H.E.S.S.: Aharonian et al., Nature 440, 1018 (2006)

TeV gamma-ray absorption on EBL (2)

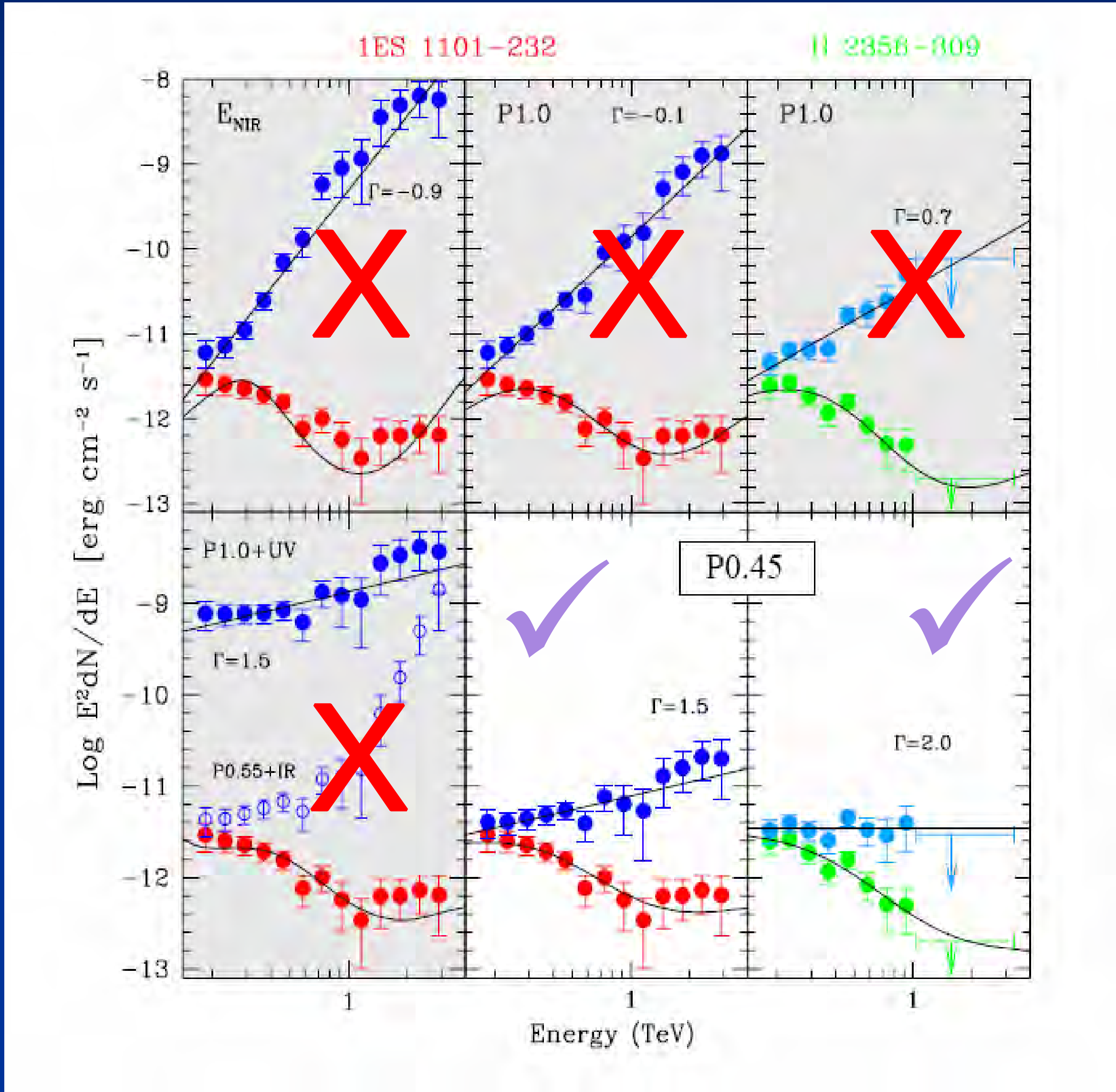

H.E.S.S.: Aharonian et al., Nature 440, 1018 (2006)

EBL Spectra

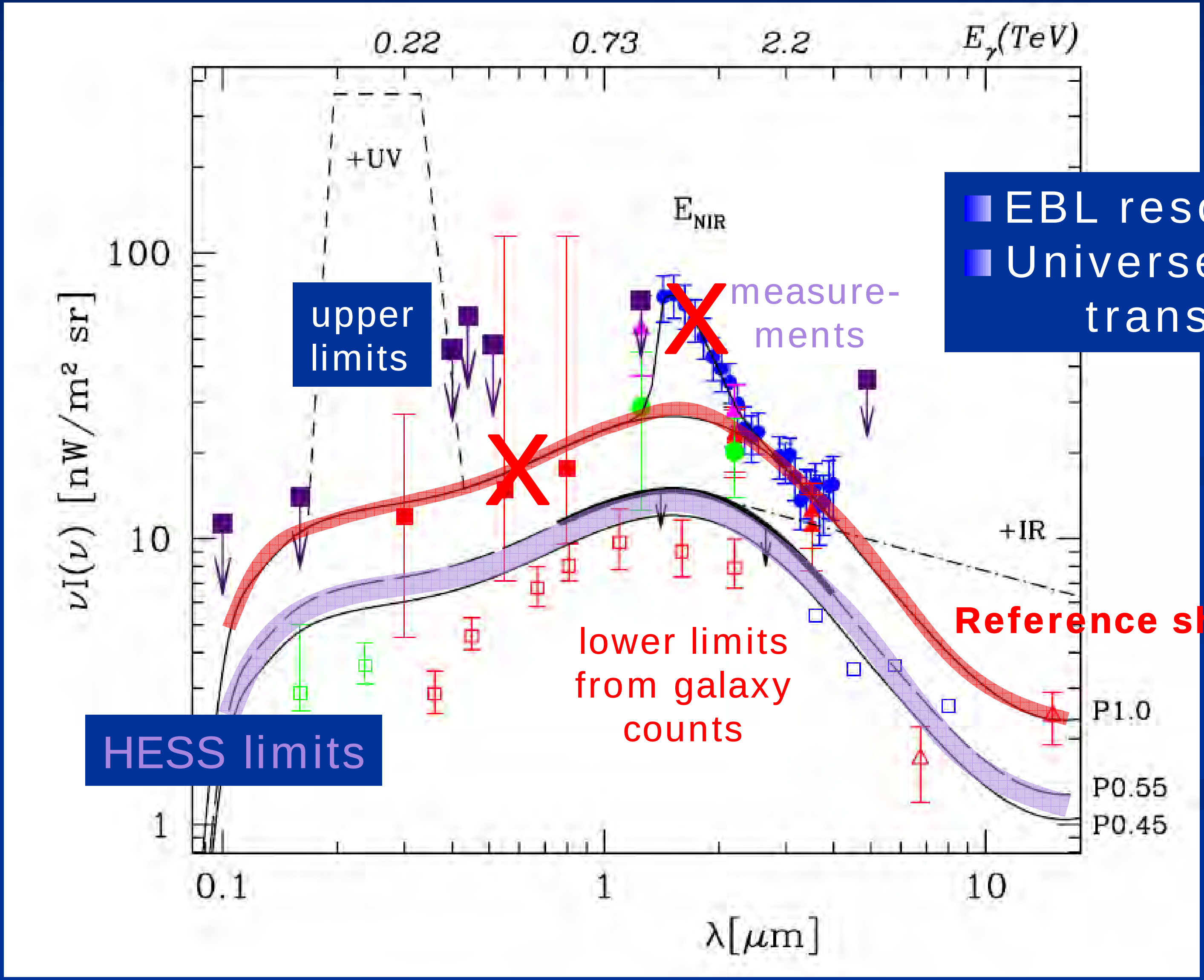

- EBL resolved
- Universe more transparent

Flare of PKS 2155-304 in 2006 (1)

PKS 2155-304: 2006 outburst, VERY PRELIMINARY

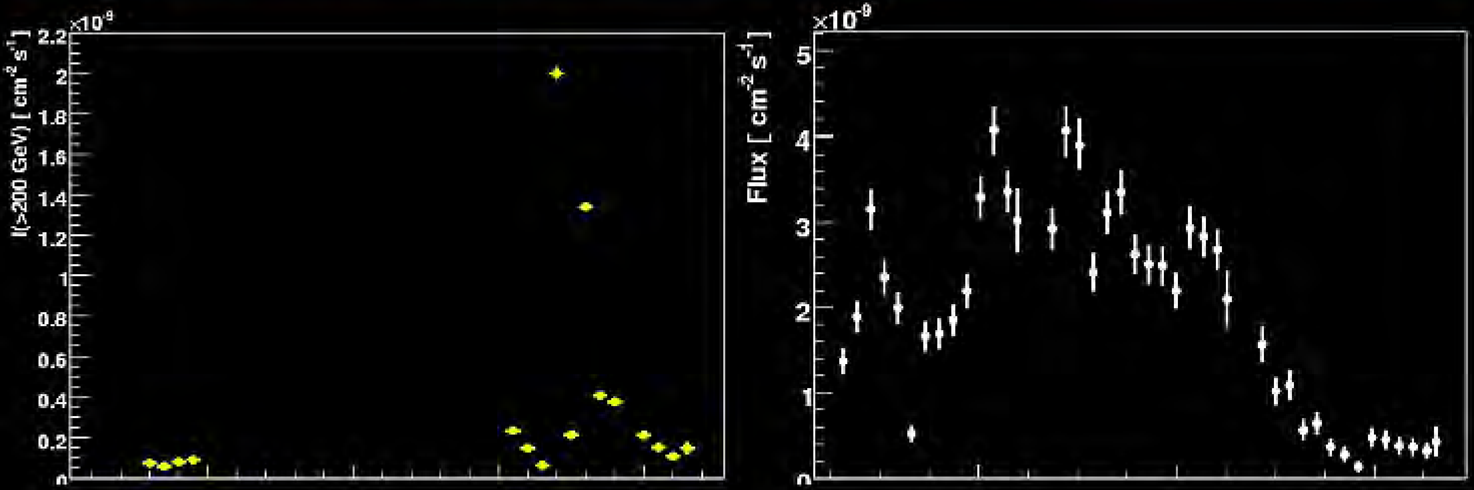

- Huge flux level triggered ATel, MWL observations
- $2'$-minute lightcurve binning shows doubling timescales at $\approx 5'$
- Complex lightcurve with possibly substructures (to be confirmed with final analysis)
- Simultaneous RXTE, Swift, Chandra, optical observations

Flare of PKS 2155-304 in 2006 (2)

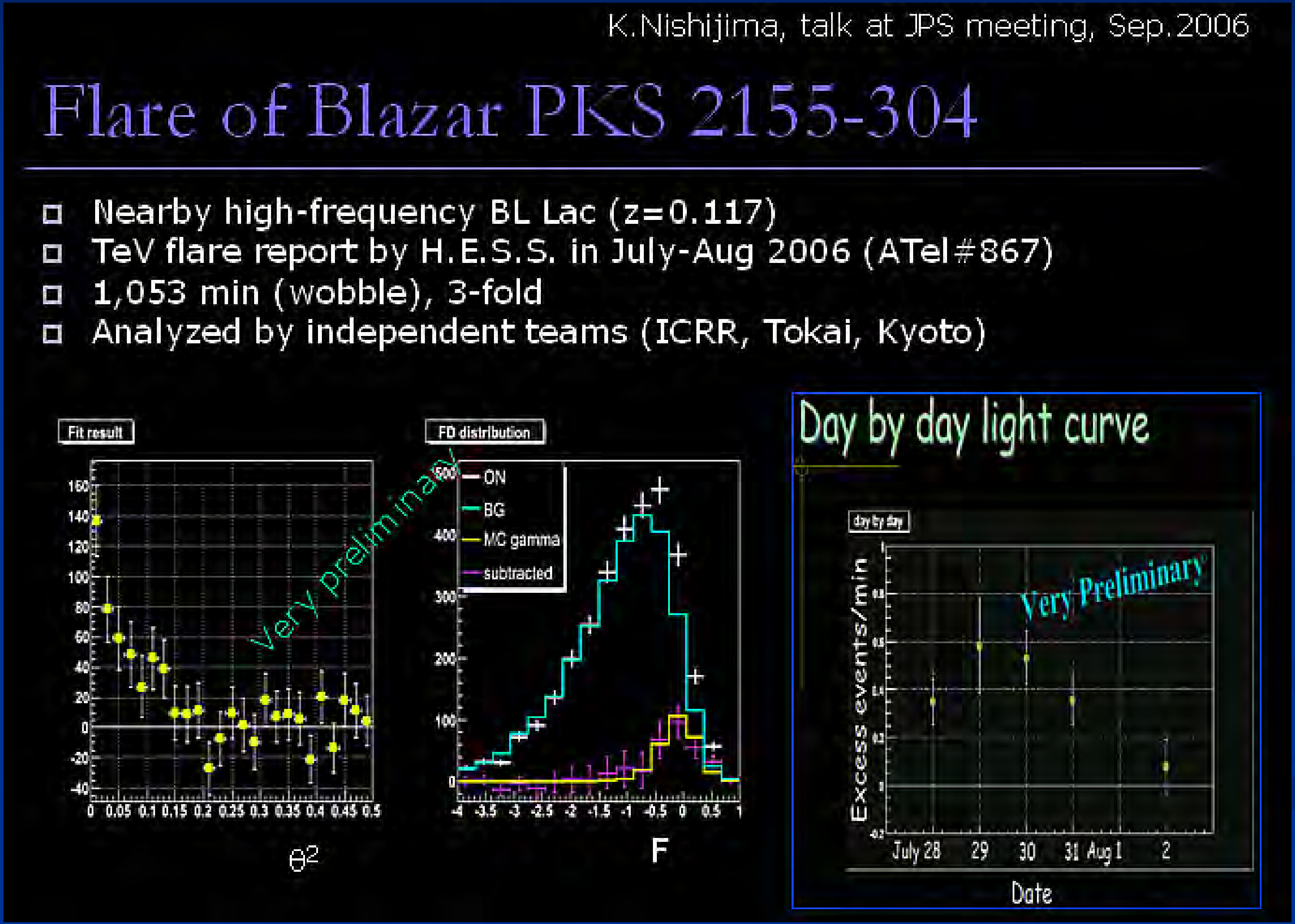

TeV gamma-ray absorption on EBL (3)

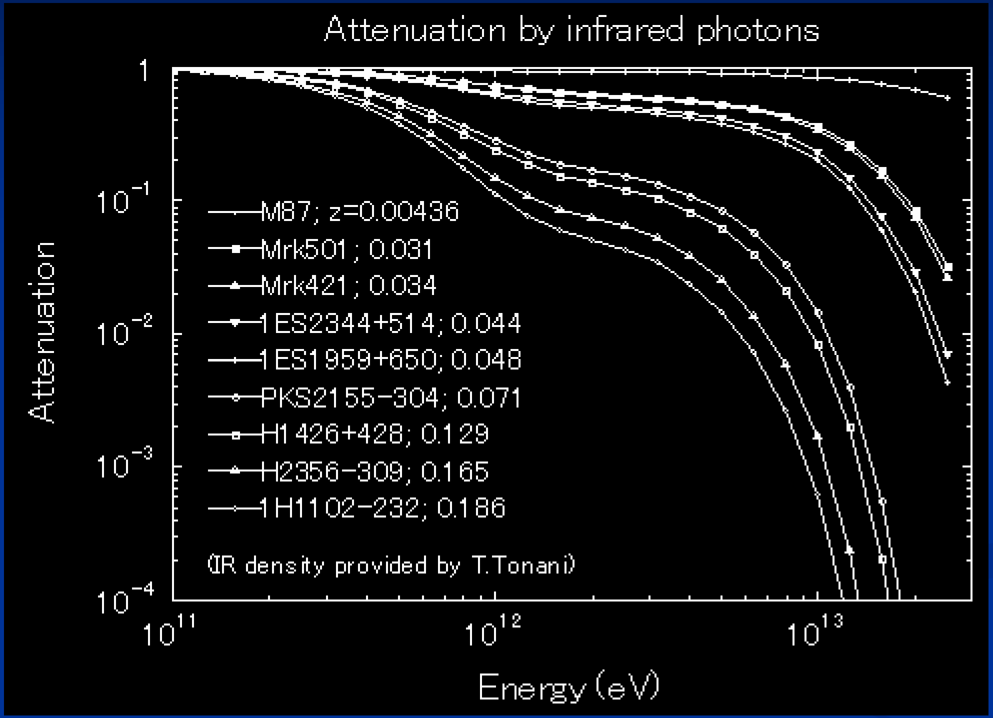

We need many samples of AGNs at various redshifts!

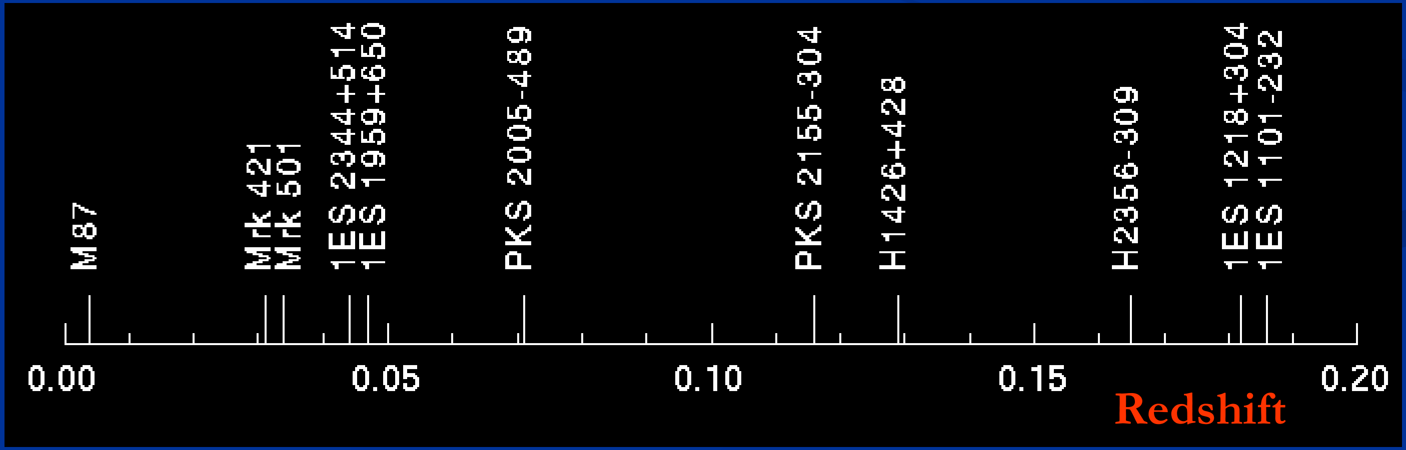

H.E.S.S.: F. Aharonian et al., Astron. Astrophys. 446, L19 (2006)

PG1553+113: even further away?

BL Lac, z >0.25 (possibly >0.78 ?)

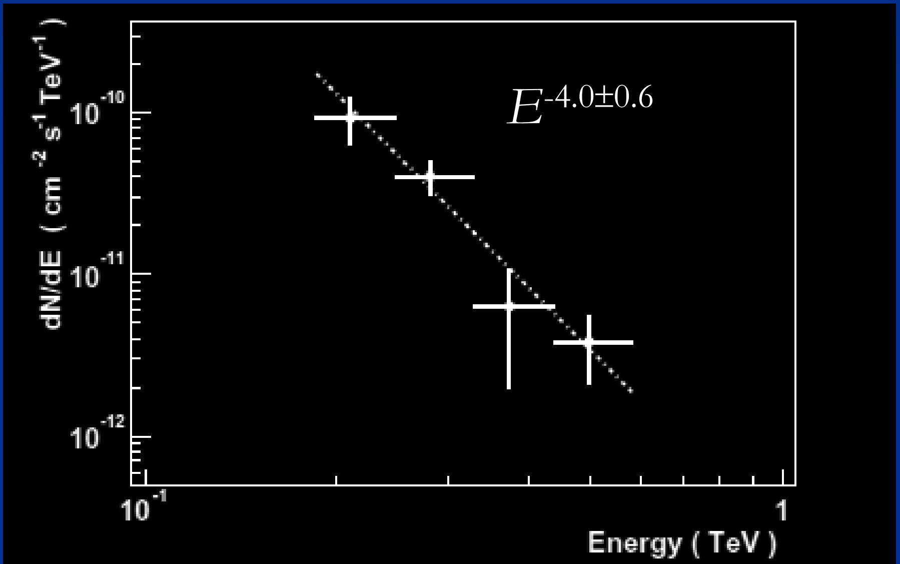

Fig. 2. The energy spectrum of PG 1553+113. The horizontal error bars indicate the energy bin size. The dashed line represents the best χ^2 fit of a power law.

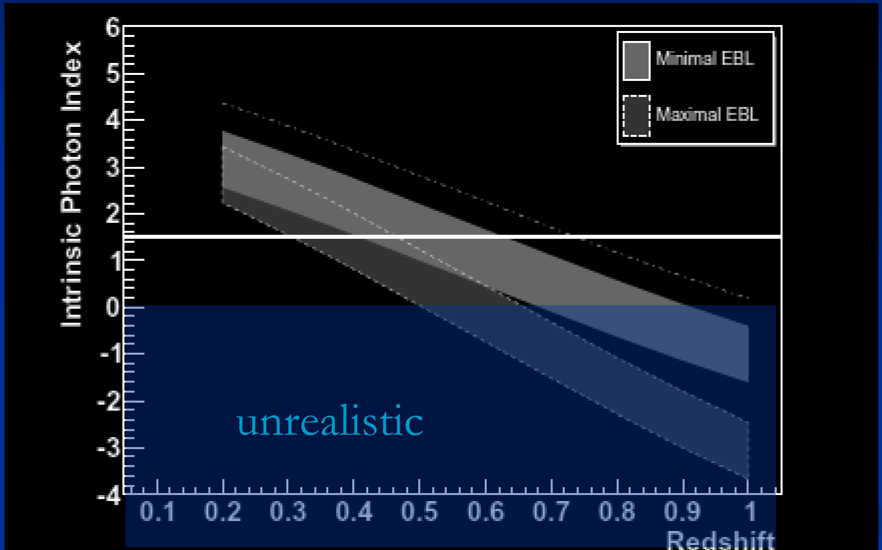

Fig. 3. The intrinsic photon index of PG 1553+113, with 1σ statistical error contours, versus redshift for the cases of *minimal* and *maximal* EBL absorption. An intrinsic photon index below the horizontal line ($\Gamma_{\rm int}$=1.5) is not considered realistic. The uppermost (dashed-dotted) curve is the sum of the intrinsic photon index and 2σ statistical error for the case of minimal EBL absorption.

⇒ Upper limit: z < 0.74

Cf. Conservative limit from non-detection of features by VLT: z>0.09
Sbarufatti et al., astro-ph/0601506

Confirmed by MAGIC: Albert et al., astro-ph/0606161

Costamante and Ghisellini A&A 384 (2002) 56

TeV blazar population

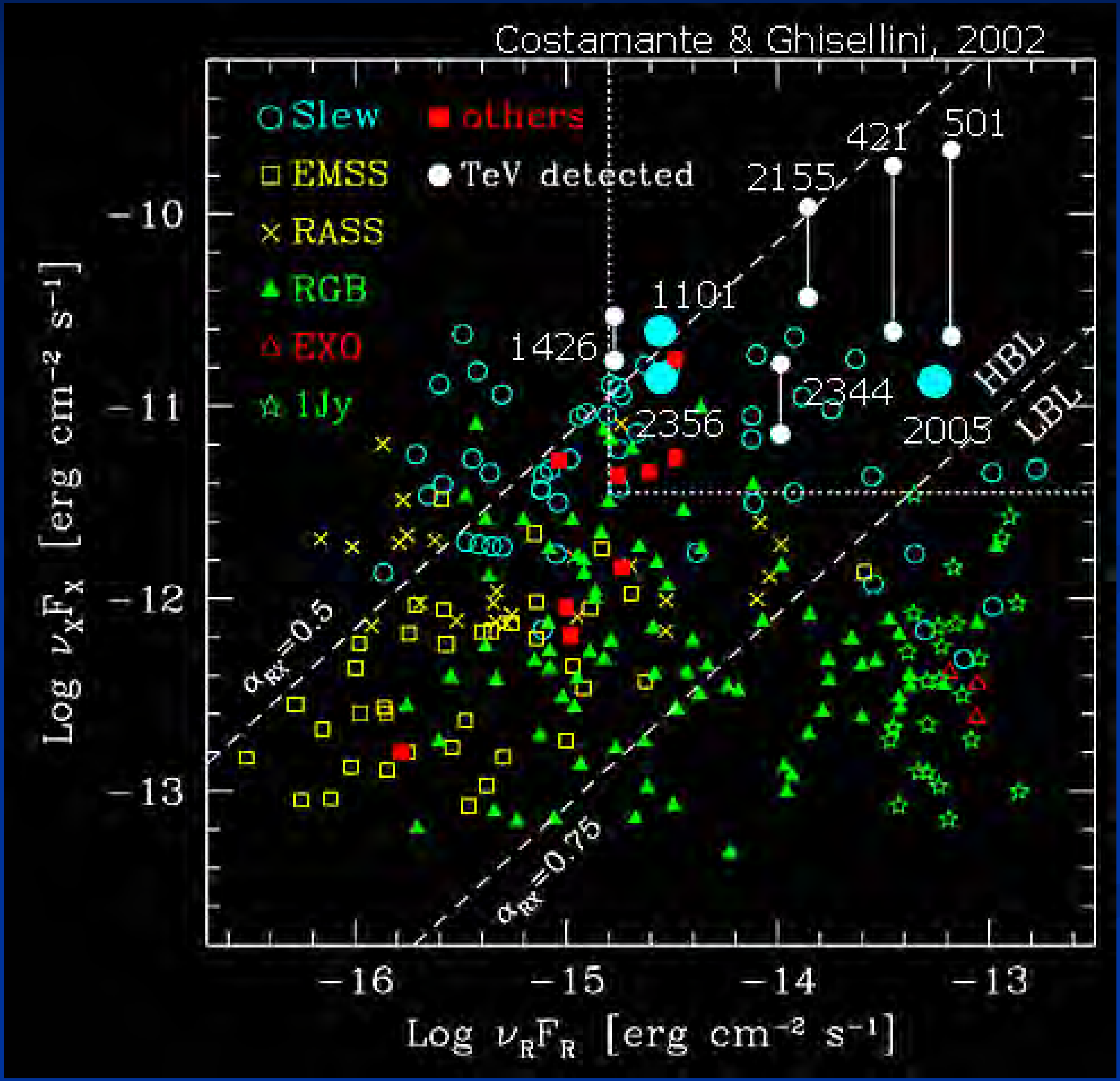

Redshift distribution of blazars

Model Fit to Blazar Redshift Distribution

Fit parameters for the FSRQs are Γ = 8 and comoving directional luminosity $l = 10^{40}$ ergs sr^{-1} s^{-1}; EC statistics

Fit parameters for the BL Lacs are Γ = 5 and $l = 10^{42}$ ergs sr^{-1} s^{-1}; syn/SSC statistics

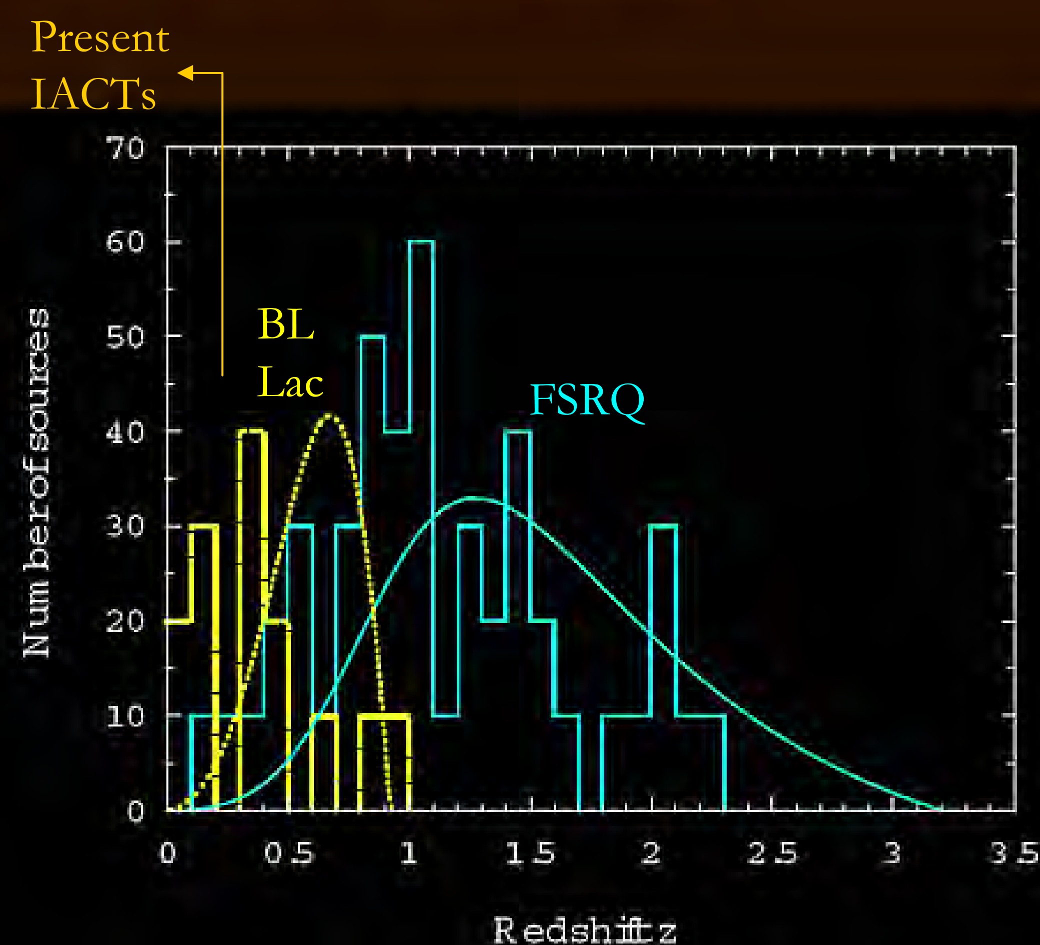

H.E.S.S.: F. Aharonian et al., Science Express, Oct.26, 2006

Radio galaxy M87 (1)

Or Vir A, Giant radio galaxy, z=0.00436 or 16Mpc)

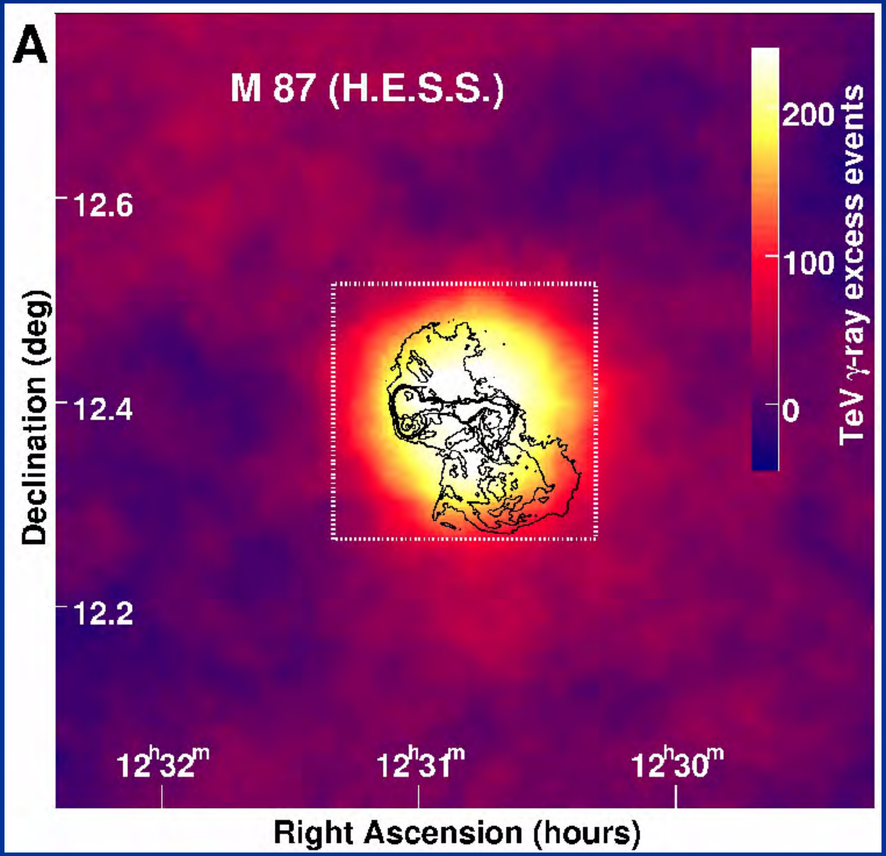

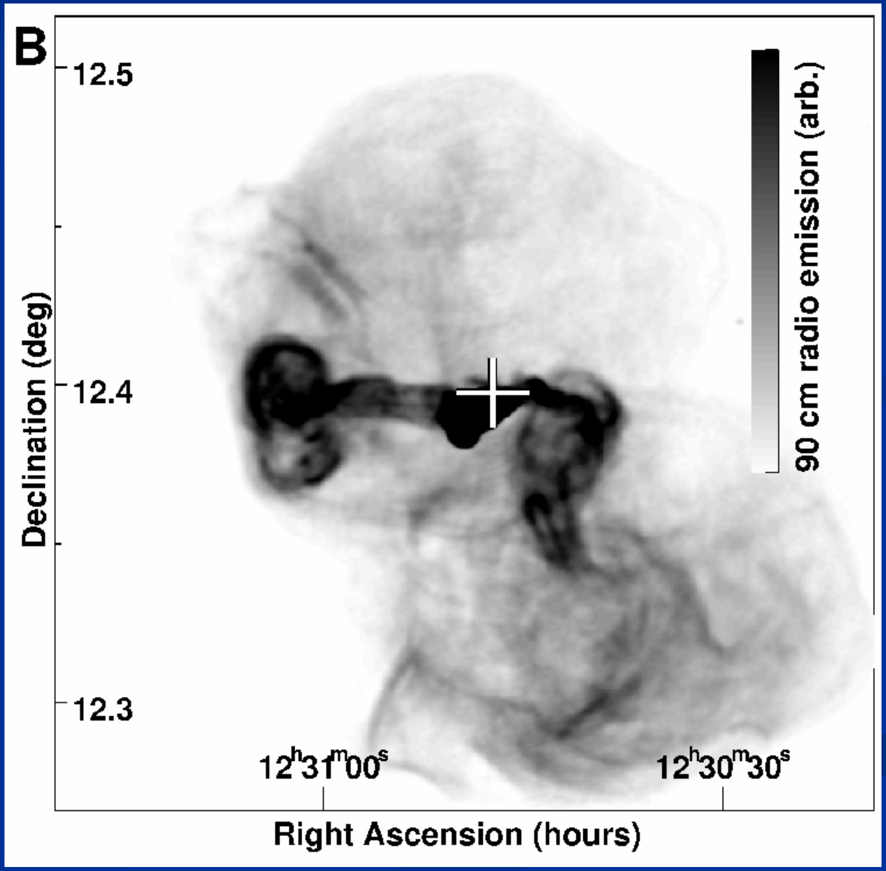

H.E.S.S.: F. Aharonian et al., Science Express, Oct.26, 2006

Radio galaxy M87 (2)

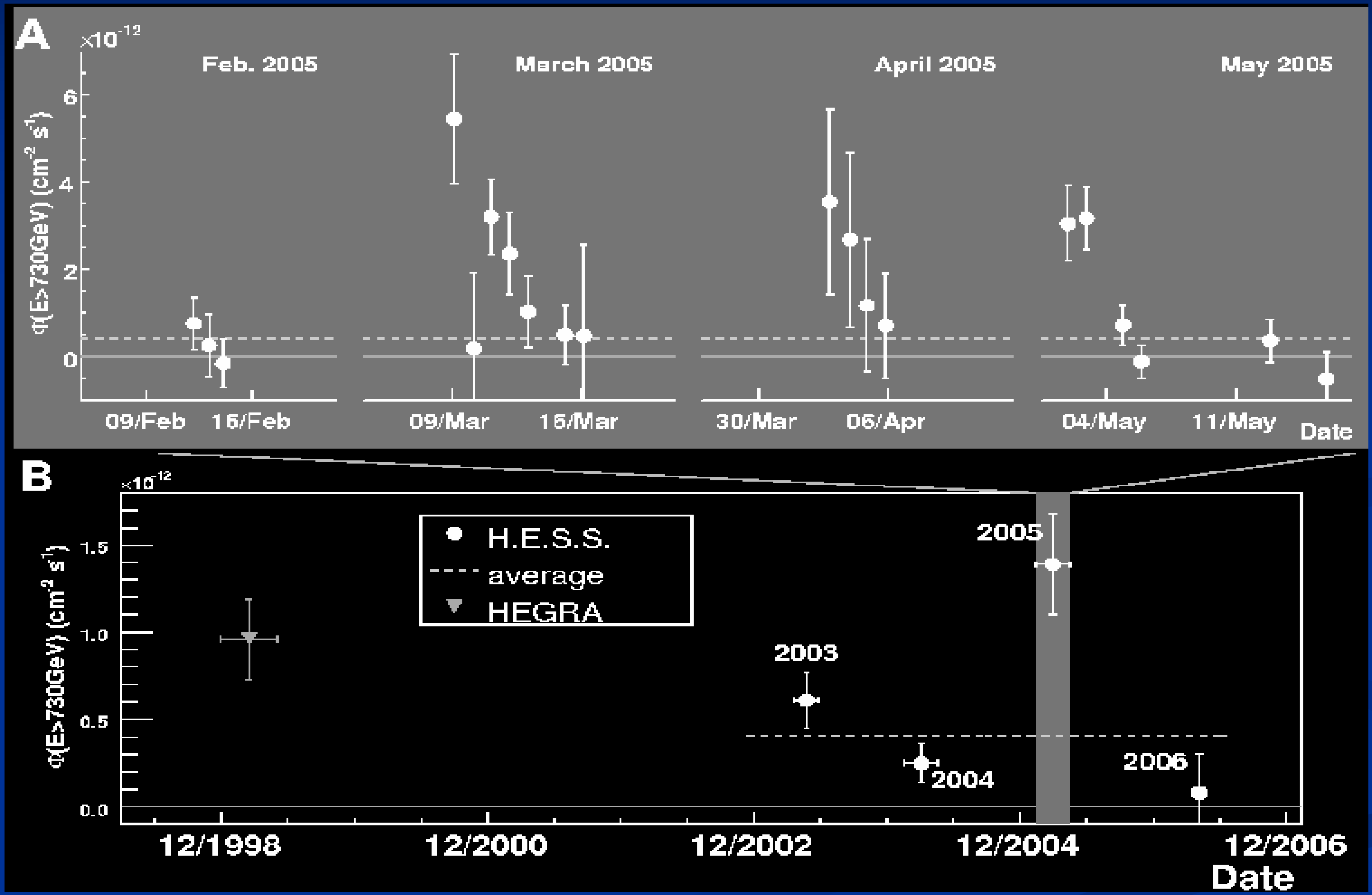

Time scale of a few days ↔ Region size ~ 10^{13}m ≈ $R_{Sch}(3\times10^9 M_\odot)$!

↔ Particle acceleration near the central black hole !

Galactic diffuse gamma-rays (1)

EGRET >100MeV

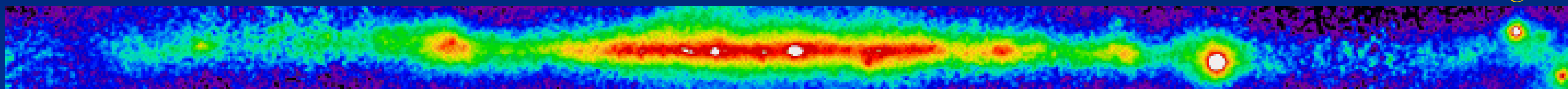

>90% of EGRET-detected photons are diffuse!

- EGRET "GeV bump" (Hunter et al. ApJ 1997)

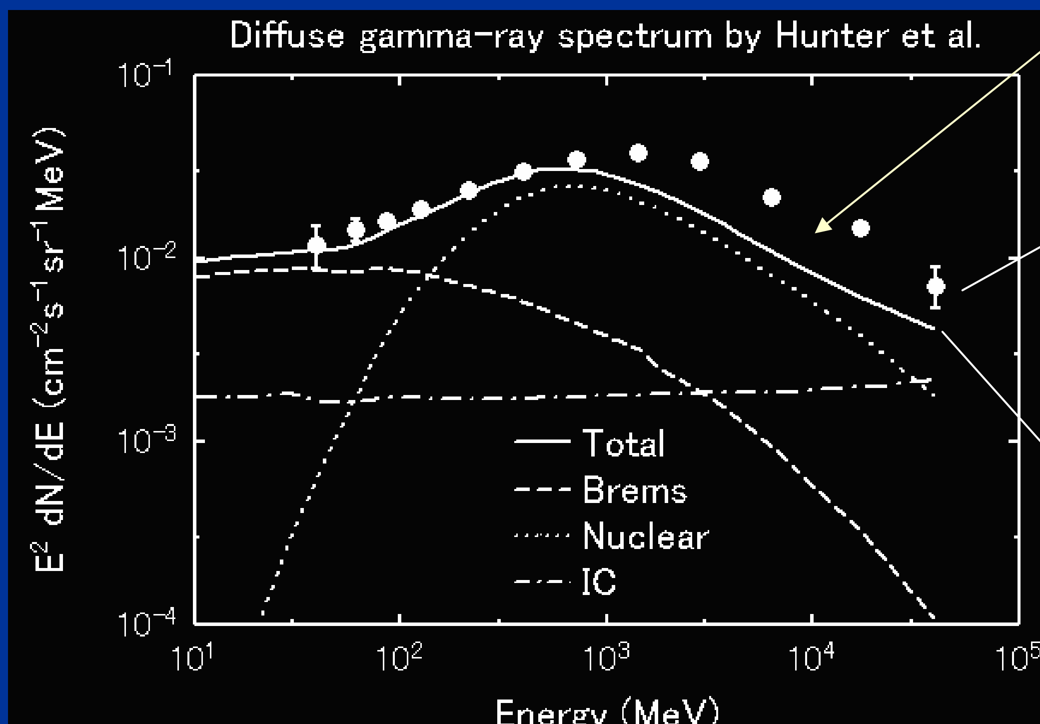

Galactic diffuse gamma-rays (2)

OG 2.1: Diffuse γ-ray Sources

1. Galactic Plane

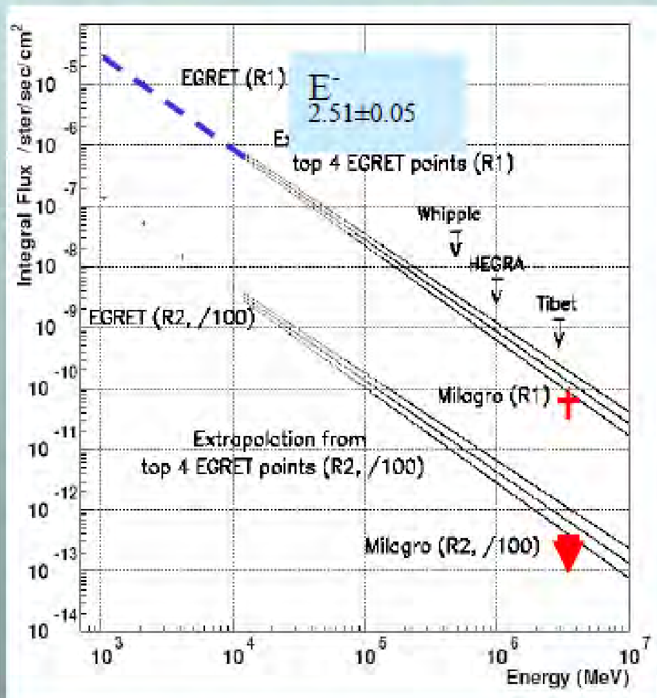

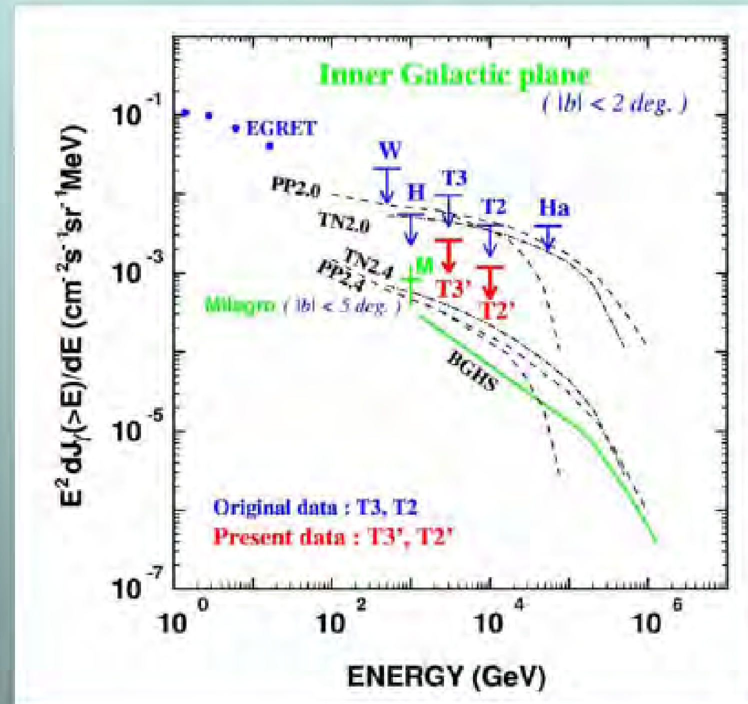

Milagro [Sinnis]
~ 4.5σ detection in 3 yr data set.
Inner region:
40-100° in longitude, ± 5° in latitude

Tibet [Ohnishi]
Flux upper limit, consistent with Milagro detection.

H.E.S.S.: F.Aharonian et al., Nature 439, 695 (2006)

Diffuse gamma-rays along the plane (1)

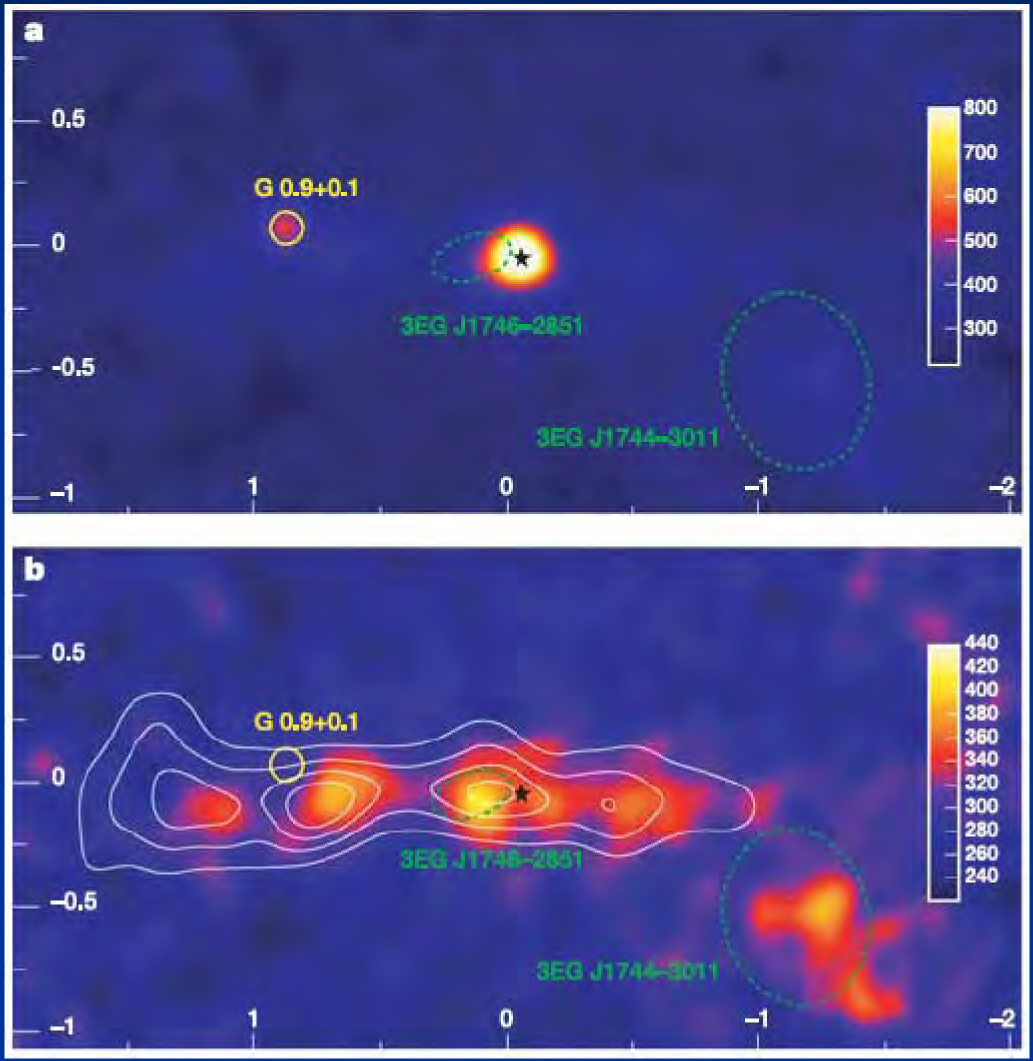

Figure 1 | VHE γ-ray images of the Galactic Centre region. a, γ-ray count map; **b**, the same map after subtraction of the two dominant point sources, showing an extended band of gamma-ray emission. Axes are Galactic latitude (x) and Galactic longitude (y), units are degrees. The colour scale is in 'events' and is dimensionless. White contour lines indicate the density of molecular gas, traced by its CS emission. The position and size of the composite supernova remnant G0.9+0.1 is shown with a yellow circle. The position of Sgr A* is marked with a black star. The 95% confidence region for the positions of the two unidentified EGRET sources in the region are shown as dashed green ellipses[20]. These smoothed and acceptance-corrected images are derived from 55 hours of data consisting of dedicated observations of Sgr A*, G0.9+0.1 and a part of the data of the HESS Galactic plane survey[21]. The excess observed along the Galactic plane consists of ~3,500 γ-ray photons and has a statistical significance of 14.6 standard deviations. The absence of any residual emission at the position of the point-like γ-ray source G0.9+0.1 demonstrates the validity of the subtraction technique. The energy threshold of the maps is 380 GeV, owing to the tight γ-ray selection cuts applied here to improve signal/noise and angular resolution. We note that the ability of HESS to map extended γ-ray emission has been demonstrated for the shell-type supernova remnants RXJ1713.7–3946 (ref. 22) and RX J0852.0−4622 (ref. 23). The white contours are evenly spaced and show velocity integrated CS line emission from ref. 11, and have been smoothed to match the angular resolution of HESS.

H.E.S.S.: F.Aharonian et al., Nature 439, 695 (2006)

Diffuse gamma-rays along the plane (2)

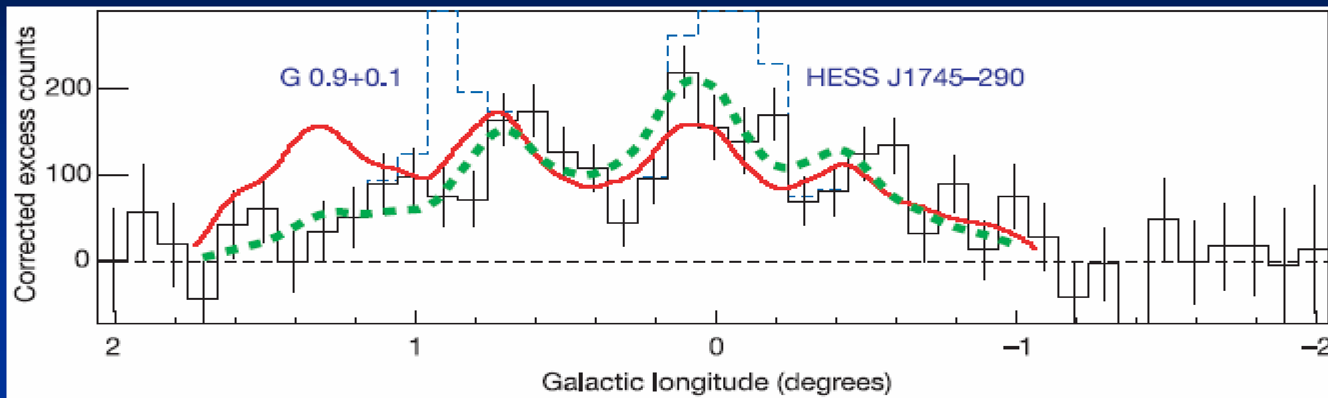

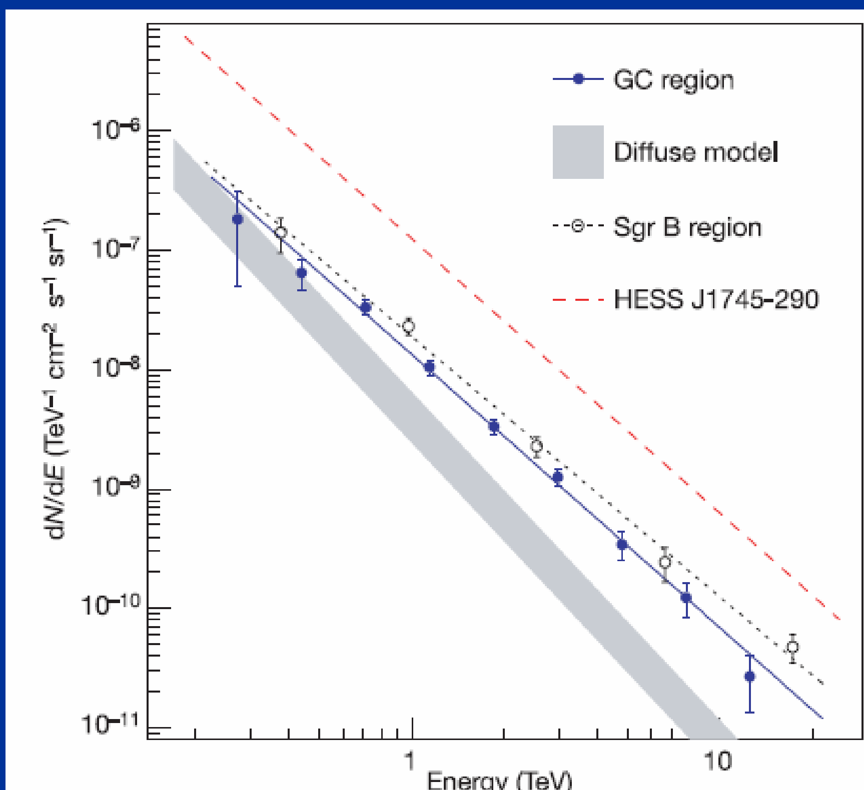

Figure 3 | Energy distribution of Galactic cosmic rays. γ-ray flux per unit angle in the Galactic Centre region (data points), compared with the expected flux, assuming a cosmic-ray spectrum as measured in the solar neighbourhood (shaded band). The spectrum of the region $|l| < 0.8°$, $|b| < 0.3°$ is shown using full circles. These data can be described by a power law: $dN/dE = k[E(\text{in TeV})]^{-\Gamma}$, with $k = (1.73 \pm 0.13_{stat} \pm 0.35_{sys}) \times 10^{-8}\ \text{TeV}^{-1}\ \text{cm}^{-2}\ \text{s}^{-1}\ \text{sr}^{-1}$ and a photon index $\Gamma = 2.29 \pm 0.07_{stat} \pm 0.02_{sys}$. The shaded box shows the range of expected π^0-decay fluxes from this region assuming a cosmic-ray spectrum identical to that found in the solar neighbourhood and a total mass of 1.7–4.4×10^7 solar masses in the region $|l| < 0.8°$, $|b| < 0.3°$ estimated from CS measurements. Above 1 TeV an enhancement by a factor of 3–9 relative to this prediction is observed. Using independent mass estimates derived from submillimetre measurements[24], $5.3 \pm 1.0 \times 10^7$ solar masses, and from $C^{18}O$ measurements[25], $3^{+2}_{-1} \times 10^7$ solar masses, results in enhancement factors of 4–6 and 5–13, respectively (see Supplementary Information). The strongest emission away from the bright central source HESS J1745–290 occurs close to the Sgr B complex of giant molecular clouds[26]. In a box covering this region ($0.3° < l < 0.8°$, $-0.3° < b < 0.2°$), integrated CS emission suggests a molecular target mass of 6–15×10^6 solar masses. The energy spectrum of this region is shown using open circles. The measured γ-ray flux (>1 TeV) implies a high-energy cosmic-ray density which is 4–10 times higher than the local value. Standard γ-ray selection cuts are applied here, yielding a spectral analysis threshold of 170 GeV. The spectrum of the central source HESS J1745−290 is shown for comparison (using an integration radius of 0.14°). All error bars show ±1 standard deviation.

Diffuse source in Cygnus? (1)

- Crosses are EGRET sources
- Contours are EGRET diffuse model
- TeV/matter correlation good in Galactic latitude
- Brightest TeV Region
  - Coincident with 2 EGRET sources (unidentified) 3EG J2016+3657 3EG J2021+3716
- *Analysis in progress*

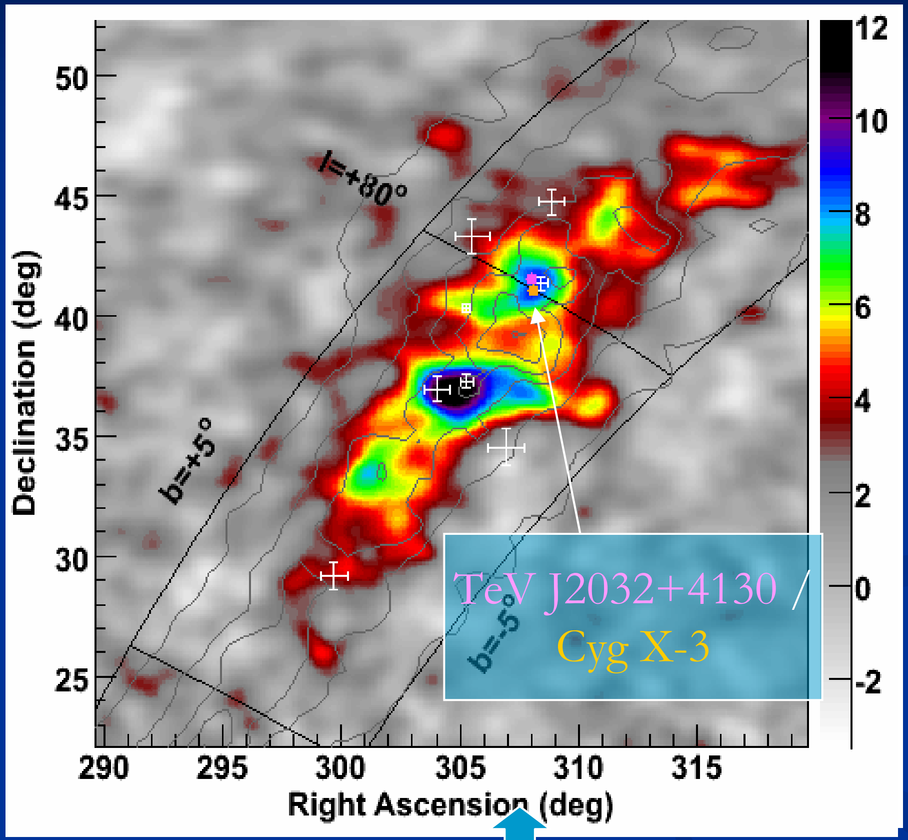

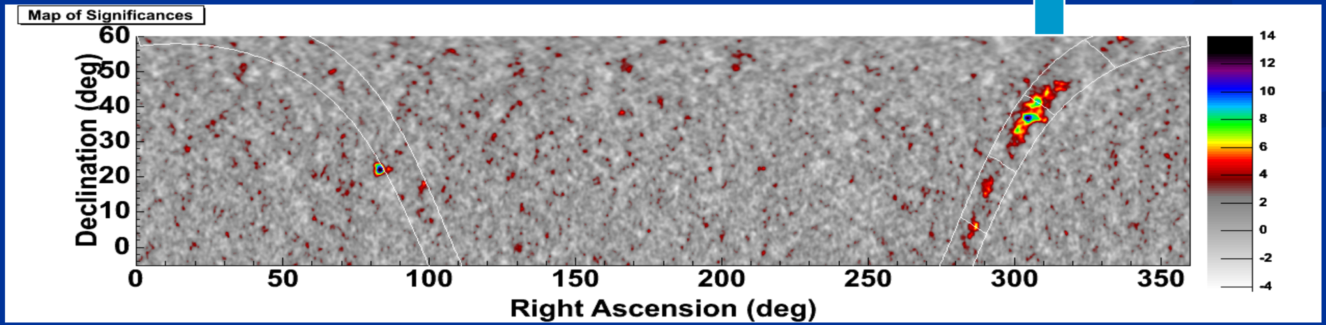

Tibet: Amenomori et al., Science 314, 439 (2006)

Diffuse source in Cygnus? (2)

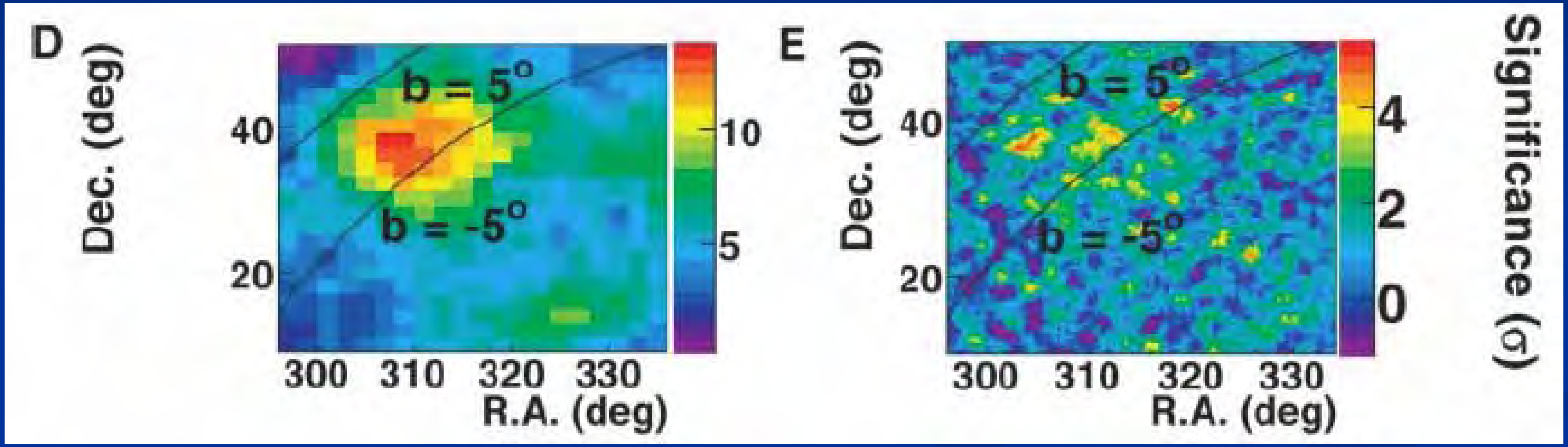

(D) and (E) show significance maps of the Cygnus region [pixels in radius of 0.9° and sampled over a square grid of side width 0.25° for (E)] for data from 1997 to 2005. The vertical color bin widths are 0.69 SD and 0.42 SD for significance in (D) and (E), respectively. Two thin curves in (D) and (E) stand for the Galactic parallel b=±5°. Small-scale anisotropies (E) superposed onto the large-scale anisotropy hint at the extended gamma-ray emission.

Diffuse source in Cygnus? (3)

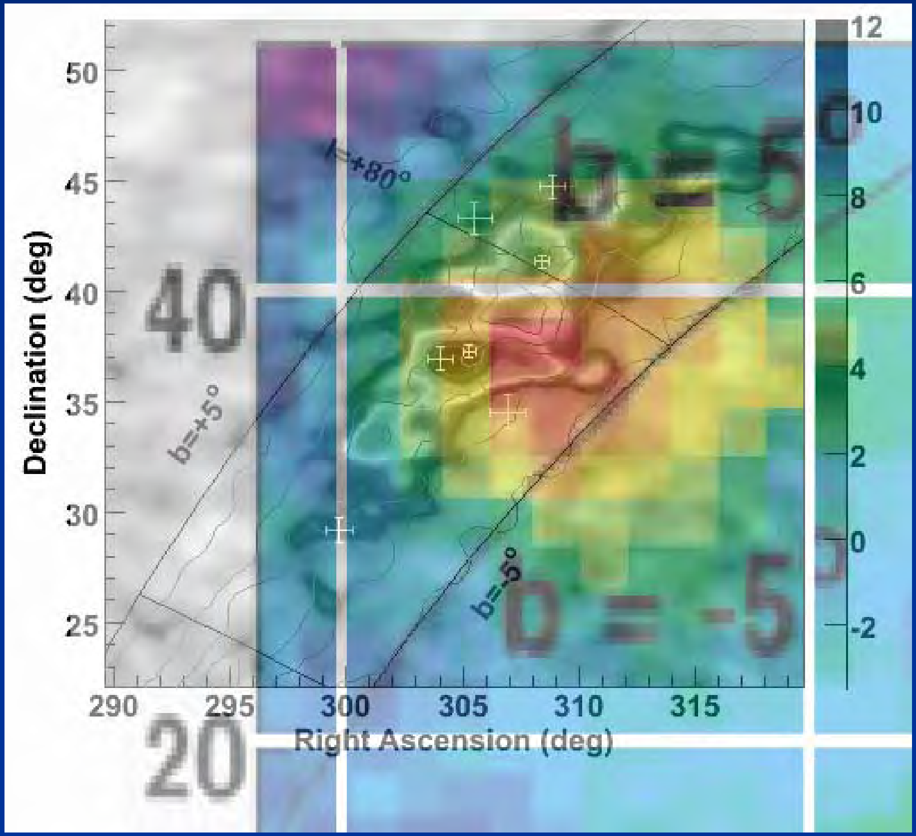

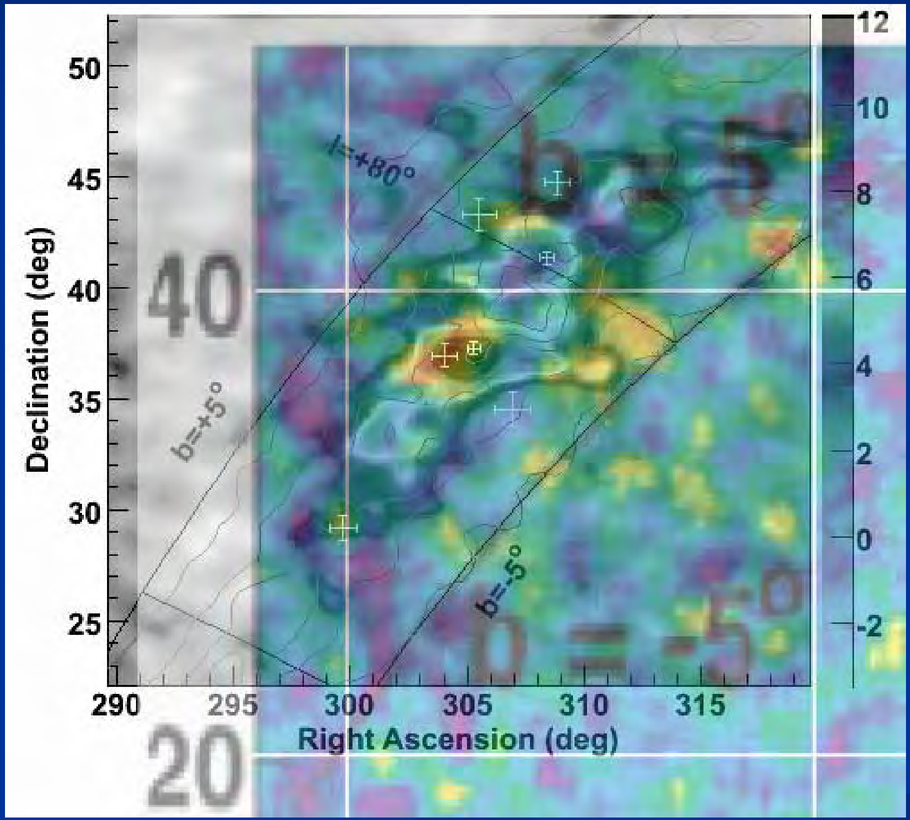

MILAGRO: A. Abdo, Santa Fe Workshop, May 2006

Tibet: Amenomori et al., Science 314, 439 (2006)

Gamma Ray Bursts

- Ground-based experiments?
  - TeV gamma-rays (afterglow)
    - MAGIC a few per year expected
  - Air shower rate
    - Tibet-III
  - Single particle rate
    - GRAND
    - ARGO-YBJ
    - Tibet-III
  - All-sky monitor
    - Ashra
- Need fast and precise GRB alerts!

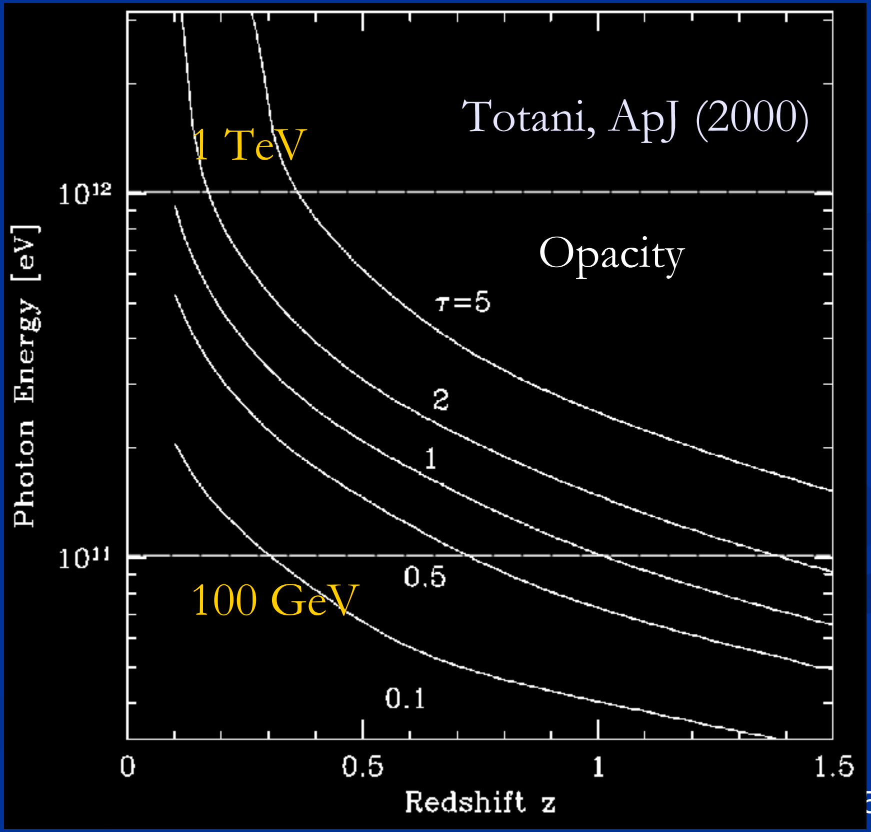

Hisano, Matsumoto, Nojiri PRL 92 (2004)

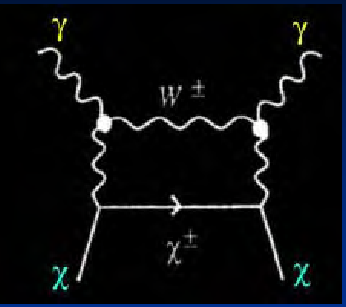

Dark matter annihilation

Signal enhancement due to `cusp' structure toward the center?

"Explosive annihilation" by non-perturvative effect

Line

Flux (cm^{-2}sec^{-1}) $\Delta\Omega = 10^{-3}$

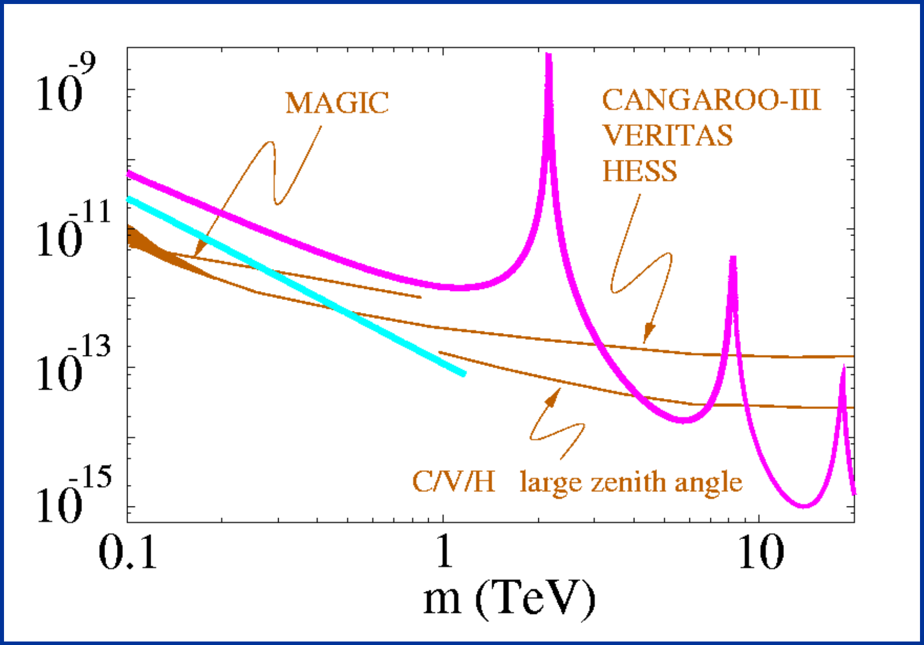

Continuum

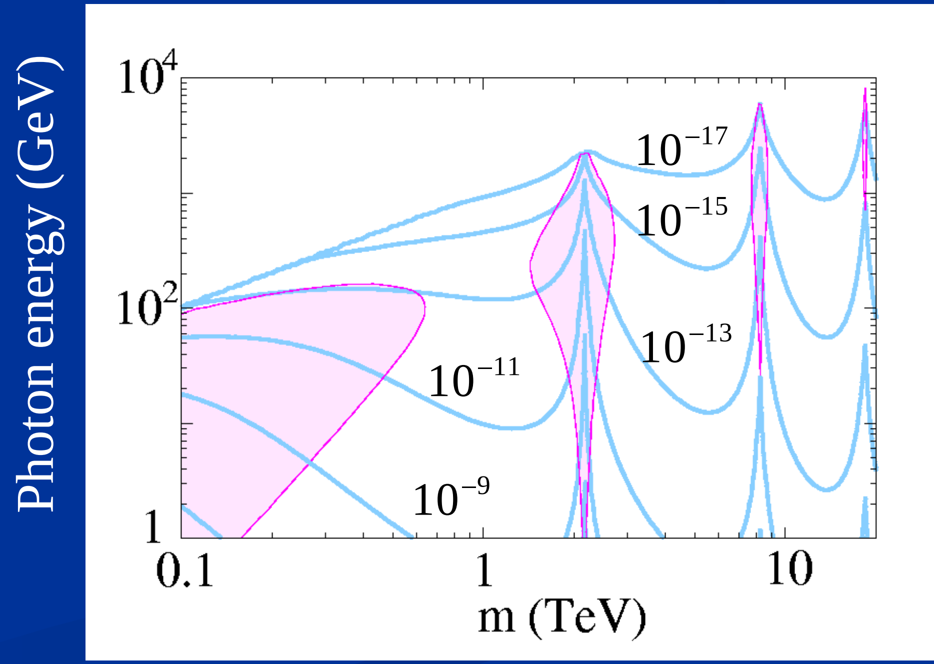

Source counts

Source Type*	2003	2005
Pulsar Wind Nebula (e.g. Crab, MSH 15-52 …)	1	6
Supernova Remnants (e.g. Cas-A, RXJ 1713 …)	2	6
Binary Pulsar (B1259-63)	0	1
Micro-quasar (LS 5039)	0	1
Diffuse (Cygnus region)	0	1
AGN (e.g. Mkn 421, PKS 2155 …)	7	11
Unidentified	2	6
TOTAL	**12**	**32**

* Includes likely associations of HESS unid sources.

→ **Explosion in the number of VHE sources.**

"Evolution" of the TeV gamma-ray sky

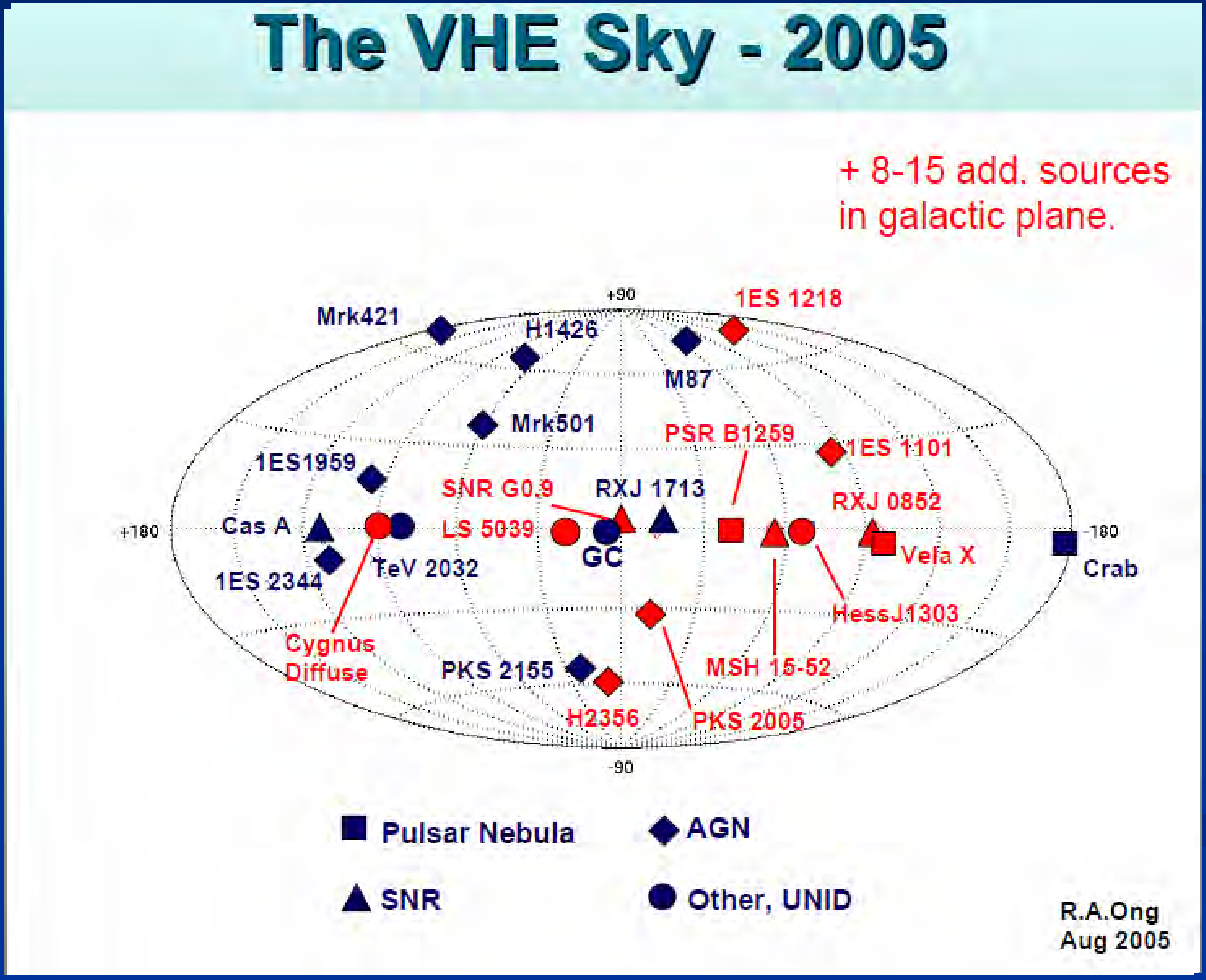

GeV vs TeV

Thrid EGRET catalog: Hartman et al, ApJS 123, 79 (1999)

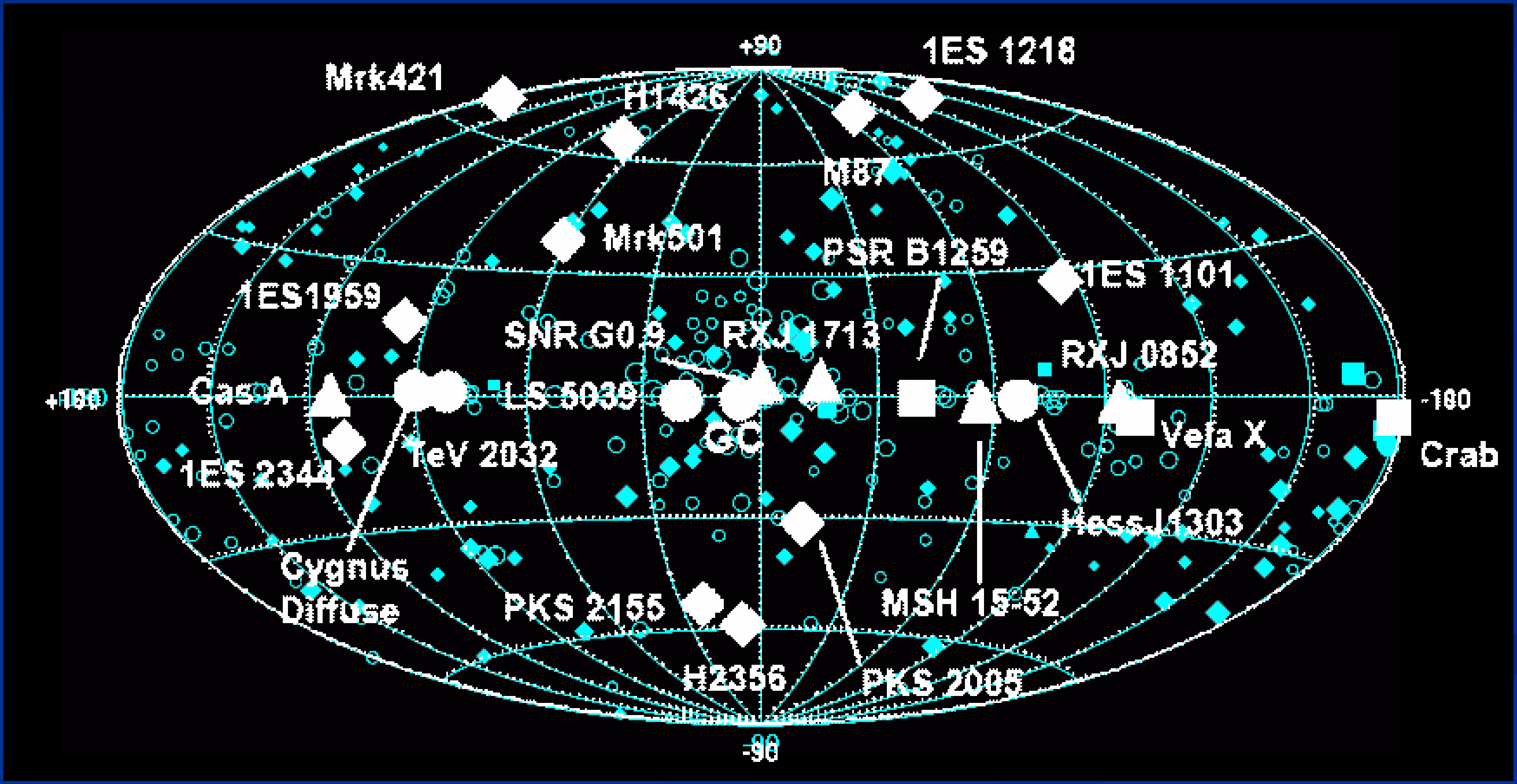

"Evolution" in number of objects

"Kifune Plot"

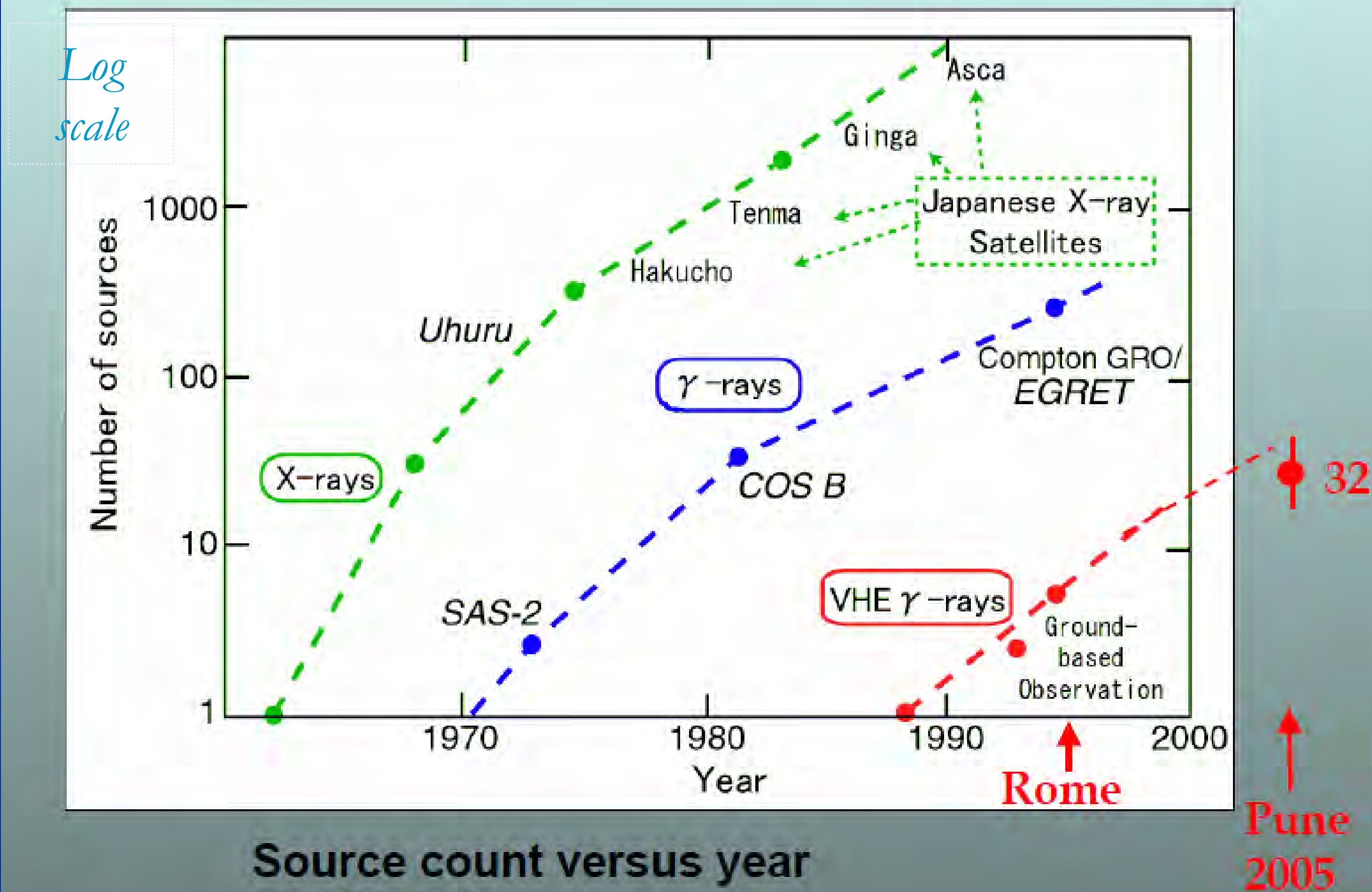

Source count versus year
[T. Kifune]

S. Funk, ICRC2005

Large area left unexplored at TeV

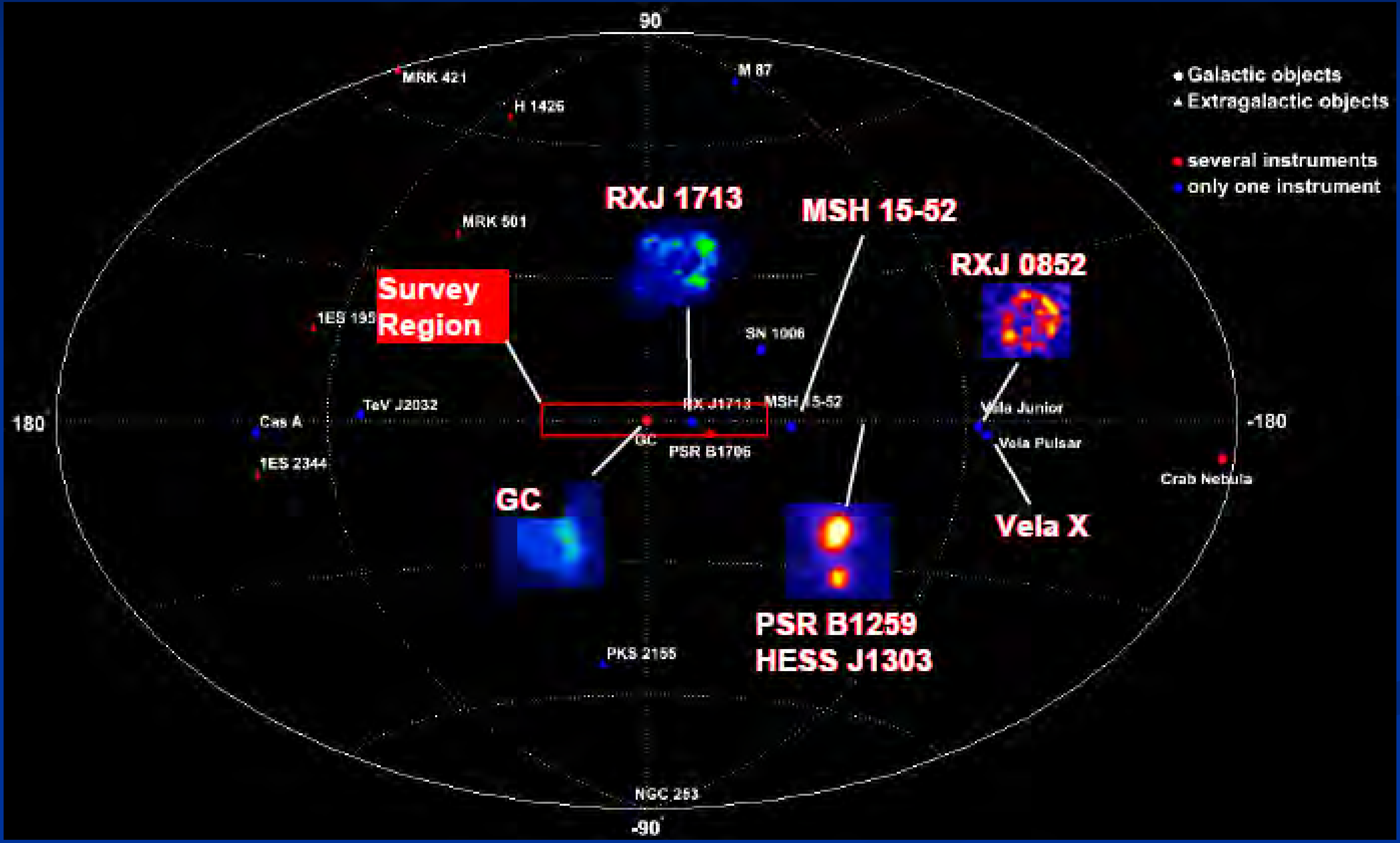

Near future

Which Direction Should We Go?

- Low energy extension
  - Unopened window
- High sensitivity or high energy extension
  - More statistics
- Better time coverage
  - Transient sources

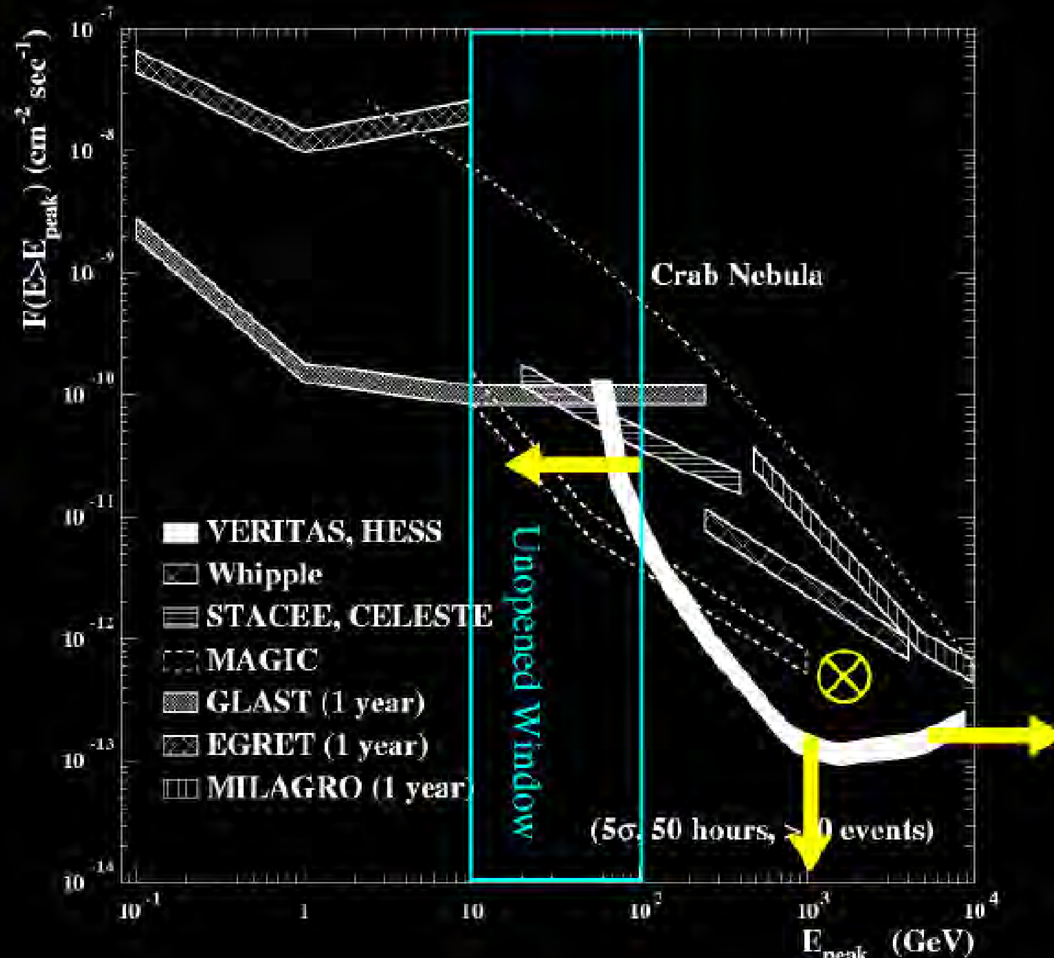

T. Yoshikoshi, Cherenkov2005

VERITAS: VERITAS-4 by 2006

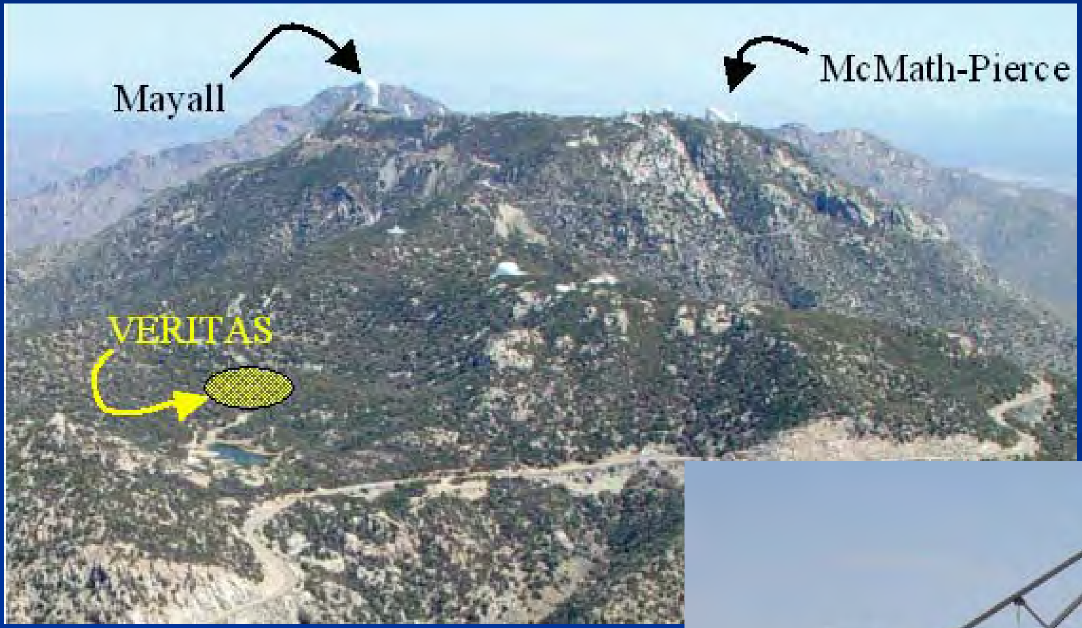

~~New site: Horseshoe canyon, Kitt Peak, Arizona~~

Smithonian Inst. etc.

Prototype (Aug '03)

Nov 2005: New Environmental Assessment

~~Oct 2006: Completion of Phase I: 4 telescope array~~

Then VERITAS-7 in 200X

M. Punch, Cherenkov2005

H.E.S.S.-II

Khomas highland, Namibia (1800m a.s.l.)

M. Teshima, Cherenkov2005

MAGIC-II and III

Canary island (2200m a.s.l.)

R. Koul, Cherenkov2005

MACE

Hanle, North India (4200m a.s.l.): 2010?

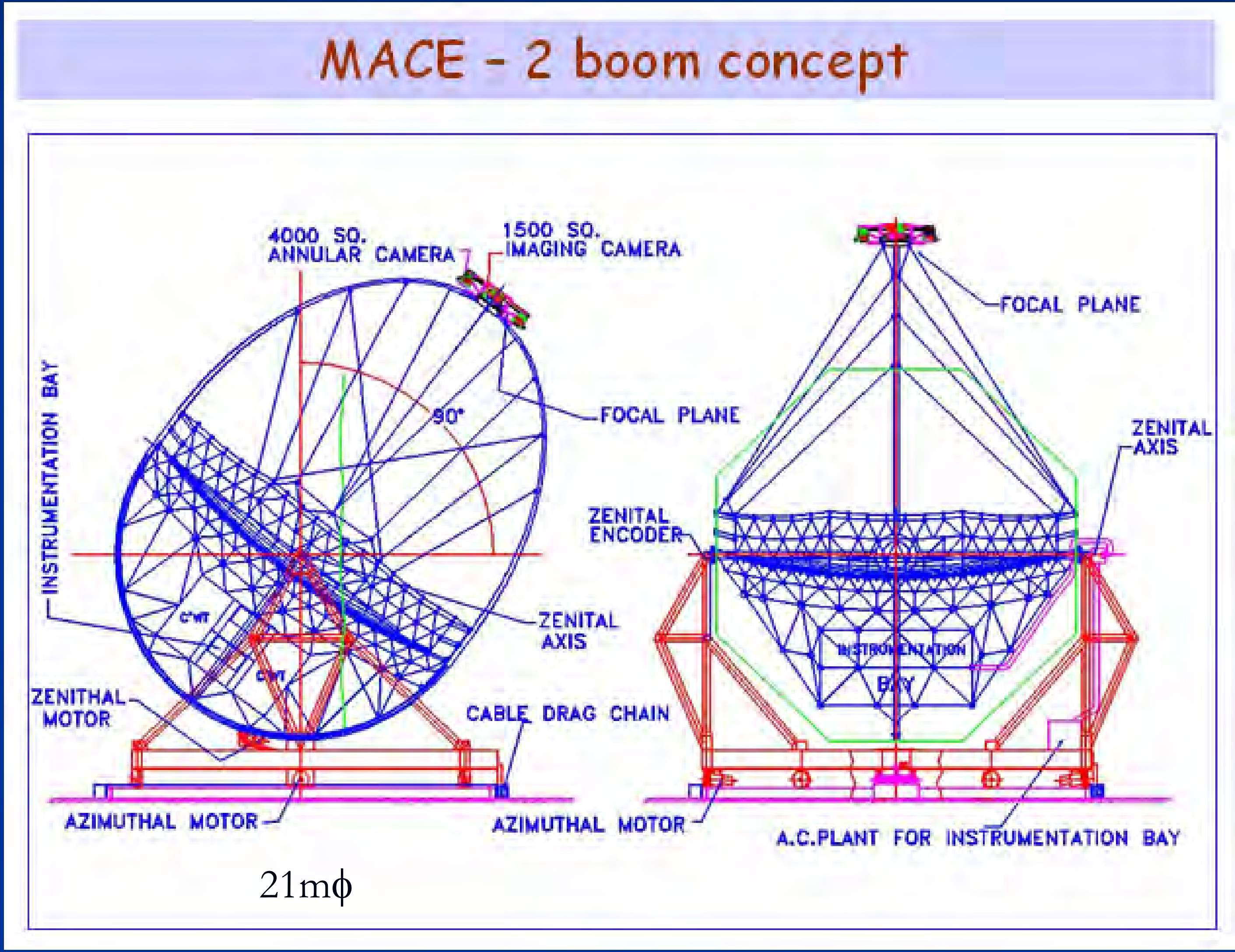

Midsized-telescope arrays

Many conceptual designs: for example,

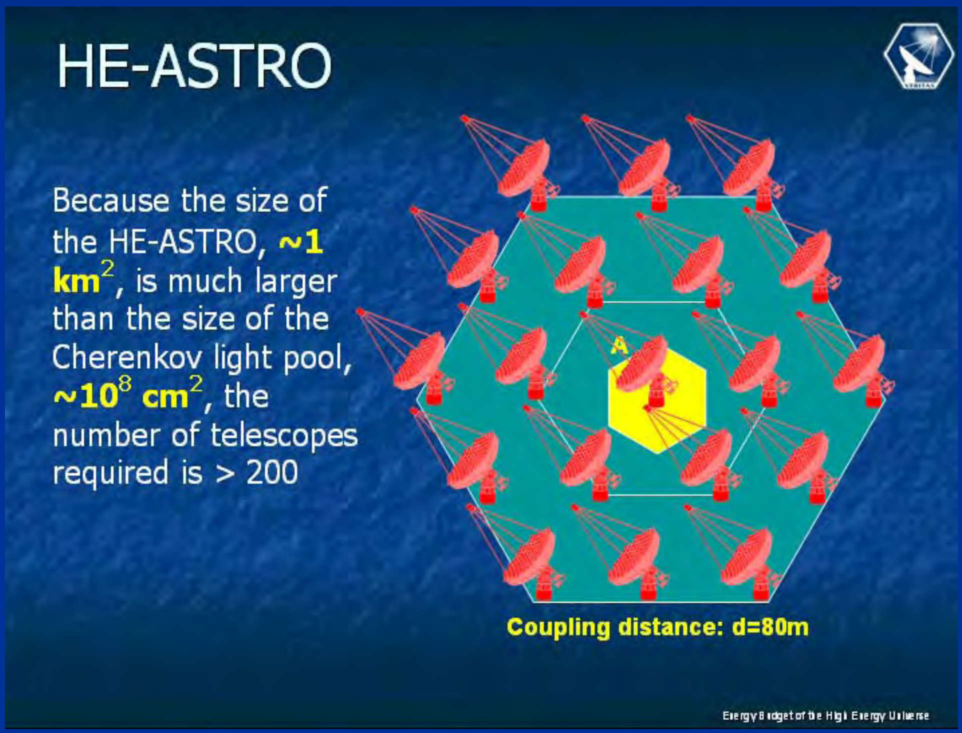

T. Weekes, Energy Budget in the High Energy Universe, 2006

TenTen (10km2 at 10TeV)

- 30-50 telescopes
- 10-20 m^2 each, 5-10 deg FOV
- >250m spacing

GRATIS

- 37 x 6 m diameter telescopes
- moderate field of view (3.5 deg.)
- 0.2 deg. pixel/optical resolution
- small off-axis aberration design
- energy threshold ~ 20 … 200 GeV with high QE

Wide-field optics

GAW (Gamma Air Watch)

- Flat, single-side lens
- Lens Diameter = 2,1 m
- Focal length = 2,5 m
- f/# = 1.2
- Field of view = ± 12 deg.

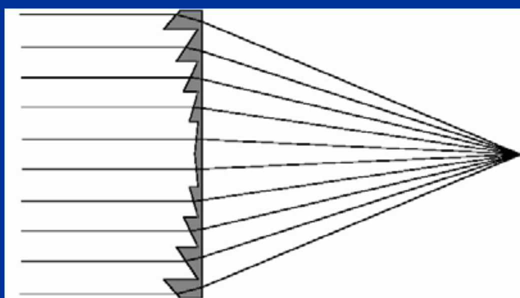

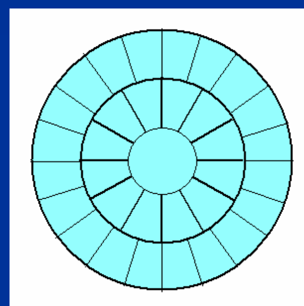

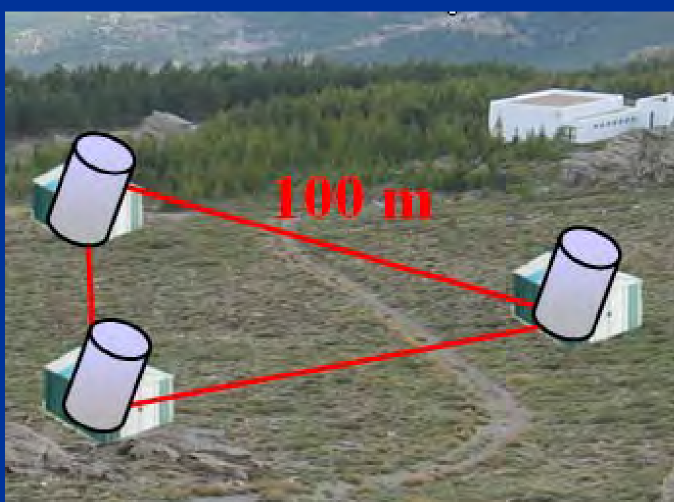

Mineo et al., NewHEGE3, 2005

ASHRA

M.Sasaki, Energy Budget in the High Energy Universe, 2006

G. Sinnis, Cherenkov2005

Particle detector: HAWC

- 300m x 300m pond
- Wide FOV: ~2sr
- 100% duty cycle

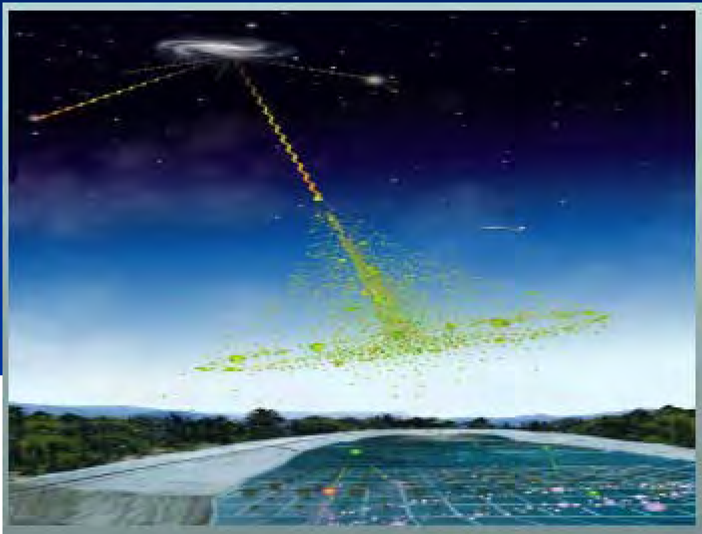
HAWC Concept

- Build pond at extreme altitude (Tibet 4300m or Chile 5200m)
- Incorporate new design
  - Optical isolation between PMTs
  - Larger PMT spacing
  - Deeper PMT depth (in top layer)

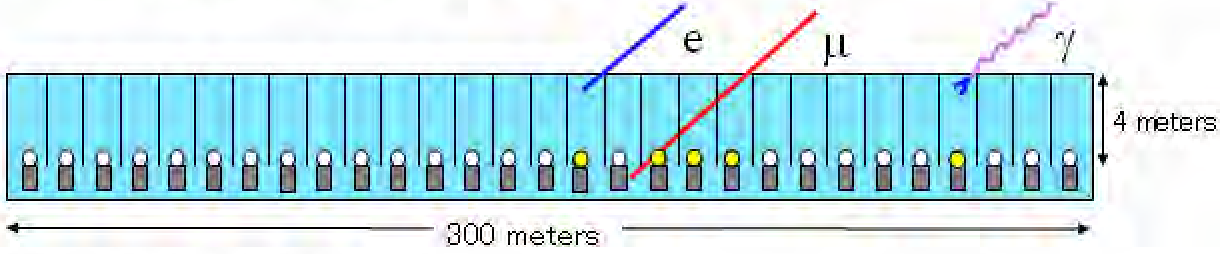

~$20M for complete detector

~60x sensitivity of Milagro – instantaneous sensitivity of Whipple over 2 sr

Crab Nebula in 30 minutes (now 1 year)

GRBs to redshift of >1 (now 0.4)

CTA (Cherenkov Telescope Array)

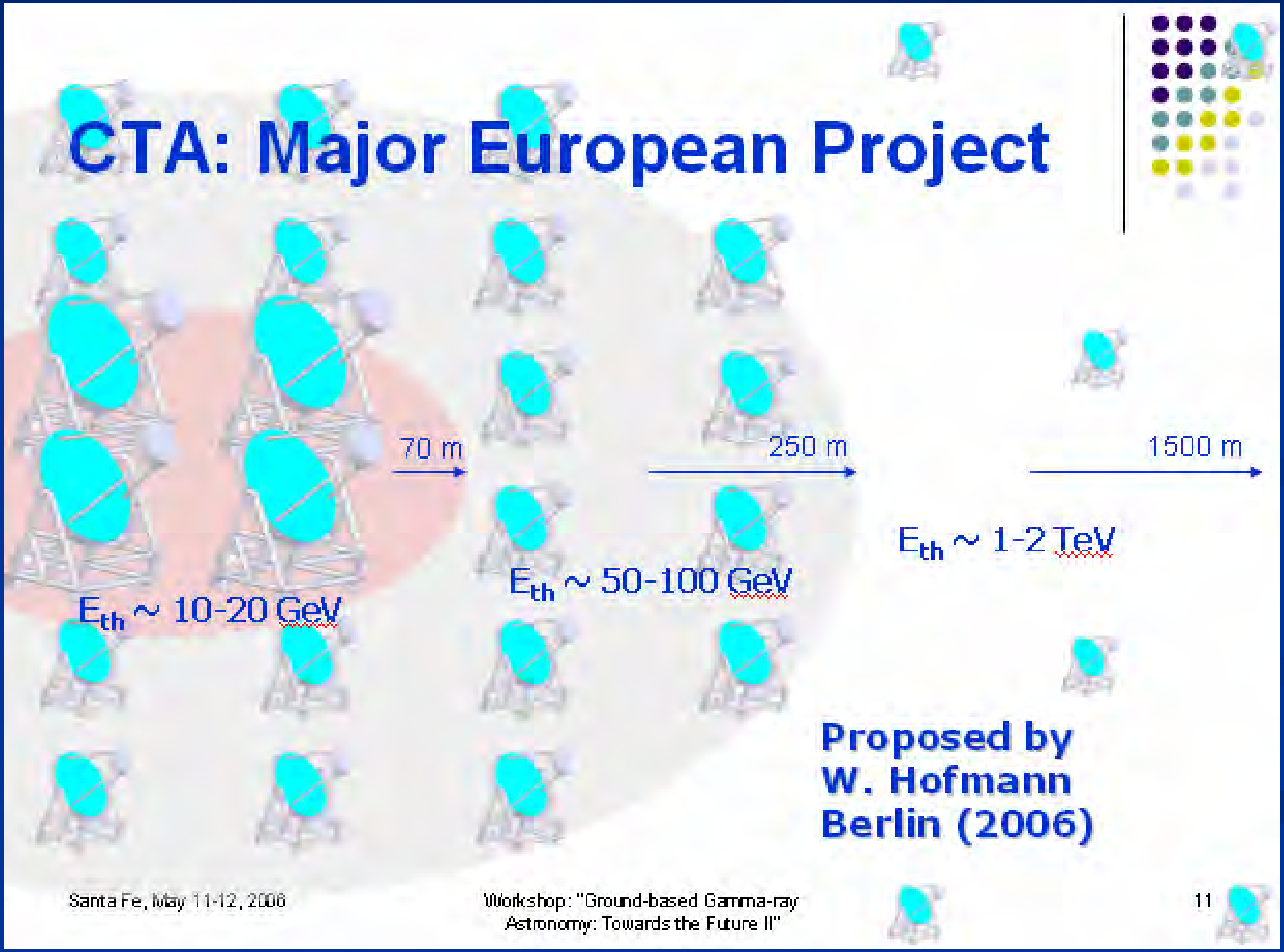

International coordination

- Monitoring of time-variable objects (e.g. blazars)
- Multiwavelength observation campaign

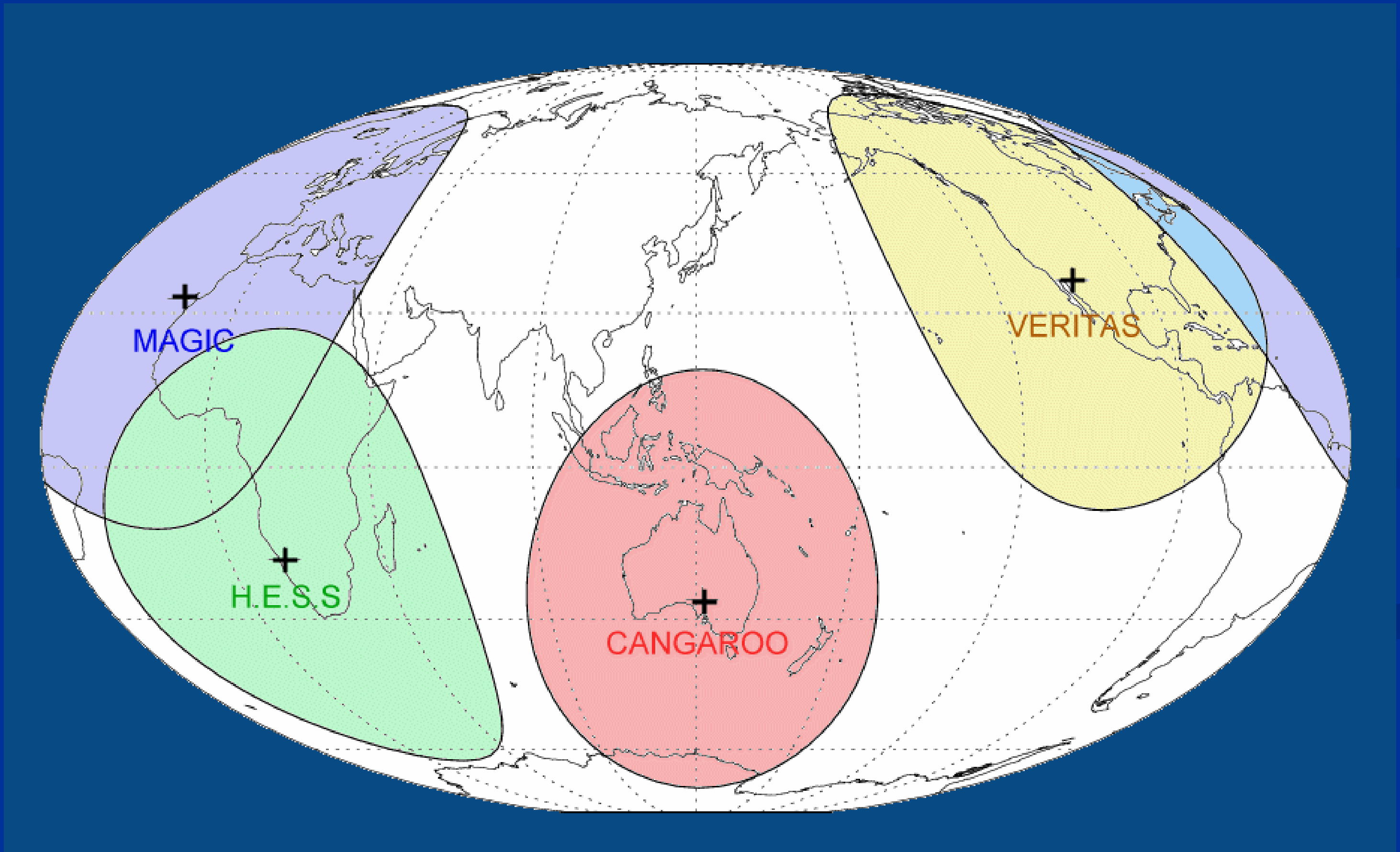

An example: MAGIC & H.E.S.S. campaign on Mrk 421

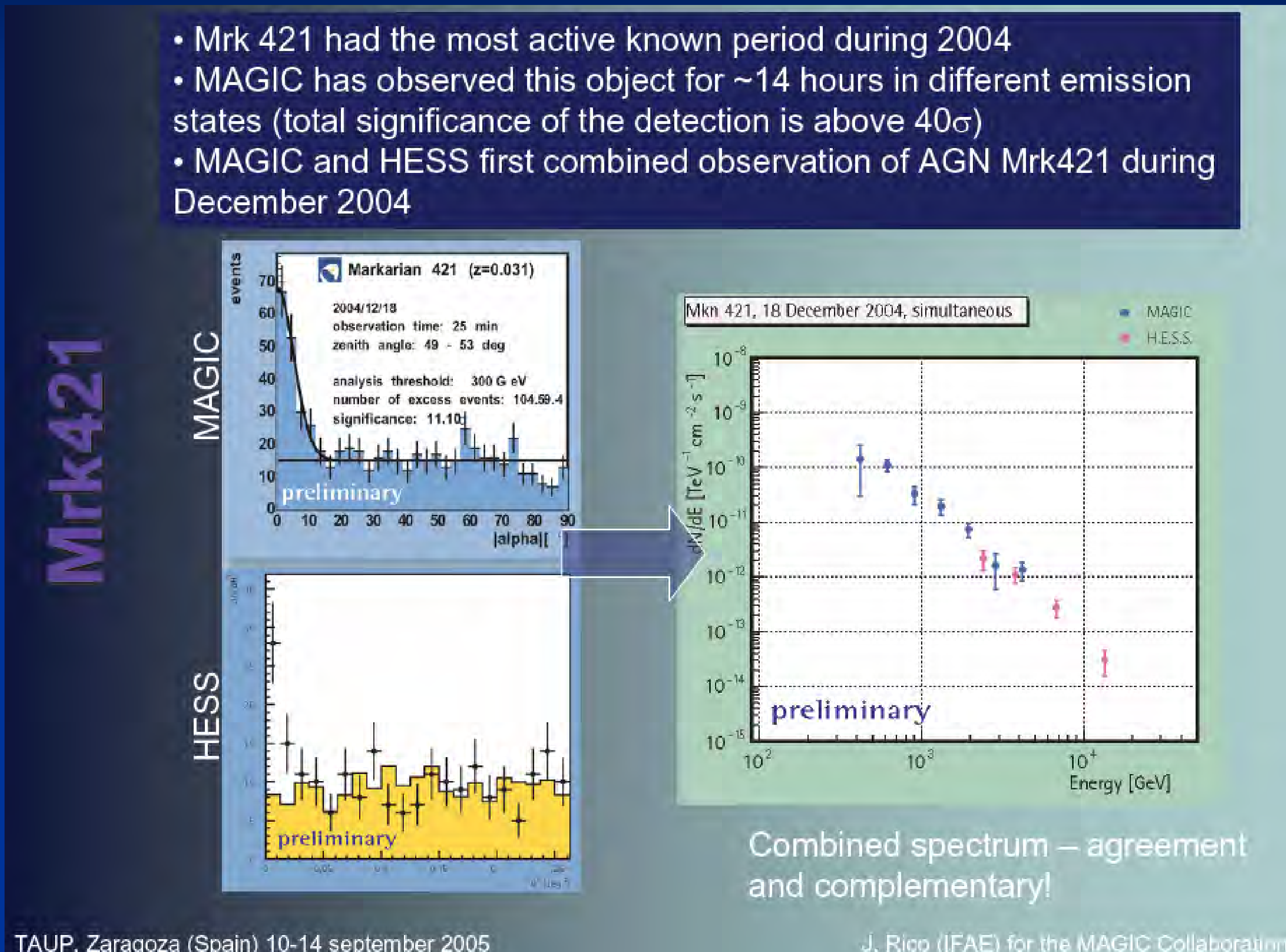

Summary

- Very high energy gamma-ray sources may contain large varieties, including both galactic and extragalactic objects.
- TeV gamma-ray astronomy is becoming an indispensable field of astronomy.
- Supernova remnants are confirmed to be very-high-energy particle accelerators: an important evidence of cosmic ray origin!
- Basic problem still remains: electron origin or proton origin?
- The "third generation" Cherenkov telescopes are working hard (and "fourth" ones are planned)– more fun!